INVESTIGATING ON-BOARD FE FERTILIZATION EXPERIMENTS USING FAST REPETITION RATE FLUOROMETRY IN THE SOUTHERN OCEAN.

By

Fiona Kate Preston-Whyte

Dissertation submitted in fulfilment of the requirement for the degree of Masters of Science in the Department of Zoology, University of Cape Town

Date: 11 February 2013

Supervisors: Associate Professor Mike Lucas and Dr Sandy Thomalla

Plagiarism Declaration

1. I know that plagiarism is wrong. Plagiarism is to use another's work and pretend that it is one's own.
2. Each contribution to, and quotation in, thesis from the work(s) of other people has been attributed, and has been cited and referenced.
3. This thesis is my own work.

Date: .....

Signature: .....

Abstract

In the face of increasing carbon dioxide (CO_2) accumulation in the atmosphere and associated climate change, an understanding of important global carbon sinks such as the Southern Ocean becomes imperative. Phytoplankton, being the major driver of the biological pump, need to be understood at the level of photosynthetic efficiency, especially in relation to growth limiting factors such as iron (Fe). This study reports both observational and experimental phytoplankton growth rate observations from the summer months of 2009/10 and 2010/11, focusing on the Southern Ocean area between South Africa, Acta Bukta (Antarctica) and South Georgia. The study includes six ship based Fe enrichment incubation experiments to examine the interaction of Fe and light controls on photosynthesis. This study focuses on the phytoplankton photosynthetic responses using Fast Repetition Rate fluorometry (FRRf). Throughout the study area phytoplankton photosynthetic efficiency (F_v/F_m) increases in response to Fe alleviation, as is the case in the on-deck Fe-supplemented incubations. Chlorophyll-a (chl-a) increase due to Fe alleviation is not guaranteed, however it is dependent on initial community structure, the light environment and grazing rates. This research implies that the majority of the Southern Ocean is Fe limited, and that an increase in Fe would lead to an increase in photosynthetic efficiency, but not necessarily biomass or carbon export.

Acknowledgments

I would like to thank Captain Hall and Captain Freddie Ligthelm, the Offices and Crew of the *MV SA* Agulhas for their unending support during the collection of the data and their interest in our work. My unending thanks to Steve Yaxley (The Chief Engineer) for his insightful problem solving without which our lives at sea would have been fraught with difficulties. To the Bosons team for their help in the movement of my incubation stand throughout the cruise. To the SANAE 49 Oceanography Team: Dr Sandy Thomalla (chief scientist), Dr Bob Scholes, Dr Thato Mtshali, Dr Yuri Controneo, Patrick Hayes-Foley, Sarah Nicholson, Amy Harington, Cienwein Smith and Samantha Maxwell-Hafen for the hard work and high spirits that went into collecting the data that contributed to this thesis. Another thank-you to Samantha Maxwell-Hafen, for calculating the SANAE 49 f-ratio's. To the SANAE 50 team: Dr Sebastiaan Swart (chief scientist), Patrick Hayes-Foley, Luke Gregor, Mutshutshu Tsanwani, Craig Attwood, Dr Pasquale Castagno, Katherine Hutchinson, Philip Massie, Raimund Rentel, Sarah Yates and Damian Weldon for data collection which contributed towards this thesis. Specifically to the extra work contributed by Isabelle Giddy and Ceinwen Smith.

I would also like to sincerely thank my supervisors, A/Prof Mike Lucas and Dr Sandy Thomalla, for insight and support throughout the project; as well as, Michael John Gibberd, Dr Sebastiaan Swart, Dr Isabelle Ansorge and Andrew Timm for answering endless queries regarding MATLAB, defining water masses, statistical advice and computer problems.

I would also like to thank the University of Cape Town Postgraduate Funding for funding part of my fees for my Masters. I would especially like to thank the trustees of the Max & Lillie Sonnenberg Scholarship for sponsoring my two-month trip to the National Oceanography Centre (NOC), Southampton that enabled the running of the HPLC (High Performance Liquid Chromatography) samples and the opportunity to work with world-class scientists at an international facility. I would like to thank Dr Mark Moore, Dr Duncan Purdie, Dr John Grittens and Dr Alex Poultan for their time, patience and knowledge shared during my time at NOC. Thanks also to the trustees of the MA-RE Basics Travel Award 2012, for co-funding my travel expenses to The 15th Biennial Challenger Conference for Marine Science (held at the University of East Anglia, United Kingdom) to present my thesis in the form of an oral presentation. A sincere thank-you to my primary supervisor A/Prof Mike Lucas for providing subsistence and living funds during the extent of this study, as well as co-funding my travel expenses to the Challenger Conference, from his South African National Antarctic Program (SANAP) grant.

Perhaps the biggest thank-you is extended to The Southern Ocean Carbon and Climate Observatory (SOCCO) at the Council for Scientific and Industrial Research (CSIR) who led the Southern Ocean scientific research programme as well as the Department of Environmental Affairs and SANAP for funding and support on the two cruises. A last official thank-you is directed towards NOAA's (National Oceanic and Atmospheric Administration's) Office of Global Programs as part of their High Density XBT (Expendable Bathythermograph) project at NOAA/AOML (Atlantic Oceanographic and Meteorological Laboratory) for the funding of the 166 Sippican Deep Blue XBTs.

My unending thanks to my friends and family who ensured that I carried on standing throughout my thesis, who were happy to listen to unending theories on the technicalities involved in marine biology, despite their glazed looks.

List of Abbreviations

ρNO_3/Total ρN	f-ratio calculation: (uptake Nitrate/total nitrogen uptake)
σ_{PSII}	The functional absorption cross section of photosystem II
ºC	Degrees Celsius
AASW	Antarctic Surface Water
ACC	Antarctic Circumpolar Current
AOML	Atlantic Oceanographic and Meteorogical Laboratory
APF	Antarctic Polar Front
APZ	Antarctic Polar Zone
ATP	Metabolic energy
$CaCO_3$	Calcium carbonate
CH_2O	Glucose
chl-a	Chlorophyll-a
CO_2	Carbon Dioxide
CROZEX	The Crozet Natural Iron Bloom and Export Experiment
CSIR	Counsel for Scientific and Industrial Research
CTD	Conductivity, Temperature and Depth
DIC	Dissolved Inorganic Carbon
DOC	Dissolved Organic Carbon
F_v/F_m	Photochemical efficiency
Fd	Ferredoxin
Fe	Iron
$FeSO_4$	Iron Sulphate
FIRe	Fluorescence, Induction and Relaxation

FRRf	Fast Repetition Rate fluorometry
Fuc:Hex	Fucoxanthin:19'-hexanoyloxyfucoxanthin
GF/F	Glass Fibre Filter
GtC	Giga tons of carbon
H_2O	Water
HNLC	High-Nutrient-Low-Chlorophyll
HPLC	High Performance Liquid Chromatography
IPCC	Intergovernmental Panel on Climate Change
IR	Infra-Red
Km	Kilometer
Kg m^{-3}	Kilogram per cubic metre
NADPH	Nicotinamide Adenine Dinucleotide Phosphate
NH_4	Ammonium
Nm	Nautical miles
NO_3	Nitrate
NO_2	Nitrite
NOAA	National Oceanic and Atmospheric Administration
NOC	National Oceanography Centre
m	Metre
MATLAB	MATrix LABoratory
ml	Millilitres
MLD	Mixed Layer Depth
MTF	Length of the multi-turnover flash phase in msMultiple Turnover Flash
MTRI	The initial interval between relaxation pulses
MTRP	The number of pulses in the relaxation sequence

O_2	Oxygen
PAR	Photosynthetically Active Radiation
Pc	Plastocyanin
PgC y^{-1}	Petagrams of carbon per year
pH	Measure of the acidity of a solution
PO_4	Phosphate
POC	Particulate Organic Carbon
PON	Particulate Organic Nitrogen
ppm	Parts per million
Pq	Plastoquinone
PS	Photosystem
PSU	Practical salinity unit
UCTD	Underway Conductivity, Temperature and Depth
$\mu g.l^{-1}$	Micrograms per litre
$\mu molL^{-1}$	Micromoles per litre
VNO_3 d^{-1}	Specific uptake rate of NO_3 per day
s	Seconds
SACCF	Southern Antarctic Circumpolar Current Front
SAF	Subantarctic Front
SANAE	South African National Antarctica Expedition
SANAP	South African National Antarctic Program
SBdy	Southern Boundary of the Antarctic Circumpolar Current
Si	Silicon
SiO_4	Silicate
SOIREE	Southern Ocean Iron Release Experiment

LSTF	Length of a single turnover flash in μsec
STF	Subtropical Front
STRI	Initial interval between relaxation pulses in μsec
STRP	Number of pulses in the relaxation sequence
XBT	Expendable Bathythermograph
UCDW	Upper Circumpolar Deep Water
WOCE	World Ocean Circulation Experiment
WW	Winter Water

Contents

CHAPTER 1: INTRODUCTION

1.1) Climate change

The last century has seen a significant warming across the globe, with the global average temperature increasing by 0.76ºC between 1850 and 1899 as well as between 2001 and 2005 (IPCC, 2007a). Although there is a natural background climatic variation, a substantial climate change signal has emerged from this natural variability (Field *et al.,* 2002; Sabine *et al*., 2004b), with the warming trend increasing significantly over the second half of this century (IPCC, 2007a). Further indications of climate change have been observed in the oceans. The latent heat differences existing between water and gas, means that the oceans have heated 20 times more than the atmosphere since 1960 (Levitus *et al.,* 2005). This has been observed specifically in warming of Southern Ocean Mode Waters and the Upper Circumpolar Deep Waters over this time period. Apart from warming, climate change can be seen in changes in global precipitation, which along with melting of the ice caps (Haeberli *et al.,* 2005a; Haeberli *et al*., 2005b; Kaser *et al.,* 2006) is linked to changes observed in ocean salinity. Between 1955 and 1998, freshening has occurred in subpolar latitudes and in the Pacific Ocean, while the Atlantic, Indian and shallower parts of the tropical and subtropical oceans have become saltier (IPCC*,* 2007d).

Geological and ice-core data provide our principle records of past climatic cycles, their changes and the long-term effects of climate change (Hughes *et al.,* 2003). These records reveal long-term cooling of Earth over the last 60 million years, while more recently cycles in global climate have resulted in regular shifts between ice ages and eras of warming. The past shifts in our climate are attributed to either natural climate variability or climate change (where the changes occur outside of the natural cycles). The natural climate

variability results from cyclical variations in earth's orbit around the sun, and in the angle of tilt of the earth's axis of rotation (MacCarthy and Rubidge, 2005), this effect on climate by the earths' movements are known as Milankovitch cycles which are clear throughout the earth's climate history. The less regular and modern variability since the 1750's is regarded as human-induced climate change.

Climate change can be (and has been in the past) caused by various factors such as volcanic eruptions, variability in solar luminosity, changes in the position of land masses, ocean currents due to plate tectonics, as well as Milankovitch forcing over longer periods (23 000, 40 000 and 100 000 years). New to this list since the 1750's is rapid human-forced change over tens to hundreds of years due to anthropogenic aerosols and greenhouse gas emissions that cause the corresponding greenhouse effect (Field *et al.,* 2002). There is mounting evidence (Robock, 1979; Wigley and Raper, 1990; Friis-Christensen and Lassen, 1991; Kelly and Wigley, 1992; Crowley and Kim, 1993; Rind and Overpeck, 1993; Cubasch *et al.*, 1997; Briffa *et al.,* 1998; Mann *et al*., 1998; Crowley and Kim, 1999; Damon and Peristykh, 1999; Free and Robock, 1999; Lean and Rind, 1999) that volcanic activity significantly contributed to decadal-scale climate variability in the little ice age (Crowley, 2000). A prime example of the influence of volcanic eruptions on the world's climate was seen by the effects of the large dust cloud present in the stratosphere in the years following Mount Pinatubo's eruption (Bluth *et al*., 1992; Krueger *et al.,* 1995), which cooled earth by about 0.5ºC. Furthermore, volcanism in the Southern Hemisphere north of 20º S influences Northern Hemispheres temperatures (Crowley, 2000). Variation in solar luminosity caused by sun-spots is believed to affect the climate due to variations in the radiation entering the atmosphere (Hoyt, 1979).

However, neither of these natural processes can explain rapid global warming experienced since the 17th century (Foukall *et al.,* 2006). The tectonic movement over this time is not sufficient to alter the Earth's climate. Instead, anthropogenic influences provide the most plausible cause of recent global warming. The two principle causes are due to aerosols and greenhouse gases.

Anthropogenic aerosols pollute the atmosphere causing changes in the Earth's albedo (which alters the fraction of solar radiation reflected both back to earth and space). Aerosols are tiny liquid droplets in the air which cause the scattering of light, and affect cloud formation and hence, rain patterns. This without a doubt is a global problem, as seen by the many Clean Air Acts around the world; United States of America (Clean Air Act of 1963, amended in1970, 1977 and 1990), South Africa (Air Pollution Prevention Act in 1965 and the National Environmental Management: Air Quality Act 2004), Philippine (Clean Air Act of 1999) and Britain (Clean Air Act of 1956, updated in 1993) all have individual Clean Air Acts. These acts were drafted in response to human health issues with amendments being adjusted to include the health of the atmosphere itself. It should be recognised that while some aerosols cause cooling (e.g. sulphate aerosols), others cause warming (e.g. dark soots). These contradictory effects are due mainly to the type of aerosol, their height in the atmosphere, as well as their light scattering or absorption properties. Either way, anthropogenic aerosols are not the main cause of current global warming trends, though they are responsible for effecting precipitation patterns (Ramanathan *et al.,* 2001; Menon *et al.,* 2002) and possibly enhancing bush encroachment (Wigley *et al.,* 2010).

More significant are the greenhouse gases. An *elevated* greenhouse effect is caused by elevated greenhouse gas concentrations of (e.g. carbon dioxide [CO_2], methane, nitrous oxide

and fluorocarbons) in the atmosphere, which in turn alters the balance between long-wave infra-red (IR) radiation lost to space, or re-radiated back to Earth (IPCC, 2007a). Where the radiation balance results in more reflected IR, this leads to an accumulation of excess heat within the atmosphere. The greenhouse effect is primarily anthropogenic, due to fossil fuels combustion, land use change (primarily in the tropics), as well as various industrial processes (Field *et al.,* 2002) such as cement production (Hendriks *et al.,* 2003). Although the causes of climate change over the last century are still argued, within scientific circles it is almost unanimously agreed that such changes stem from anthropogenic activities and that "*the link between greenhouse gases and observed climate change are now incontrovertible*" (Hoegh-Guldberg, 1999; IPCC, 2001).

Present atmospheric CO_2 concentration is rising between 10 and 100 times faster than at any other time in the past 420 000 years (Falkowski *et al.,* 2000). This is due to the rapid industrialization that occurred after the 1750's, when burning fossil fuels provided the energy for great industrial advancements, but with corresponding growth in CO_2 emissions. This development has continued into the 21st century with "*56.6% of all anthropogenic greenhouse gas emissions coming from 85% of the global economies that are primarily energy driven through the consumption of fossil fuels*" (IPCC, 2011). At the end of 2010, atmospheric CO_2 exceeded pre-industrial levels by 39%. In the absence of any further climate change policies, climate models are predicting a global average surface temperature rise of 1.5 – 5ºC (Field *et al.,* 2002; IPCC, 2007b) over the next century (relative to 1999).

"*Anthropogenic caused climate change is already having a significant impact on multiple systems globally*" (Rosenzweig *et al.,* 2008). These include melting Arctic ice, shrinking mountain glaciers (Haeberli *et al.,* 2005a; Haeberli *et al.,* 2005b; Kaser *et al.,*

2006), and more extreme weather patterns, with wet areas receiving more precipitation, and dry areas less, leading to the intensification and spread of deserts (Hillel and Rosenzweig, 2002; IPCC, 2007c).

Because modern societies are non-nomadic, climate change has important social and economic consequences. To reduce the impact of such threats, the Cancun agreement (2010) called for limiting the maximum global average temperature rise to 2ºC above pre-industrial values. To achieve this, CO_2 would need to stabilize in the atmosphere between 445 - 490 ppm (at the end of 2010, atmospheric CO_2 was at 390 ppm) (IPCC, 2011). Current global agreements on CO_2 emissions are insufficient to limit us to such a goal (Cuypers *et al*., 2011).

1.2) The carbon cycle

There is a continual carbon cycle that has existed throughout out Earth's history which has varied over time, in response to climate change (Barnola *et al*., 1987; Petit *et al.,* 1999; IPCC, 2007a; Sundquist and Visser Ackerman, 2014). Industrialization has seen disruption in the natural carbon cycle (IPCC, 2013), with anthropogenic released carbon in to the atmosphere estimated at a net flux of 8.4 PgC y^{-1} (Sabine *et al.,* 2004b) The oceans are naturally both a major source (~70.6 PgC y^{-1}) and sink (~70 PgC y^{-1}; Sabine *et al*., 2004b), for atmospheric CO_2 (Siegenthaler, 1986). Human perturbations have altered this natural cycle by ~20 PgC y^{-1} and ~21.9 PgC y^{-1} for source and sink respectively, resulting in a net overall sink of ~1.3 PgC y^{-1} (Sabine *et al*., 2004b). The net uptake of carbon by the ocean since global industrialization had by 1994 increased the oceanic carbon inventory by 118 ± 19 GtC (IPCC, 2007d). Though the oceans continue to take up CO_2, the rate at which they succeed in doing so has decreased since the 1980's (IPCC, 2007d).

Trends in atmospheric CO_2, such as the slowing of emitted CO_2 (from 0.5% per year to 0.3% per year (Hansen *et al*., 1998) in the late 1990's (despite a period of worldwide increased economic and industrial growth (Zagha and Nankani, 2005), puzzle the scientific community (Field *et al.,* 2002). Associated changes in the terrestrial carbon sinks such as bush encroachment in grasslands (Bond and Midgley, 2000; Morgan *et al.,* 2007; Kgope *et al*., 2009; Wigley *et al*., 2010) occurred at this time (Higgins *et al.,* 1999; Roques *et al*., 2001; Moleele *et al*., 2002). The economic and social consequences of such changes (Bond and Midgley, 2000) lead to the necessity of better understanding the carbon sinks, such as within the oceans. It is also key to understand processes that influence the carbon cycle, such as photosynthetic responses (Coale *et al.,* 1996), and how these respond to changing environmental conditions whether due to geo-engineering consequences or to natural changes that occurs with climate change or climate variability.

1.3) The role of the oceans

"*Although the intricate two-way relationship existing between the Earth's oceans and climate is not fully understood*" (Field *et al.,* 2002), the oceans have a fundamental influence on the global climate system with regard to both variability and change (Field *et al.,* 2002; IPCC, 2007d). The oceans have already reduced the magnitude of human-driven climate change (Fung *et al*., 2005; Friedlingstein *et al*., 2006) through the uptake of CO_2. Over the last two centuries, the oceans have been the primary sink for anthropogenic carbon, taking up ~23% of collective fossil fuel emissions in 2008 (anthropogenic atmospheric carbon 9.9 +/- 0.9 PgC y^{-1} and CO_2 by ocean sinks 2.3 +/- 0.4 PgC y^{-1}) (Le Quere *et al.,* 2009), thus successfully slowing the growth rate of atmospheric CO_2 and its effects on the earth's climate.

The short and long term effects of the oceans on life on Earth can be seen in the transport of heat around the globe via the oceans and the corresponding weather patterns that are regulated by ocean-atmosphere coupling. The long-term effect of the oceans on climate however, is of vital interest. The CO_2 flux depicted in figure 1 represents the integrated relationship between the oceans and the atmosphere, which affects climate in the long term. With rising atmospheric CO_2 concentrations, the mechanisms affecting CO_2 flux, it's basic limitations and influencing features become key to understanding and making possible mitigation plans as "*alterations in these fluxes could buffer or enhance climate change*" (Field *et al.,* 2002).

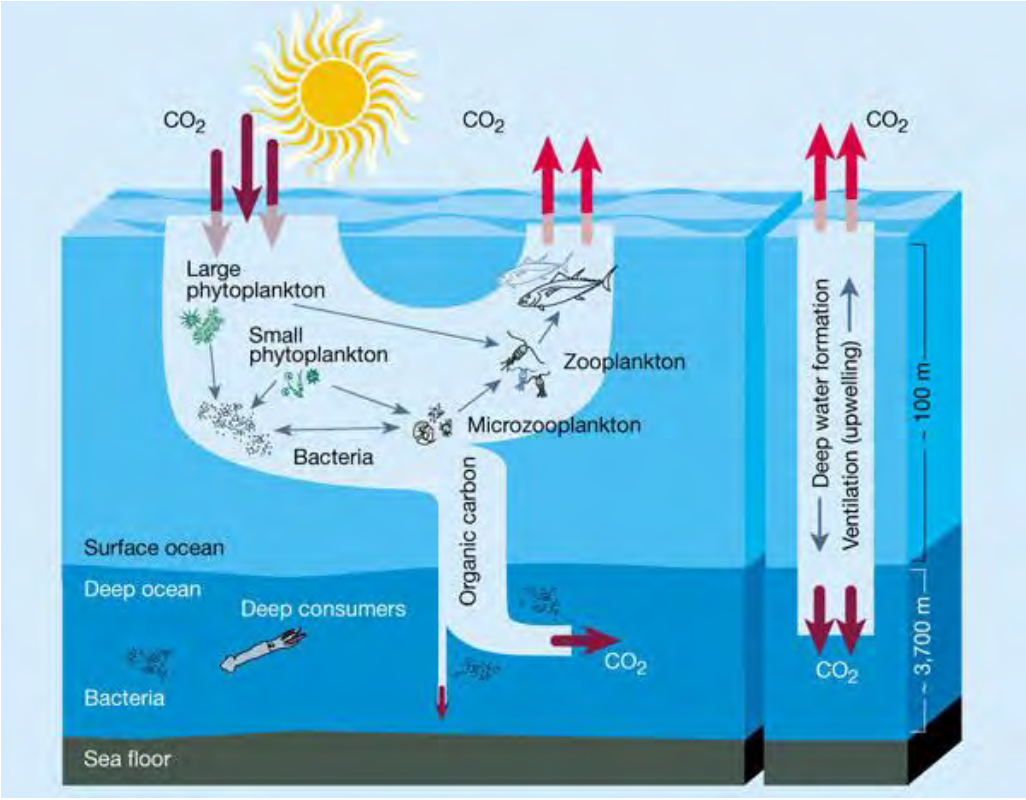

Figure 1: Ocean carbon flux (http://www.acecrc.org.au/Research/Southern%20Ocean%20Carbon%20Sink)

The oceans are an enormous reservoir for carbon (Field *et al*., 2002), and are currently a net carbon sink of ~1.3 $PgCy^{-1}$ (Sabine *et al.,* 2004b). CO_2 is drawn out of the atmosphere by two basic processes: the "physical solubility pump" and the "biological carbon pump".

1.3.1) The physical solubility pump

The strength of the physical solubility pump is set primarily by temperature and the degree of warming and cooling that, together with salinity, regulates density and the rate of surface water sinking, taking with it atmospheric CO_2 (Watson and Orr, 2003). The expulsion of salt during winter seawater freezing and ice formation in Polar latitudes (Warren and Wunsch, 1981) leads to deep-water formation due to sinking of the resulting cold, dense water. Furthermore, as the waters cool, gases (including CO_2) become increasingly soluble in it (Cutnell and Johnson, 2007). Subduction of this water therefore carries with it the CO_2 signal of the atmosphere, carrying the CO_2 into deep reservoirs within the oceans. However, eventual over-turning of the ocean by the thermohaline circulation (Gordon, 1986; Broecker, 1991; Schmitz, 1995) will result in CO_2 'outgassing' around 1 000 years later in the Equatorial Pacific, the largest 'source' of CO_2 to the atmosphere (Petit *et al*., 1999; Toggweiler, 2008). Over such a long time scales, sequestered CO_2, is isolated from further interactions with the atmosphere (IPCC, 2007d).

Removal of CO_2 into the deep ocean lowers the concentration of CO_2 in surface layers, which creates an atmosphere-ocean concentration gradient that allows further uptake of CO_2 by the oceans. It is this physical process that forms part of the carbon sink within the oceans, termed the physical solubility pump.

The oceans have warmed since the 1950's, with a rise in the average global surface (to 700m) ocean temperature of 0.10ºC (IPCC, 2007b; IPCC, 2007d). This is a matter of concern, as the solubility of CO_2 in the ocean is an inverse function of temperature (Field *et al*., 2002). Warming of the oceans therefore threatens the efficiency of the "physical solubility pump". A thirty-year study currently by Rintoul *et al.,* (in press) further supports

this concern as it reveals that Antarctic Bottom Water formation has declined by up to 60% over that period.

Rising temperatures are less of a concern for phytoplankton communities (Chisholm *et al*., 2001), which are affected more by other factors associated with temperature, rather than by small temperature changes themselves. However, as warming oceans lead to stronger stratification, which reduces upward nutrient flux, this will negatively influence the biological carbon pump.

1.3.2) The biological pump

The biological pump (Volk and Hoffert, 1985; Longhurst, 1991; Falkowski and Raven, 2007) refers to the transfer of CO_2, fixed during photosynthesis, into the deep ocean through the sinking of particulate detritus. Phytoplankton are responsible for approximately half of the carbon fixation on earth even though they make up less than 1% of the earth's photosynthetic biomass (Falkowski *et al*., 2000). The fraction of this particulate organic carbon (POC) that is not respired back into surface waters as CO_2, sinks below the euphotic zone (Chisholm *et al*., 2001) into the deep ocean, where it too no longer interacts with the atmosphere. But apart from POC, photosynthesis also produces dissolved organic carbon (DOC) that does not itself sink, but represents a principal store of organic carbon (Tranvik and Jansson, 2002). Where subduction occurs, DOC is exported into the deep ocean, where together with POC; both forms are re-mineralised by bacteria into dissolved inorganic carbon (DIC) (Orr *et al.,* 2005). The deep ocean contains the largest store of mobile carbon on Earth, amounting to about 38,110 PgC, or about 50 times more carbon than is present in the atmosphere (Sabine *et al.,* 2004b; Sabine and Tanhua, 2010), and 10 times more than the earths plant and soil carbon stores (Sabine *et al.,* 2004b).

The vast expanse of the oceans, along with the presence of phytoplankton in surface waters ensures that the oceans play a key role in the global carbon cycle and hence climate regulation (Chisholm *et al.,* 2001; Sabine *et al.,* 2004a, 2004b; Orr *et al*., 2005; Canadell *et al.,* 2007). Each year, about 45% of photosynthesis on Earth occurs in aquatic environments (Falkowski, 1994; Field *et al*., 1998), the rate of which places an upper bound on the overall biomass and productivity of ecosystems (Falkowski and Raven, 2007). This in turn controls the potential of CO_2 uptake by photosynthetic organisms. The ability to influence the rate of photosynthesis thus becomes a relevant interest. As 23% of anthropogenic CO_2 is absorbed by the oceans (Le Quere *et al.,* 2009), this makes the oceans a key area of study as a CO_2 sink.

The geological record of past climate change (Hughes *et al*., 2003) is limiting because it cannot predict what future changes in ocean chemistry, due to higher atmospheric CO_2, may have on the photosynthetic ability of phytoplankton. Current systems, their physical properties, the phytoplankton communities found within them, and their photosynthetic abilities provide different scenarios for predicting this response. Past climates suffered from unexpectedly rapid climatic shifts over decades or less. These changes were especially prominent at high latitudes, with ice-age transitions being linked to abrupt changes in the North Atlantic circulation (Broecker, 2000; Hughes *et al.,* 2003). As current climate change is approached with unprecedented interference in the atmosphere, there is uncertainty in relating the speed of predicted climate change to the past (Hughes *et al.,* 2003). As marine life is reliant on the biogeochemical status of the ocean, it is heavily influenced by changes in the physical state and circulation (IPCC, 2007d), this provides a further area of uncertainty that one must be aware of when considering climate change and oceanic research.

As the biological pump faces climate change the most pressing concern is the effects that changing surface temperatures will have on the system. Increases in surface temperatures affect the mixed layer depth (MLD) and stratification, which in turn affects the light environment, as well as upward nutrient supply. The interconnected relationship between light and nutrient supply controls the phytoplankton bloom, which regulates CO_2 export. Most studies of climate change on phytoplankton production are model based (Cox *et al.,* 2000; Bopp *et al.,* 2001; Fung *et al.,* 2005; Taucher and Oschlies, 2011), showing the same main result: an overall decrease in export production in response to global warming (Taucher and Oschlies, 2011). The metabolic sensitivity of individual phytoplankton species to temperature is also an important component to consider. However more research is needed in this field before conclusive conclusions can be drawn.

One area of concern is potential degradation in the functioning of the biological pump due to changes in ocean pH. Additional absorption of CO_2 by the ocean leads to an increase in ocean acidity, while the concentration of carbonate ions decreases. The exact effect of this on marine biology is poorly documented; however, there are two emerging effects. Firstly, as the saturation state of calcite and aragonite in the oceans fall, a community shift is seen away from the abundance of the most pH sensitive calcifying species. For example, the rate at which coral reefs and coccolithophores form Calcium carbonate ($CaCO_3$) decreases and the dissolution rate may increase. As coccolithophores act as 'ballast' for other less dense decaying matter, this may reduce carbon export into deeper waters (IPCC, 2007d; Archer, 2009); thus, decreasing the strength of the biological pump.

1.4) The Southern Ocean

The Southern Ocean is found south of 30° S - 40º S, uniquely connecting the Pacific, Atlantic and Indian Oceans. A combination of the active subduction of high latitude surface waters rich in CO_2 into the deeper ocean (IPCC, 2007d), and the region's strong biological carbon pump estimated to be 3 PgC (Schlitzer, 2002), accounting for 20% of the global annual phytoplankton production (Orr *et al.,* 2001; Hassler *et al.,* 2012), entitles the Southern Ocean to be viewed as one of the most important ocean sinks of anthropogenic CO_2 (Berger and Wefer, 1991; Caldeira and Duffy, 2000; Sigman and Boyle, 2000) with a disproportionate global impact (Boyd, 2002) on biogeochemical cycles, biodiversity and climate regulation (Hassler *et al.,* 2012).

Of all the world's oceans, the Southern Ocean contains the highest inventory of unused macronutrients (Levitus *et al*., 1993; Boyd *et al*., 2002), yet there is only low and varied phytoplankton biomass and productivity throughout the ocean (Sullivan *et al*., 1993; Seeyave *et al.,* 2007). It is this high-nutrient-low-chlorophyll (HNLC) nature of the Southern Ocean that makes it so interesting. The limited biomass accumulation and hence limited export of CO_2 into deeper waters (de Baar *et al*., 1997; Blain *et al.,* 2007; Pollard *et al.,* 2009) despite high residual nitrate (NO_3) concentrations has made the Southern Ocean a centre for many studies on primary production. One factor known to limit phytoplankton growth in this HNLC ocean is iron (Fe) (Pollard *et al*., 2009). The absence of a continental land-masses in the Southern Hemisphere makes the Southern Ocean one of the most Fe-impoverished of the world's oceans (Duce and Tindale, 1991; de Baar *et al.,* 1995; de Baar *et al.,* 1997; de Baar and Boyd 2000; Mahowald *et al*., 2005; Wagener *et al*., 2008).

1.5) The role of Fe in the Southern Ocean

The 'iron hypothesis,' originally proposed by Martin (1990), espoused elevated phytoplankton production and enhanced carbon export during glacial-interglacial transitions (Sigman and Boyle 2000) due to Fe-stimulated growth. Antarctic and Greenland ice-cores dating from the Last Glacial Maximum revealed a 30x increase in Fe-rich dust flux (Yung *et al*., 1996; Aumont *et al.,* 2008; Mackie *et al.,* 2008), prompting detailed studies on the role of Fe in the control of phytoplankton growth rates.

The HNLC status of the Southern Ocean is thought to be consistent with a Fe limited regime and this argument has been well documented (Martin and Fitzwater 1988; Martin, 1990; Martin, 1992; de Baar *et al.,* 1995; Coale *et al.,* 1996; Boyd *et al.,* 2000; de Baar and Boyd, 2000; Blain *et al.,* 2001; Gervais *et al.,* 2002; de Baar *et al.,* 2005; Blain *et al.,* 2008; Pollard *et al.,* 2009; Smetacek *et al.,* 2012).

Fe-limitation affects the efficient functioning of phytoplankton, both in terms of their photo-physiology and nitrogen metabolism (Raven, 1990; Cochlan *et al*., 2008). Fe limitation impairs pigment synthesis, so reducing the efficiency of the electron transport system in photosystem (PS) I and PS II (Behrenfeld *et al.,* 1996). Fe is critical for the assimilation of NO_3 and is also needed in the biosynthesis of chlorophyll (Miller *et al.,* 1984), without which chlorosis occurs (Lawrence, 2005), substantially decreasing the photosynthetic energy conversion efficiency of the phytoplankton (Laws and Bannister, 1980; Kolber *et al.,* 1988), and so impairs the plants ability to fix carbon. The combination of the above severely affects Fe limited cells, particularly where there is potential light limitation (Sunda and Huntsman, 1997; Lindley and Barber, 1998; Timmermans *et al.,* 2001; Moore *et al.,* 2007a, 2007b). In

the high latitude South Ocean, with its low light levels and cloudy conditions, this is of particular importance.

Now, in the face of climate change, where current predictions forecast an increase in atmospheric dust (Hillel and Rosenzweig, 2002) and hence changes in Fe-flux, as well as deepening the MLD (Sarmiento *et al*., 1998; Boyd, 2002) there are concerns that phytoplankton bloom productivity may decline (Smetacek and Nicol, 2005) concurrent with shifts in species composition; both affecting the efficiency of the "biological carbon pump".

1.6) Experimental evidence supporting the importance of Fe

To determine whether Fe was indeed a limiting factor in HNLC oceans (Martin 1991, 1990), two forms of experiments began to occur: small-scale open ocean Fe fertilization experiments (Martin *et al.,* 1994; Coale *at al.,* 1996; Boyd *et al.,* 2000; Gervais *et al*., 2002; Hoffmann *et al*., 2006; Smetacek *et al.,* 2012), and on-board Fe enrichment experiments (Martin, 1990; Moore *et al*., 2007a, 2007b). These experiments, summarised by De Baar *et al*., (1995) and Boyd *et al*., (2007) have confirmed that Fe limits phytoplankton growth in HNLC oceans.

The first open-ocean Fe enrichment experiment (IronEx1- Martin, *et al.,* 1994) occurred in 1993, in the eastern equatorial Pacific Ocean, showing a "*clear unambiguous physiological response to the addition of Fe, resulted in the doubling of biomass, tripling of chl-a* [chlorophyll-a] - *and quadrupling primary productivity*". Unexpectedly, there was however, no observed NO_3 drawdown. Fe limitation of algae blooms in HNLC waters was further confirmed by Coale *et al*., (1996) (IronEx II), however the link between NO_3 uptake

and Fe was found to be contradictory; with nutrient measurements by Martin *et al*., (1994) indicating "*little or no systematic difference in nitrate"* while Coale *et al*., (1996) reported "*a strong drawdown of approximately 5 µM nitrate as the biological response developed*".

The success of these experiments, was followed by two small-scale Fe fertilisation experiments in the Southern Ocean (Boyd and Law, 2001; Pollard *et al*., 2007). Though both showed an increase in phytoplankton productivity in response to the addition of Fe (Chisholm *et al*., 2001), these experiments differ fundamentally. The Southern Ocean Iron Release Experiment (SOIREE) (Boyd and Law, 2001) was the first *in situ* Fe fertilization experiment in the Southern Ocean (1999), which showed an increase in chlorophyll and a 10% increase in CO_2 draw down. The Crozet Natural Iron Bloom and Export Experiment (CROZEX) (Pollard *et al*., 2007, 2009) differed in that it was the first planned natural Fe fertilization experiment, studying a natural Fe-enriched bloom off the Crozet Islands. These two studies are fundamentally important, as together they show an undeniable response, with increased chlorophyll and increased photosynthetic efficiency (Boyd and Abraham, 2001; Moore *et al*., 2007a, 2007b) in response to both artificial and natural Fe fertilization in the Southern Ocean.

On board Fe enrichment experiments, such as those run in the Ross Sea by Martin, (1990), and on *RRS Discovery* during CROZEX (Moore *et al*., 2007a, 2007b) and on *MV SA Agulhas* in the austral summer of 2010/11, allows phytoplankton responses to Fe and macronutrient additions to be carefully assessed.

1.7) Fe and light co-limitation in the Southern Ocean

The 'iron hypothesis' in the Southern Ocean, though strongly supported, is not sufficient to fully explain the dynamics of chlorophyll blooms that occur in this ocean. The

Southern Ocean, being so far South, and often under cloud cover is exposed to low yearly light. Additionally, the development of phytoplankton blooms increases light attenuation with depth, suggesting that light limitation becomes important in areas of deep MLD's, or near the bottom of the euphotic zone in stratified waters (Sunda and Huntsman, 1997). The co-limitation of Fe and light in the Southern Ocean was first proposed by Raven (1990), who anticipated that at low irradiances, the Fe requirement of phytoplankton would increase with the light-harvesting requirements (Boyd, 2002). This is due to the increased chlorophyll:carbon ratio needed to capture sufficient photons (Venables and Moore, 2010). This co-limitation was confirmed by Sunda and Huntsman, (1997), through culture experiments.

The variation of phytoplankton growth between night and day, highlights the importance of light (Hassler *et al.,* 2012). Using naturally Fe fertilized areas such as downstream of South Georgia, the Crozet and Kerguelen Islands as examples, Venables and Moore, (2010) conclude that although blooms in these areas only begin in spring when light is sufficient, they are not limited by light for the three months of summer.

Satellite imagery coupled with *in situ* measurements advocate that the Southern Ocean contains more phytoplankton then the available Fe can theoretically sustain, suggesting that Fe is recycled during bloom events. The development of small cells in Fe limited areas, and the resulting increased grazing by microzooplankton, is conducive to material and Fe recycling (Sunda and Huntsman, 1997). This yet unmeasured dynamic complicates the understanding of the Fe-light integration on phytoplankton (Strzepek *et al*., 2005; Hassler *et al.,* 2012).

Southern Ocean phytoplankton blooms are still poorly understood, doubtless due to the complex and dynamic interplay between Fe availability, chemistry (whether Fe is biologically available or not) and biology in surface waters (Raven, 1990; Boyd *et al.,* 1999; Boyd, 2002; Hassler *et al.,* 2012). However, as current climate projections involving the Southern Ocean predict warming, causing "*stratification and an alteration of the MLD*" (Sarmiento *et al*., 1998; Boyd, 2002). By contrast, MLD's in mid-latitude regions of the Southern Ocean appear to be deepening because of increased wind stress. These projections highlight the importance of understanding the effect of Fe-light limitation in phytoplankton photosynthetic processes in the Southern Ocean.

1.8) Understanding photosynthetic processes

Knowledge of photosynthetic processes in marine organisms provides an understanding of how they might respond to changes in the light environment they experience. Such interpretations are essential to understand the influence of community structure on global biogeochemical cycles in marine environments (Falkowski and Raven, 2007), and hence enhance predictions of possible changes in the future.

Photosynthesis is the process by which plants convert the sun's energy into chemical energy, which is stored as sugars or other organic molecules. Species of phytoplankton require these organic compounds for phytoplankton growth and reproduction, as well as cellular tissue. The simplified equation of photosynthesis shows the carbon fixation process:

$$CO_2 + 2H_2O \leftrightarrow [CH_2O] + H_2O + O_2$$

Photosynthesis is divided into two separate phases - the so-called 'light reactions' and the 'dark reactions'. In the 'light reactions', light is captured by plant pigments, notably by chl-a, a green pigment located in the chloroplasts. This 'light reaction' can be affected by light limitation as it converts solar energy into chemical energy in the form of ATP:

$$2H_2O + \text{light} \rightarrow 4[H^+] + ATP + O_2$$

It is this reaction that allows fast repetition rate fluorometry (FRRf) to be used as a measure of the photosynthetic efficiency of phytoplankton. In the 'dark reactions', the ATP is used to fix inorganic CO_2 within the Calvin Cycle (Campbell and Reece, 2005), synthesising the production of sugars.

$$4[H^+] + ATP + CO_2 \rightarrow CH_2O + H_2O$$

The effect of Fe limitation effects photosynthesis in two ways. Firstly, it is necessary in PS II and PS I. Secondarily, it is needed in NO_3 assimilation.

1.8.1) The effect of Fe on PS II and PS I

PS II and PS I are concerned with the light phase of photosynthesis. As the majority of cellular Fe is contained in PS II and PS I, this is heavily affected by Fe-limitation (figure 2).

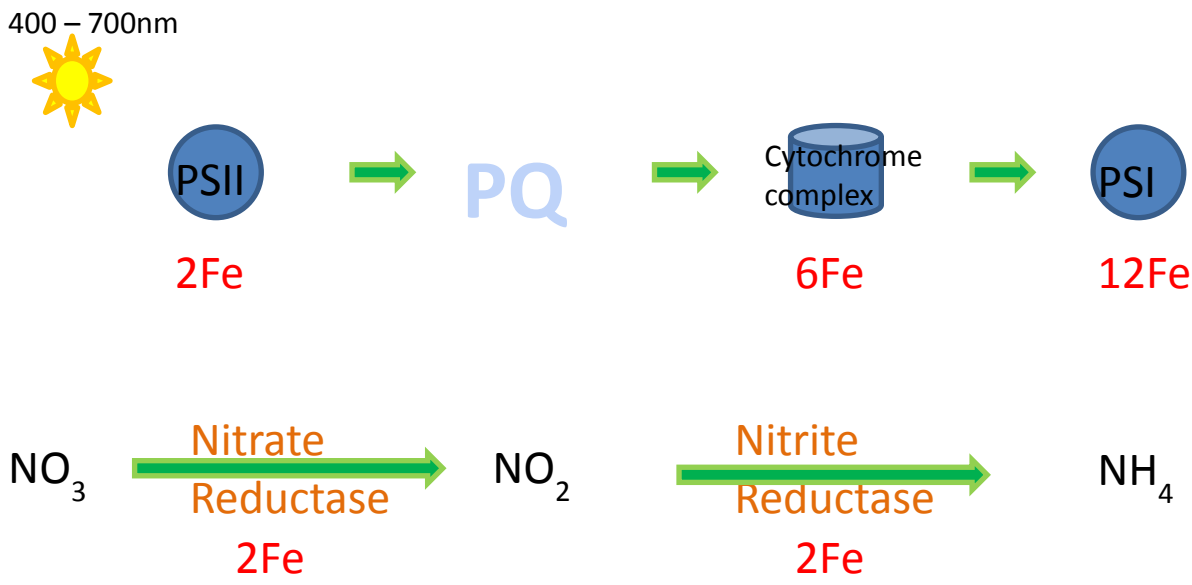

Figure 2: Light and Fe dependency of photosynthesis and NO_3 assimilation (Lucas, 2009).

Ultimately, light drives the synthesis of NADPH (Nicotinamide adenine dinucleotide phosphate) and ATP by energizing PS II and PS I, which are both found in the thylakoid membrane of chloroplasts. Non-cyclic flow is the primary pathway of energy transformation in light reactions (includes both PS's) and is shown in figure 3. This reaction begins with a light photon striking a pigment molecule in the light-harvesting complex of PS II. This photon is passed along the pigment molecules to the P680 chl-a molecule, exciting it's electrons to a higher energy state. The excited electron is both captured by the primary acceptor, and replaced in the P680 molecule by splitting a water (H_2O) molecule into oxygen (O_2) and two hydrogen ions. The excited electron is passed from PS II's primary accepter to PS I via an electron transfer chain consisting of the electron carrier plastoquinone (Pq), a cytochrome complex and a plastocyanin (Pc) protein. This transfer reduces the energy level of the electron, hence providing the energy needed for ATP synthesis. This electron replaces an electron captured from P700 by PS I's primary acceptor (P700 loses its electron through a pathway mirroring that of P680). Similarly, the new photoexcited electron moves down the second transport chain from PS I's primary acceptor through the ferredoxin (Fd) protein to be

one of the two electrons to connect with $NADP^+$ to form NADPH (Campbell and Reece, 2005).

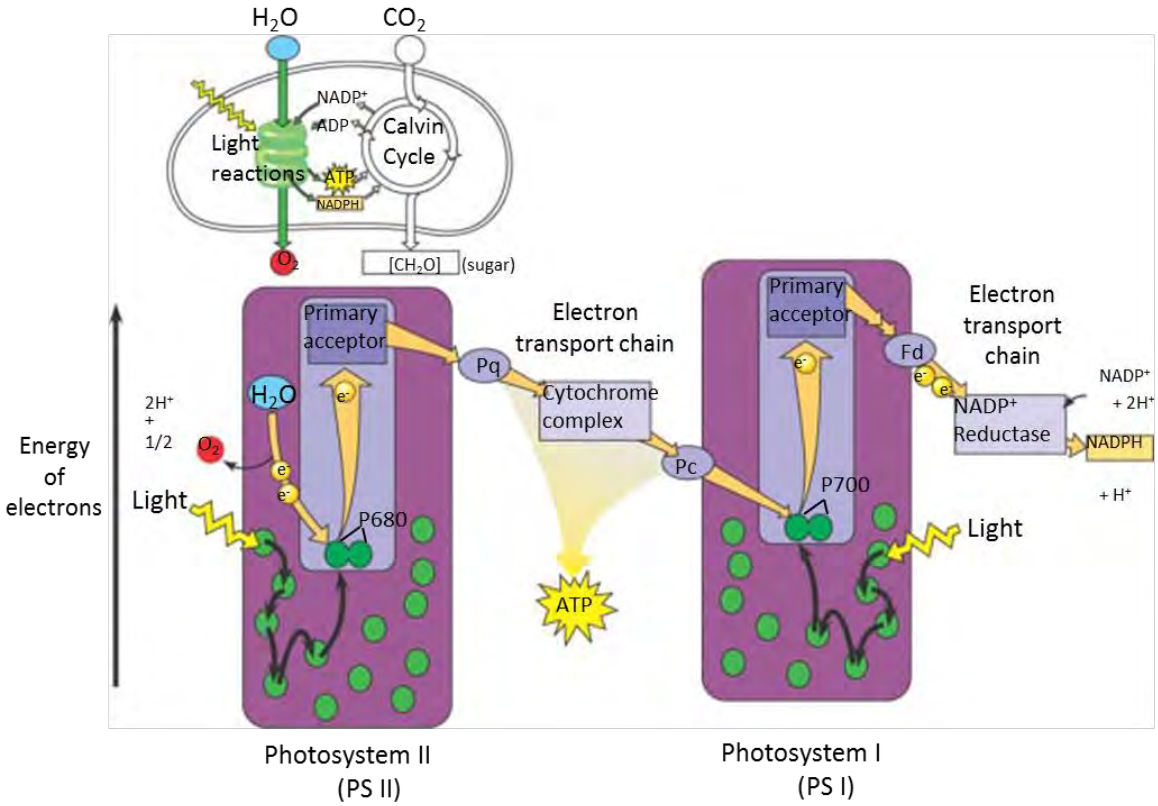

Figure 3: How noncyclic electrons flow during the light reaction that generates ATP and NADPH (Cambell and Reece, 2005).

The effect of Fe limitation on the photosynthetic apparatus means that not all available light can be used. When Fe deficient, phytoplankton not only decrease their absorption of light, but also dissipate (during the electron transfer chains) a large part of the light absorbed by the PS II antenna (Morales *et al.,* 1998).

1.8.2) The effect of Fe in nitrate assimilation

Fe is necessary in the enzymes involved in NO_3 reduction by plants (Raven, 1990; Sunda and Huntsman, 1997; Boyd *et al*., 1999; De Baar *et al*., 2005; Lucas *et al*., 2007) as seen in figure 2.

It has been estimated that 80% of Fe required by phytoplankton is used in photosynthesis (Raven *et al*., 1999). Fe is an essential element required in diverse metabolic pathways: Fe functions as a catalyst in electron transfer reactions, is needed in chlorophyll synthesis and is critically involved in the assimilation of nitrogen (the enzymes nitrate and nitrite reductase both contain Fe and are necessary to reduce NO_3 to ammonium (NH_4). These combined processes limit the photosynthetic yield under Fe limited conditions (Hassler *et al.,* 2012).

1.8.3) Fast Repetition Rate Fluorometry

FRRf allows one to investigate the photosynthetic efficiency of phytoplankton in terms of PS I and PS II's electron transport system, indirectly measuring the phytoplankton's ability to utilize CO_2 in carbon fixation during photosynthesis. Thus it measures changes in the basic photosynthetic processes, which can loosely be related to carbon fixation by phytoplankton.

Changes in photochemical reactions and photosynthetic parameters measured by FRRf have been widely used as a diagnostic tool for nutrient-related changes in photosynthetic efficiency (Kolber *et al.,* 1988; Kolber and Falkowski, 1993). The FRRf protocol allows the simultaneous assessment of the parameters in phase two (light reactions) of photosynthesis: i.e. σ_{PSII} (the functional absorption cross section) and F_v/F_m (photochemical efficiency, as described by the relationship between variable fluorescence [F_v] relative to the maximum theoretical fluorescence [F_m]) (Suggett *et al.,* 2009). This method uses active chl-a fluorescence measurements to evaluate the efficiency by which absorbed light is utilized during photosynthesis (Suggett *et al.,* 2009). Chl-a fluorescence is a

biophysical bi-product re-emitting light not utilized in photosynthesis (Suggett *et al.,* 2009), and so provides a measure of how efficient phytoplankton are at using light.

FRRf measurements are strongly dependent on prior light exposure, thus after a period of dark acclimation, PS II photochemical efficiency is at its maximum, as the quinones (the primary acceptor molecules of PS II) are then fully oxidised. Since the maximum photosynthetic efficiency of phytoplankton decreases under stressful growth conditions (Kolber *et al.,* 1988), this concept has led to the use of FRRf to assess the large-scale photosynthetic condition of entire photosynthetic communities (Behrenfeld *et al.,* 1996; Moore *et al.,* 2005, 2006; Suggett *et al.,* 2006). High values of F_v/F_m and corresponding low values of σ_{PSII} indicate a high photosynthetic efficiency, whereas the inverse indicates that phytoplankton are experiencing physiological stress (Holeton *et. al.,* 2005; Suggett *et al*., 2006).

Variability of these parameters has in the past been attributed to two very different controls; the first being NO_3 or Fe stress (Kolber *et al.,* 1988; Greene *et al.,* 1991; Boyd and Abraham, 2001), and the second being the species composition of phytoplankton (Suggett *et al.,* 2004, 2009; Moore *et al.,* 2005). The high macronutrient concentrations found within the Southern Ocean (Levitus *et al.,* 1993) makes the direct effect of NO_3 limitation in this region obsolete. However, as Fe is required for the efficient uptake and utilization of NO_3, in Fe limited seas, Fe limitation can directly influence photosynthetic efficiency.

1.9) Community structure

Southern Ocean phytoplankton communities are mostly dominated by diatoms and haptophytes, frequently *Phaeocystis antarctica* (Boyd, 2002; Hassler *et al.,* 2012). Diatoms dominate mainly near frontal zones (Sakshaug *et al*., 1991; Laubscher *et al*., 1993; Smetacek *et al*., 1997) corresponding with relatively higher Fe concentrations found in these zones (Laubscher *et al*., 1993; de Baar *et al*., 1995; Boyd, 2002). There is contradictory information regarding the seasonal shifts in diatom-*Phaeocystis* community structure. In the Ross Sea, haptophytes are particularly noticeable during spring (Arrigo *et al*., 1999) as *Phaeocystis antarctica*'s photo-physiology is efficient at low irradiance (Boyd, 2002), thus allowing these blooms to appear before those of diatoms. However, off sub Antarctic islands such as Crozet, a spring diatom dominated community is succeeded by smaller taxa in summer as Fe concentrations decline (de Baar and Boyd, 2000; Smetacek *et al.,* 2004; Seeyave *et al.,* 2007).

Limiting nutrient concentrations have a profound effect on the community structure of phytoplankton. Small phytoplankton thrive in Fe-limiting areas because their lower surface:volume ratio allows Fe to be scavenged at low concentrations. Even so, different phytoplankton taxa have various Fe requirements and are known to adapt to environmental changes (Strzepek *et al.,* 2011; Hassler *et al.,* 2012), for example, when facing depleting Fe conditions, diatoms shrink in size (Sunda and Huntsman, 1995). Modification of the light-harvesting antenna can also occur to maximize light photosynthetic efficiency (Michel and Pistorius, 2004). And as a balance between Fe and light efficiency, a decrease in pigment concentration can occur in low Fe conditions (Timmermans *et al.,* 2001).

A dominance by small phytoplankton classes is suggested (Price *et al.,* 1994) to indicate an Fe-limited ecosystem further controlled by microzooplankton grazers. Conversely, Fe alleviation promotes a disproportionate response from larger phytoplankton that can also escape the pressures of grazing (Cullen, 1991; Morel *et al*., 1991; Price *et al*., 1994; Hoffmann *et al.,* 2006; Moore *at al.,* 2007a).

"*Diatoms appear to be primarily limited by iron supply, because in virtually all iron enrichments there has been a floristic shift toward this algal group*" (de Baar and Boyd, 2000). This is further confirmed in a Pacific Ocean study by Coale *et al.,* (1996), where Fe enrichment favoured diatom production and a corresponding draw down of NO_3 and silicate (SiO_4). The response of *Phaeocystis antarctica* to Fe fertilization is however unknown (Boyd, 2002), although it may encourage colony formation (Lucas *et al.,* 2007).

As few Fe enrichment experiments have been carried out in relation to the vast expanse of the Southern Ocean, let alone the world's oceans, current knowledge on different community responses to Fe alleviation is relatively sparse. Moore *et al.,* (2007a) stated that the outcome of Fe alleviation experiments was strongly influenced by the initial community structure.

1.10) Rational for this investigation

FRRf allows one to investigate the photosynthetic efficiency of phytoplankton in terms of PS I and II's electron transport system, indirectly measuring the phytoplankton's ability to fix CO_2 during photosynthesis. Thus it allows measurement of changes in the basic

photosynthetic responses to light and Fe co-limitation and hence indirectly, assess the carbon fixation potential.

1.11) Research hypotheses:

The research carried out in this study strives to test three principal hypotheses:

1) The photosynthetic efficiency of phytoplankton within the Southern Ocean will increase with the addition of Fe. However, the degree to which it increases will differ, depending on the area within the Southern Ocean.

2) The nutrient uptake and chl-concentrations of phytoplankton within the Southern Ocean will increase with the addition of Fe. However, the degree to which it increases will differ, depending on the area within the Southern Ocean.

3) The response of phytoplankton in the Southern Ocean to Fe-fertilization is depended on the initial community structure.

CHAPTER 2: METHODS

2.1) General

All fieldwork was carried out on the South African polar resupply vessel, *MV SA Agulhas*. Data were collected over two summer cruises in 2009/10 and again in 2010/11. The first cruise occurred between Acta Bukta (Antarctica) and South Georgia (figure 4).

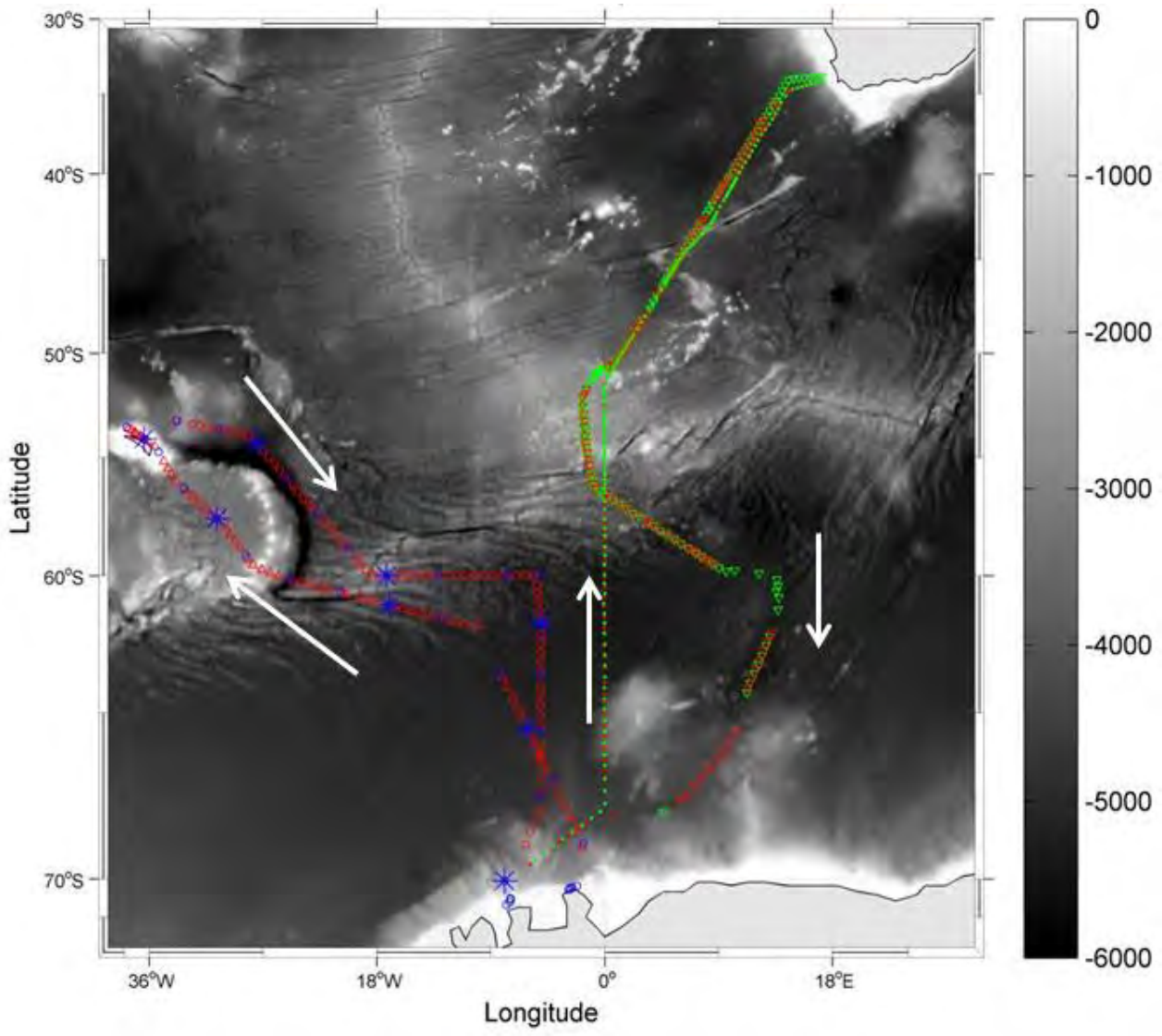

Figure 4: Chart of the research area occupied during SANAE 49 in the austral summer of 2009/10. The following stations appear on the map; CTD (blue), productivity CTD stations (blue *), underway UCTD stations (red) and XBT stations (green). Legs are divided into southward (**∇**), north westward (Δ), south eastward (○) and northward (•). Background map data and script courtesy of Wessel and Smith (1996).

This cruise (AGU 148) was part of the SANAE (South African National Antarctica Expedition) 49 cruise from December - February, 2009/10. The cruise consisted of a Southward leg from Cape Town, South Africa to Acta Bukta, Antarctica (9 December - 22 December), a north westward leg from Acta Bukta to South Georgia (16 - 4 January) and back (25 January - 2 February), followed by a return journey to Cape Town (13 - 23 February).

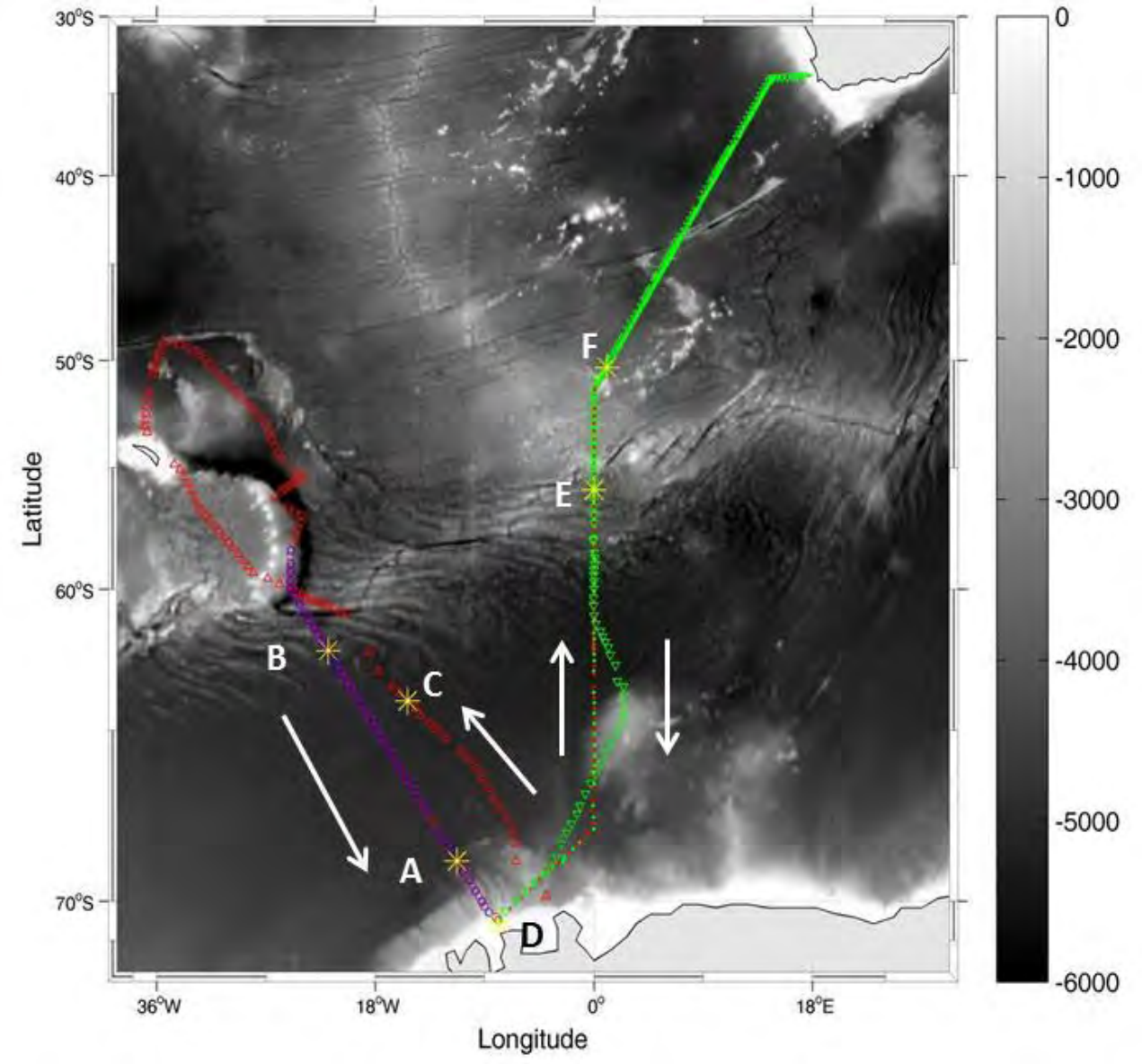

Figure 5: Chart of the research area occupied during SANAE 50 in the austral summer of 2010/11. With sites of the CTD (blue), underway UCTD (red) and XBT stations (green) marked on the map. Fe enrichment experiments are labelled and appear in (yellow *). Legs are divided into, into southward (∇), north westward (Δ), south eastward (○) and northward (•). Background map data and script courtesy of Wessel and Smith (1996).

The second cruise (AGU 153) was part of the SANAE 50 cruise from December 2010 - February 2011 (figure 5). This cruise consisted of four legs: a southward leg from Cape Town to Acta Bukta (8 - 19 December), a north westward leg from Acta Bukta to South Georgia **(**1 January - 10 January), a south eastward Leg from South Georgia to Akta Bukta (10 January - 20 January) and the Northward Good-hope line (5 February - 16 February), from Acta Bukta to Cape Town, South Africa.

2.2) *In situ* measurements and sample collection

2.2.1) In situ measurements and sample collection: SANAE 49

On the north westward and south eastward legs of SANAE 49, CTD (conductivity, temperature and [pressure] depth) profiles were conducted (using a Sea-Bird 911+ CTD) every day at 09:00 and at 21:00 for water column sampling to 500m. Water was collected for chemical and biological analysis on the upward cast using 6 x 12 litre Niskin bottles. Two *in situ* samples from the clean seawater inflow to the engine room were collected in-between each CTD cast. A Sippican Deep Blue Expendable Bathythermograph (XBT) and UCTD (underway CTD; produced by Ocean Science) were alternatively deployed every hour (at ~10nm intervals), with XBT deployments increasing to every hour (run concurrently with the UCTD) over main frontal and topographical features. Neither instrument could be used during sea ice conditions. The use of the XBT's formed part of the long term GoodHope program (funded NOAA's Office of Global Programs as part of their High Density XBT project at NOAA/AOML).

On the Northward leg of SANAE 49, *in situ* sampling occurred for chemical and biological analysis every four hours. Physical data were collected by alternate UCTD and

XBT's every hour, except over fronts where an XBT was also discharged concurrently with the UCTD.

On SANAE 49's Southward leg, *in situ* sampling or chemical and biological analysis took place every four hours.

2.2.2) In situ measurements and sample collection: SANAE 50

On SANAE 50, the sampling strategy varied greatly depending on the leg.

The north westward leg consisted of underway stations only. Biological and UCTD stations occurred every 40nm and 20nm respectively. Between 69º S - 71º S and around 62º S, UCTD deployments were interrupted by sea ice, while over the South Georgia shelf UCTD deployments ceased due to the shallow bathymetry.

The south eastward leg was divided into two sampling strategies. The first half of this leg consisted of underway stations and second half (from 58.5º S) consisted of CTD stations. For the CTD leg, CTD's were spaced 20nm apart with UCTDs deployed between each CTD station. CTDs sampled the water column to 500m, sampling a maximum of 13 depths. Water was collected during the upwards cast of the CTD with full biological and chemical sampling occurring at each CTD. Course changes seen south of 55º S were due to poor weather conditions.

For the northward leg, XBT and UCTD deployments were alternated and occurred every 10nm, increasing to every 5nm over main frontal regions. Biological stations occurred every 40nm, except over fronts where the resolution increased to 20nm. Due to winch

problems, UCTD measurements were only conducted to 50º S, after which XBT's replaced the use of UCTD's in this region.

2.2.3) Biological stations

All biological stations included samples for chl-a, High Performance Low Chromatography (HPLC), FRRf and nutrients.

Underway

Underway Biological: SANAE 49

Discrete underway biological samples on SANAE 49 were collected from the engine room clean water supply pump (approximately 5m below the ocean surface). These water samples were analysed for chl-a, HPLC and nutrients.

Underway Biological: SANAE 50

Water for discrete underway biological samples on SANAE 50 was collected from an uncontaminated surface sea water supply using the towed Fe-fish (approximately 1 -5m below the ocean surface, depending on swell conditions). When ice and bad weather prevented deployment of the Fe-fish, samples were collected from the clean engine room supply.

Sample variables from the two water sources were compared to see if there were any statistical differences. For chl-a there was no statistical difference, but there was however a

statistical difference between FRRf results. Thus, when the Fe-fish could not be deployed, FRRf samples were obtained from bucket samples, with no statistical difference from the Fe-fish supply.

Underway biological samples for SANAE 50 were analysed for chl-a, HPLC, and FRRf and nutrients. Nutrients sampled at night were filtered and frozen for analysis the following day.

CTD

CTD Biological: SANAE 49

Biological CTD stations consisted of the top 6 depths collected in the Niskin bottles. These depths included surface, thermocline and chl-a max depth determined on the downward cast. All biological depths were analysed for chl-a, FRRf and HPLC.

CTD Biological SANAE 50

The SANAE 50 CTD biological stations consisted of the top 6 depths collected in the Niskin bottles as before. These depths included surface, thermocline and chl-a max (top and bottom), as well as additional depths below the euphotic layer. All biological depths were analysed for chl-a, FRRf and HPLC.

2.3) On-deck Fe-light enrichment experiments

2.3.1) Setting up enrichment experiments

Six on-board Fe light incubation experiments were carried out during SANAE 50 (for positions see table 3, under results) to test phytoplankton responses to Fe and light. Experiment 8 and 9 were cut after day 3 and 2 respectively after the sea water supply cooling the incubations was compromised.

For each experiment, 13 x 2L clean, uncontaminated polycarbonate bottles were randomly filled in the Fe-free tent with water obtained from the towed Fe-fish). Six of these bottles were spiked with 100µl of 2µmol $FeSO_4$ (iron sulphate), while a further six were not spiked with Fe, so were control bottles. Three of the Fe spiked bottles and three of the controls were covered with a neutral density filter to provide 50% shading. A final (13^{th}) bottle was filled with seawater, without any Fe supplement, and not reopened until day 5 of the experiment. This acted as a control to test for long-term contamination during sub-sampling.

All bottles were placed in an on-deck incubator covered in 50% neutral density filter and cooled by running surface (5m) seawater. Thus, on-deck incubations were performed for 5 days at two different irradiances as six bottles were exposed to 50% light and six bottles to ~25% light.

2.3.2) Sampling enrichment experiments

Every 24 hours, water was removed from 12 bottles for chl-a, nutrient and FRRf determinations. Samples for nutrient analysis were filtered, frozen and analysed back in Cape Town for NO_3, SiO_4 and phosphate (PO_4). Triplicate samples were taken for time zero chl-a and FRRf analysis. Sub-sampling of the incubations occurred between midnight and dawn to avoid light-shock.

Chl-a and FRRf samples were analysed immediately using the methods described later. As the incubation stations were set up concurrently with full biological stations, the starts of each experiment corresponded with HPLC, chl-a, nutrient and FRRf measurements taken from the CTD bottles.

2.4) Analytical methods

2.4.1) Water masses determined from CTD-profiles

The SeaBird 911plus CTD sensors measured temperature and salinity with each cast. Using Ocean Data View (2008), water densities were determined to establish water mass characteristics based on T-S (temperature - salinity) plots (see Appendix A). Water masses were determined according to Park *et al.,* (1998), Orsi *et al.,* (1995) and Veth *et al.,* (1997).

The CTD's auxiliary sensors also included a SBE 43 dissolved oxygen and underwater PAR (photosynthetically active radiation) sensor. Dissolved oxygen was calibrated against water samples from selected depths from the CTD casts. These samples were run on a SiS Sensoren Instrumente automated dissolved oxygen system following the

Winkler method for dissolved oxygen measurements in discrete water samples (Carpenter, 1965) and in accordance with World Ocean Circulation Experiment (WOCE) standards.

2.4.2) Phytoplankton photo-physiology (FRRf)

A bench top Satlantic FIRe (**F**luorescence, **I**nduction and **R**elaxation) System was used in discrete mode to measure a comprehensive suite of fluorescence parameters (F_v/F_m and σ_{PSII}). These photosynthetic physiological parameters can be used to provide highly sensitive and well-resolved data on phytoplankton community responses to light and nutrients. The system is well described in the Satlantic manual, and in several publications (e.g. Kolber *et al.,* 1998).

The paramenters used specifically in this study are: F_v/F_m and $\sigma_{PSII.}$ F_v/F_m represents the photochemical efficiency. This looks at the relationship between the variable fluorescence (F_v) and the maximum theoretical fluorescence (F_m). Calculations for F_v/F_m are as follows:

$F_v/F_m = (F_m-F_o)/F_m$

Where: F_v = variable fluorescence

F_m = Maximum theoretical fluorescence

F_o = minimum fluorescence yield

σ_{PSII} represents the functional absorption cross section, and is calculated as the slope between F_o and $F_{m.}$ Figure 6 is an example of the FIRe measurement protocol, showing the mathematical position so of above mentioned parameters.

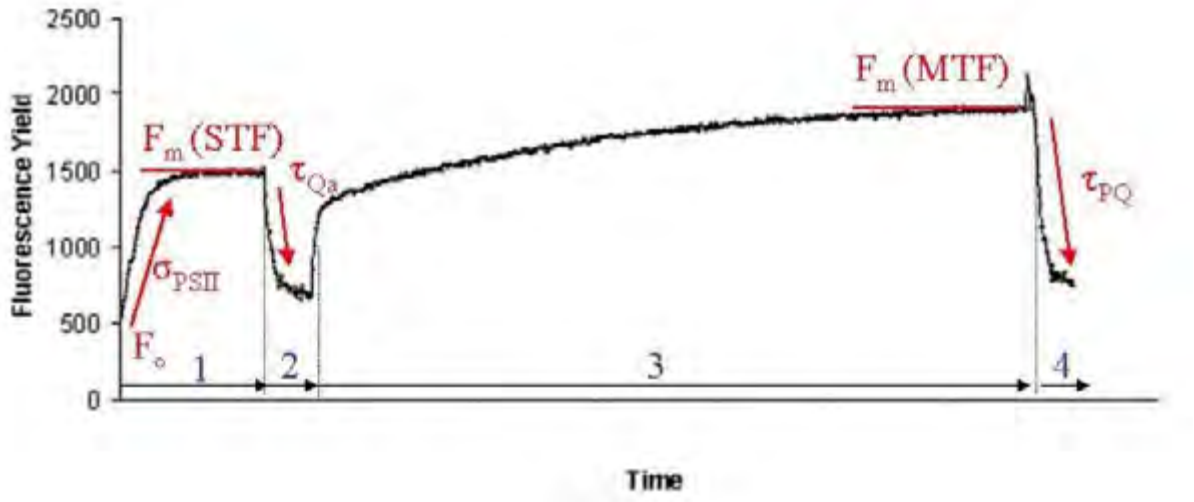

Figure 6: An example of the FIRe measurement protocol (Satlantic, 2010)

Each sample for FRRf measurements was collected in a clean dark plastic bottle and placed in a dark environment for half an hour prior to FRRf measurements in the FRRf cuvette (Behrenfeld *et al.,* 1996; Moore *et al.,* 2005, 2006; Suggett *et al.,* 2006). Just prior to placing the sample in the cuvette, the sample was inverted to ensure an even distribution of phytoplankton in each sample. These procedures ensured completion of the photosynthetic cycle at the time of collection so as not to interfere with the FRRf readings. The FRRf readings were also conducted in minimum light conditions to reduce outside light interference.

The Satlantic FIRe instrument was set at the following settings for each site:

Number of automatic samples: 16 (for SANAE 49) or 25 (for SANAE 50)

LSTF 100, STRP 60, STRI 60, MTF 600, MTRP 60, MTRI 100.

Values of F_v/F_m and σ_{PSII} were calculated by fitting a best-fit line to the measured saturation curves and by running the results through a MATLAB (MATrix LABoratory

R2008a) script code (see Appendix B) to remove the first measured value, as required by the bench top Satlantic FIRe Systems calibration procedure. The script used (courtesy of Dr Brian Hopkinson) was validated against the one used by Dr Mark Moore (Appendix C) during CROZEX (Moore *et al.,* 2007b). A comparison of the two scripts confirmed that interpretations were independent of model choice. Any values above 10% error levels were removed from the data set.

Blanks were run (at the gain setting of that station) for each site to be included in the photosynthesis parameter calculations. These were done by filtering a fraction of each sample under positive pressure through a 25mm Whatman glass fibre filter (GF/F) to remove all biological material, and the filtrate was then run through the Satlantic FIRe System at the same settings as its corresponding sample. Blanks were run both on board (SANAE 50 only) as well as back at the University of Cape Town (UCT) (SANAE 49 and SANAE 50). Sample fluorescence values were corrected for the blank values in MATLAB (Appendix B).

SANAE 49 Sampling

For the SANAE 49 cruise, water samples from the top six CTD depths were collected to measure active phytoplankton community fluorescence through the water column. At each depth, nine replicate samples were run on the FIRe instrument.

SANAE 50 sampling

CTD

For the SANAE 50 cruise, water samples from the top six CTD depths were run as above. At each depth, three replicates samples were run on the FIRe instrument. The reason for the difference in number of replicates between SANAE 49 and SANAE 50 was time constraints. The large number of samples required to be run in the experimental stage of SANAE 50, the time it took, and available personnel, lead to the decrease in the number of replicates on SANAE 50 compared to SANAE 49.

Underway

In situ FRRf samples were taken as part of the biological sampling, every four hours. As for biological samples, water was collected from the uncontaminated surface Fe-fish supply. When, however, the Fe-fish could not be deployed, the FRRf sample was collected with bucket samples. Due to time and personnel constraints during the incubations, the FRRf 4am sample was not run. This corresponded with the biological station that did not include a Fe sample. At each station, three replicates samples were run on the FIRe instrument.

Fe Incubations

At the beginning of each Fe-incubation, three replicate samples were run on the FIRe instrument. Once the incubations were running, the sub sampling saw that one sample was run from each bottle, with a corresponding blank.

Background Statistical check

For the biological station data, a brief comparison between the F_v/F_m and σ_{PSII} parameters and the time of day was run to see if the phytoplankton where being negatively affected by radiation through photo-inhibition. It was found that the time of day did not influence the F_v/F_m and σ_{PSII} parameters.

2.4.3) Nutrients

Nutrients were analysed in two different ways on the two cruises. On SANAE 49 the nutrients were analysed manually, while on SANAE 50 they were analysed automatically.

SANAE 49: Manual analysis of nutrients

Samples for analysis of inorganic nutrients were drawn from Niskin bottles from all depths sampled and analysed immediately. Concentrations of SiO_4, PO_4, NO_3, NH_4 and urea were analysed according to manual methods described in Grasshoff *et al.,* (1983) and Parsons *et al.,* (1984), scaled to 5 ml sample sizes.

Problems encountered with silicate on SANAE 49

Frozen back-up SiO_4 samples were re-run back at the UCT, using the automatic method after the manually run samples were found to be far too high. This occurred only for SiO_4 samples in very low SiO_4 regions, such as north of the Subtropical Front (STF).

Problems encountered with phosphate on SANAE 49

Manual analysis of PO_4 is run with a concurrent analysis of a standard solution. On SANAE 49, the originally standard solution of PO_4 was double the concentration that it was required to be. Due to the high concentration of this standard, and the sensitivity range of the test, one could not simple half the results of the standard. The standard is used in the calculation of the sample. Thus, to gain the true PO_4 value from the samples, a correction needed to be applied. This was corrected by using the average corrected standard (0.92 $\mu mol.L^{-1}$) from SANAE 48, the previous annual cruise run at the same time, using the same methods, through the same waters.

Problems encountered with nitrate on SANAE 49

On the Northward Leg, after 65.8º S, the ammonium chloride (used as a buffer for the cadmium column after it is repacked [Mostert, 1983]) ran out, although samples were still run. A comparison between SANAE 48 and SANAE 49 NO_3 and PO_4 data as well as the NO_3:PO_4 ratio (Appendix D) revealed that the exclusion of ammonium chloride in the method made a substantial difference (the greatest difference between the two years, at the same latitudes, reaching 20 $\mu mol\ l^{-1}$). This difference was not initially picked up by the standard, due to the difference in pH between the fresh water standard and sea water samples. See Appendix D [a]) for the NO_3 readings. An attempt was made to rebuild the NO_3 data using the combined SANAE 48 and 49 NO_3:PO_4 ratio ($y = 0.0634x + 0.2041$, Appendix E). As the analysis of NO_3 is salt sensitive, this data had to be corrected using the above mentioned ratio. The combination of this correction and the PO_4 correction does undermine the quality of this data set.

SANAE 50: Automated nutrient analysis

The Lachat QuikChem 8500 series 2 Flow Injection Autoanalyzer was used to measure NO_3 and SiO_4 concentrations on SANAE 50. However PO_4 was still determined manually according to the method described in Grasshoff *et al.,* (1983) and Parsons *et al.,* (1984).

All nutrient samples were measured during the day. Hence samples taken during the day were analysed that same day, but nutrient samples collected at night were filtered and frozen to be analysed a few days later.

All incubation nutrient samples were filtered (through Whatman GF/F), frozen, and analysed at the UCT after the cruise. Unfortunately this process renders the SiO_4 analyses suspect at best, or simply invalid.

The differences in the time lines between the underway and incubation nutrient analysis was due to an unfortunate and frustrating set of personnel, political and funding events, both on the ship and on the land. It is understood that the delay in analysis of the incubation nutrient samples compromises this data sets quality (see appendix J).

2.4.4) Chlorophyll-a

Chl-a concentrations were determined for the top six CTD depths and for the *in situ* underway biological samples. Chl-a samples were collected by vacuum filtering 250 ml of seawater through 25 mm Whatman GF/F filters to trap phytoplankton cells. Chl-a pigment

was extracted from the filter with 7 ml (SANAE 49) or 8 ml (SANAE 50) of 90% acetone over a 12 - 24 hour period a dark fridge. Samples were then read on a Turner Designs Trilogy fluorometer that was calibrated with chl-a standards (Sigma, UK) before the voyage. The sample chl-a concentration ($\mu g.l^{-1}$) was derived using the calibration curve regression.

2.4.5) Community structure: (HPLC)

For both SANAE 49 and SANAE 50, community composition was estimated from diagnostic pigment composition and the pigment ratios measured using HPLC for both CTD and *in situ* underway samples. For HPLC analysis, water samples of 1 - 2 L (depending on particulate loads), were filtered under positive pressure through 25 mm Whatman GF/F filters to capture phytoplankton. These filters were then stored immediately in liquid nitrogen.

Post-cruise, HPLC samples were stored in a -80ºC freezer. HPLC analyses were conducted at the National Oceanography Centre (NOC), Southampton. Phytoplankton cells were raptured in 90% acetone in a Sonics & Materials Inc. Vibracell sonicator (run for 30 s). Pigments were extracted by centrifugation using a MSE Mistral 1000. After filtering through a 0.2 µm filter, sample pigments were analysed on a thermo separation product following the protocol of Gibbs as described by Barlow *et al.,* (1997). This involves pigment separation through a 3 µm Hypersil MOS2 C8 column, followed by detection by absorbance and identification by retention time and online diode array spectroscopy.

Analysis of raw pigment signatures was done using ChromQuest 4.1 software. Pigment information was to characterise phytoplankton species, described by Wright and Jeffery (2006) and Jeffery *et al.,* (1997) (see Appendix F). For each species, the average

percentage of occurrence in the population was determined. Only species that occurred on average in more than 5% of the population were included in this study.

2.4.7) Physics

UCTD and XBT's

XBT's and UCTD's produce salinity and temperature profiles and were used on the cruise to determine frontal positions. UCTD data were processed using SeaBird Seasoft, and validated against CTD measurements.

CTD's

CTD measurements included a SBE 43 Dissolved Oxygen Sensor, a fluorometer, an underwater PAR unit and a surface reference PAR sensor.

Underway PAR

The underway PAR sensor was mounted on the port side of the ships 'monkey island' and provided incoming irradiance measurements (every 30 seconds). Average PAR for each experiment was calculated using standard statistical methods (average = sum of irradiance for full experiment/number of observations). This was to calculate the full irradiance available per experiment.

2.4.8) Nitrogen uptake and f-ratio

To provide a measure of nitrogen and carbon export, the f-ratio (nitrate uptake /total nitrogen uptake [ρNO_3/Total ρN]) was calculated for the surface waters using stable isotope ^{15}N uptake techniques (see Dugdale and Goering, 1967 and Lucas *et al.,* 2007). Under appropriate time and space scales, the f-ratio represents the fraction of primary production (as PON [particulate organic carbon]), fuelled by NO_3, that is potentially exported to the deep ocean through the sinking of phytoplankton particles. This can be translated into carbon (POC) export if the canonical Redfield Ratio of 6:1 (C:N) is adopted (Redfield, 1963). Uptake measurements were made at eight stations during the SANAE 49 cruise (Figure 4).

Underwater irradiance and sample depths

At each of the eight CTD stations, water samples were collected at the following light depths: 86%, 47%, 15%, 6%, 3.5% and 0.7% surface irradiance. These light depths where calculated using an underwater PAR sensor on the downward cast of the CTD. After converting PAR values into natural log values, the following equation was used to determine the depth for each sample:

$w = (-1/k) \times \ln(LD/100)$

where: k= the slope of the natural log of PAR vs. depth

LD=light depth (%)

W=depth which represents that light percentage (m)

The linear nature between PAR and depth plots within the Southern Ocean allowed k to be calculated as described above.

Sea-water samples from each depth were decanted into 3 x 1.0 L polycarbonate bottles. To measure simultaneous ρNO_3 and carbon fixation, one bottle from each depth was spiked with $^{15}N\text{-}NO_3$ (1 µmol $K^{15}NO_3$ / 100 µl) and with ^{13}C (49.4 µmol / 100µl). To separate bottles at each depth, NH_4 (0.1 µmol $^{15}NH_4Cl$ / 100 µl) and urea spikes (0.1 µmol CO $(^{15}NH_2)_2$ /100 µl) were also added at ~10% of ambient concentrations to avoid stimulating production.

After spiking, the bottles were placed in simulated *in situ* on-deck incubators for 24 hours, which were shaded to the appropriate light depth with neutral density filters, and cooled to ambient sea surface temperatures with running seawater.

At the end of the incubations, all samples were filtered onto pre-ashed Whatman GF/F filters (25 mm) and stored frozen prior to being run on UCT's Thermo Finnegan Mass Spectrometer in the Archaeometry Department. Calculation of uptake rates followed the protocol of Dugdale and Goering (1967), as well as Lucas *et al.,* (2007).

As calculation of update rates (and thus f-ratios) are strongly dependent on accurate nutrient measurements. A sensitivity study was undertaken, this sensitivity study looked at what changes would occur to the f-ratio if there was a 10% variation in the NO_3 data. Results of this study can be found under section 3.1.4.2.

2.5) Statistical analyses

2.5.1) Statistical analyses of the controls on FRRf parameters

To determine any factors that could be controlling the F_v/F_m and σ_{PSII} values (code in Appendix G), linear regressions between variables were run using the programme R (version 2.14.0, 2011). A comparison between the f-ratio, F_v/F_m and σ_{PSII} allowed one to search for a relationship between the photosynthetic "health" (F_v/F_m and σ_{PSII}) and carbon export to the deep ocean (f-ratio), based on the premise that healthy Fe-replete diatoms are likely to assimilate significant amounts of NO_3, as reflected in a high f-ratio (Lucas *et al.,* 2007).

2.5.2) Statistical analysis of results from Fe incubations experiments

For the Fe enrichment experiments, a paired-sampled t-test was conducted to separately compare the F_v/F_m, σ_{PSII} and chl-a, values under the following conditions:

1) The control bottles and the Fe addition bottles at 50% light levels
2) The control bottles and the Fe addition bottles at 25% light levels
3) The control bottles at 50% light levels and 25% light levels
4) The Fe addition bottles at 50% light levels and 25% light levels
5) All the control bottles and all the Fe addition bottles
6) The contamination control bottle and the control bottle at 50% light level (this was only done for experiments: B, C and D).

This was done in Microsoft Excel (2010) to calculate any significant difference between the two light levels, for the Fe alleviated bottles and the controls.

CHAPTER 3: RESULTS

SECTION 1: Observational Results

3.1.1) Antarctic Sea Ice Data

Table 1: A comparison of the total sea Antarctic sea ice area for the duration of the SANAE 49 and SANAE 50 cruises (NSIDC, 2012)

	Antarctic Sea Ice Area (million square km)	
	SANAE 49: 2009/2010	SANAE 50: 2010/2011
December	6.9	6.7
January	3.2	2.9
February	2	1.8

Table 1 reveals that the area covered by sea ice was greater for the full three months duration of the SANAE 49 (2009/10 cruise) compared to SANAE 50 (2010/11).

3.1.2) Water masses

The temperature sections (figures 7, 8) from the north westward legs of both SANAE 49 and SANAE 50, between Antarctica and South Georgia (see figure 4), show evidence of a subsurface temperature minimum layer. This Winter Water (WW) is cold, fresh and oxygen rich (Park *et al.,* 1998). There is a strong thermocline dividing this water from the Antarctic Surface Water (AASW) and Upper Circumpolar Deep Water (UCDW). The UCDW and Lower Circumpolar Deep Water (LCDW) is distinguished by salinity differences, with UCDW having low salinity water found between densities of 27.35 kg m^{-3} – 27.75 kg m^{-3}, while the younger, LCDW has low salinity water with a density above 27.75 kg m^{-3} (Veth *et al.,* 1997).

On the north westward leg of SANAE 49 (figure 7), the southern boundary of the Antarctic Circumpolar Current (SBdy) is positioned at 60.45º S, with the Southern Antarctic Circumpolar Current Front (SACCF) at 57.97º S. On the south eastward leg, the SBdy and SACCF shifted to 58.8º S and 58.97º S respectively. On SANAE 50 the SBdy and SACCF, although less distinct, were placed at 56.7º S or 57.3º S and 50.17º S on the south eastward leg respectively.

MLD is deeper for the south eastward legs than the north westward legs of both SANAE 49 and 50. This is specifically noticeable south of the SBdy (figures 7 and 8).

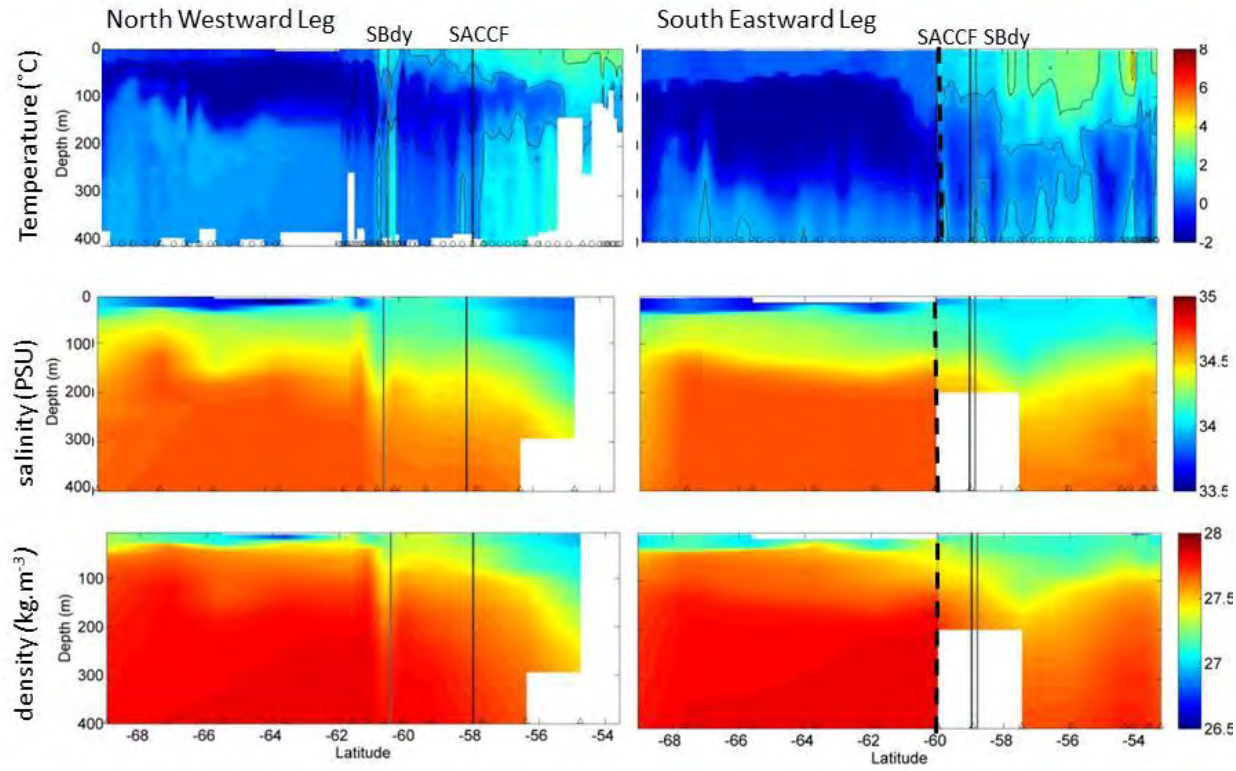

Figure 7: Vertical Temperature (˚C) salinity (PSU) and density (kg m^{-3}) sections on the north westward (left) and south eastward (right) legs of SANAE 49. The positions of the SBdy and the SACCF are shown with a grey and black lines respectively. The dotted black line at 60˚S on SANAE 49's south eastward leg represents more than one CTD deployment at that latitude (see figure 4). CTD and UCTD stations are marked with a triangle and circle respectively.

Any discontinuity seen in the plots around 60º S on the south eastward leg of SANAE 49 (figure 7) were due to numerous CTD's been conducted at one latitude (different

longitudes). This was due to an unfortunate set of weather conditions which forced the ship to follow this particular route (see figure 4).

The northward legs, from Antarctica to Cape Town, show little variability between the two years (figure 9). The presence of WW is still evident close to Antarctica, with waters warming as one approached South Africa. The presence of Agulhas Rings south of South Africa is evident during SANAE 50's northward leg south of the Southern STF (figure 9). During SANAE 50, the Northern STF (39.33º S), Southern STF (40.56º S), Subantarctic Front (SAF) (44.01º S), Antarctic Polar Front (APF) (49.36º S), SACCF (53.22º S), SBdy (55.41º S) of the Antarctic Circumpolar Current (ACC) fronts were clearly present at the latitudes indicated. During SANAE 49, the fronts were positioned as follows: Southern STF (41.59º S), SAF (43.96º S), APF (50.08º S), SACCF (53.39º S) and SBdy (55.62º S).

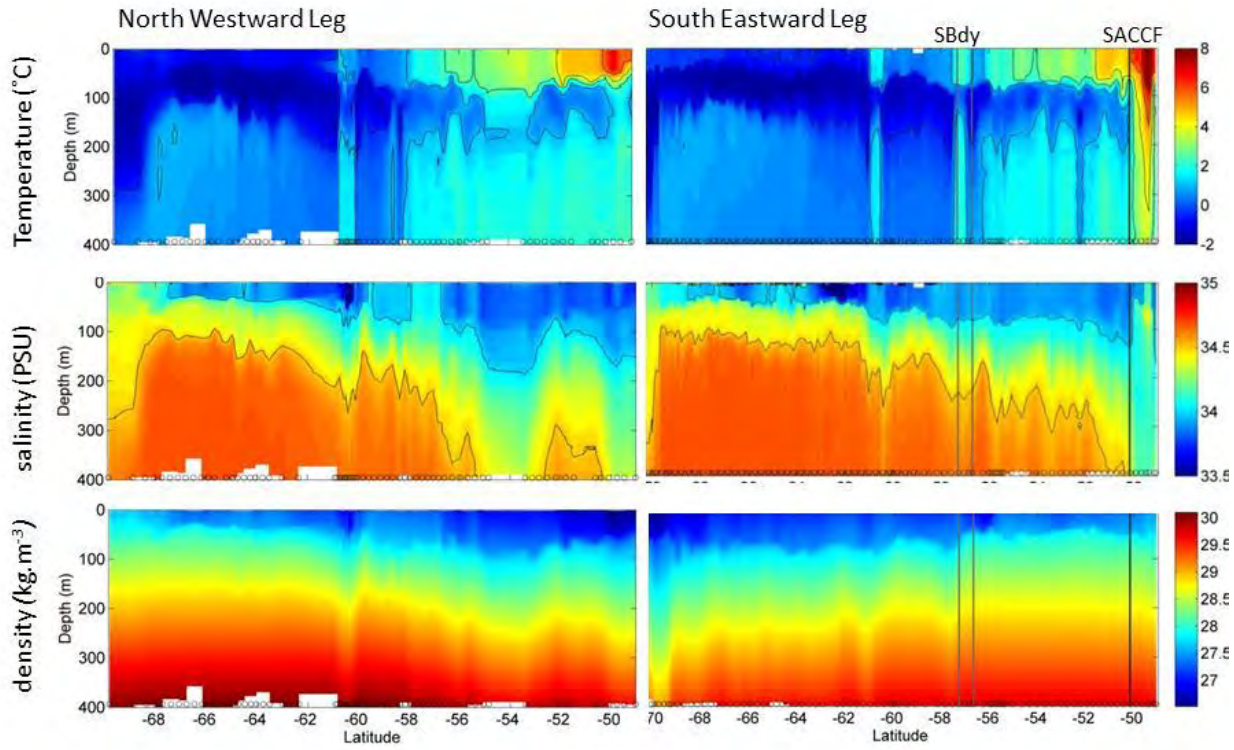

Figure 8: Vertical Temperature (˚C) salinity (PSU) and density (kg m^{-3}) sections on the north westward (left) and south eastward (right) legs of SANAE 50. The positions of the SBdy and the SACCF are shown with a grey and black line respectively. CTD and UCTD stations are marked with a triangle and circle respectively.

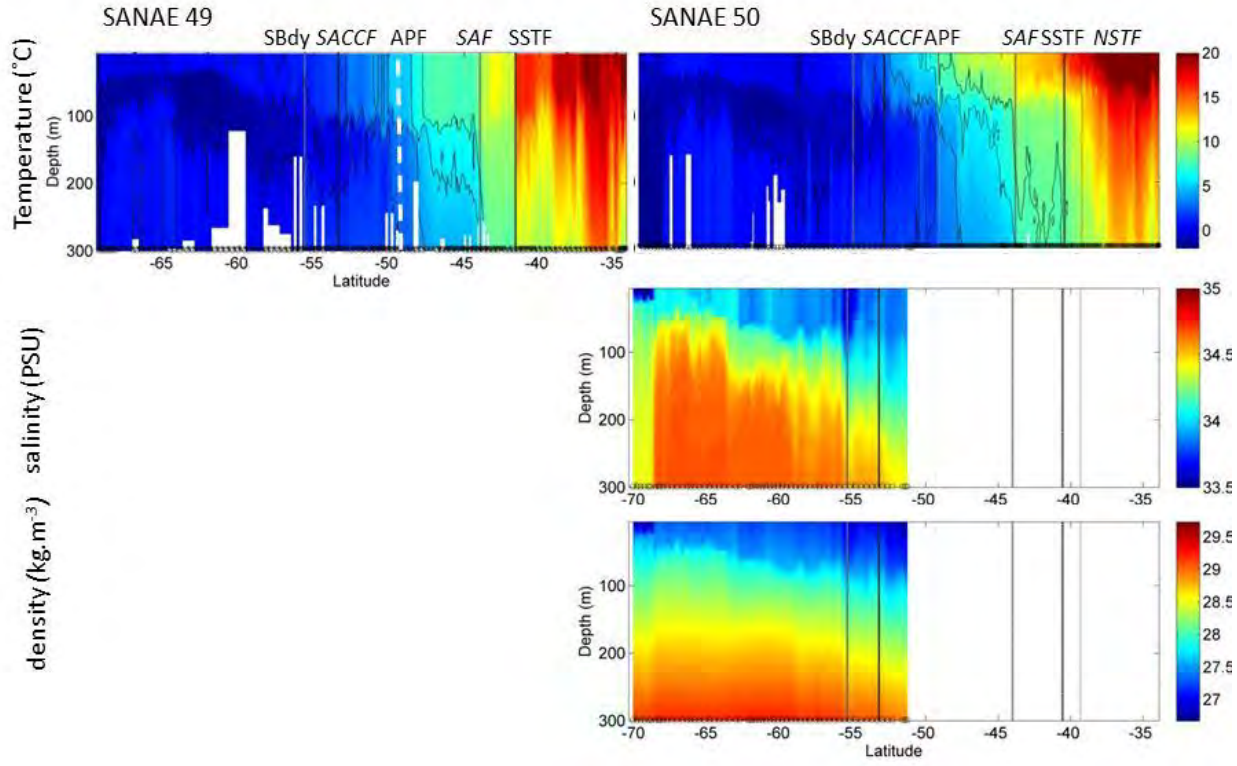

Figure 9: Vertical Temperature (˚C), salinity (PSU) and density (kg m^{-3}) sections on the northward legs of SANAE 49 (right) and SANAE 50 (left). The positions of the Northern STF (black dotted line), the Southern STF (black dashed line), the SAF (grey dashed line), the APF (white dotted line), the SACCF (black solid line) and the SBdy (grey solid line) are shown. XBT and UCTD stations are marked with a star and a circle respectively.

3.1.3) Nutrient concentrations

3.1.3.1) Nitrate

NO_3 concentrations in surface waters (AASW and upwelled UCDW) of the north westward leg of both cruises (Figures 10, 11) exceeded 25 µmol l^{-1}.

During SANAE 49, a NO_3 maximum (34.87 µmol l^{-1}) penetrated into AASW near South Georgia (figure 10), extending to just north of the SACCF (north westward leg). LCDW (lower circumpolar deep water) also contained high concentrations of NO_3, which mixed into the WW layer, reaching a maximum concentration (> 34.9 µmol l^{-1}) at about 60º S. NO_3 concentrations for AASW along the south eastward leg exceeded 16.7 µmol l^{-1}, with

minima concentrations occurring between 65.1º S and 62º S, as well as between 54º S - 56º S. On this leg the NO_3 concentrations increased substantially (>30 µmol l^{-1}) in deep waters (> 500m). In increase in NO_3 concentrations is noted in the deeper waters between 62º S and 66º S on the south eastward leg.

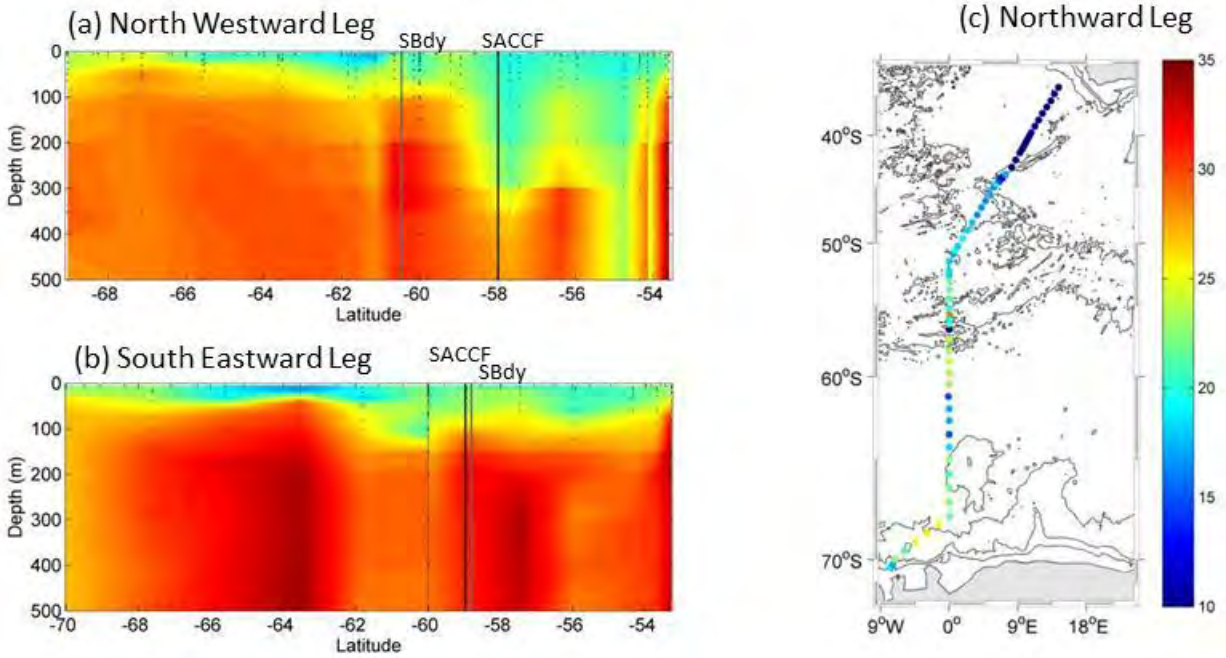

Figure 10: Vertical section of a) $N0_3$ (µmol l^{-1}) from the north westward, b) south eastward and c) northward legs of SANAE 49. The SBdy and the SACCF are shown in (a) and (b) with a grey and black line respectively. The thin black line in (b) represents the region where more than one station occurred at 60º S on the south eastward leg.

During SANAE 50 along the south eastward leg, NO_3 concentrations decreased throughout the water column between 67º and 61.5º S, where surface concentrations were 15 µmol l^{-1} (figure 11). Similar concentrations were evident in the surface waters just off Antarctica.

Along the northward legs of both SANAE 49 and SANAE 50 cruises, there were clear southward increases in NO_3 concentrations. Notable increases occurred before the fronts (figure 10 and 11), specifically at the SAF.

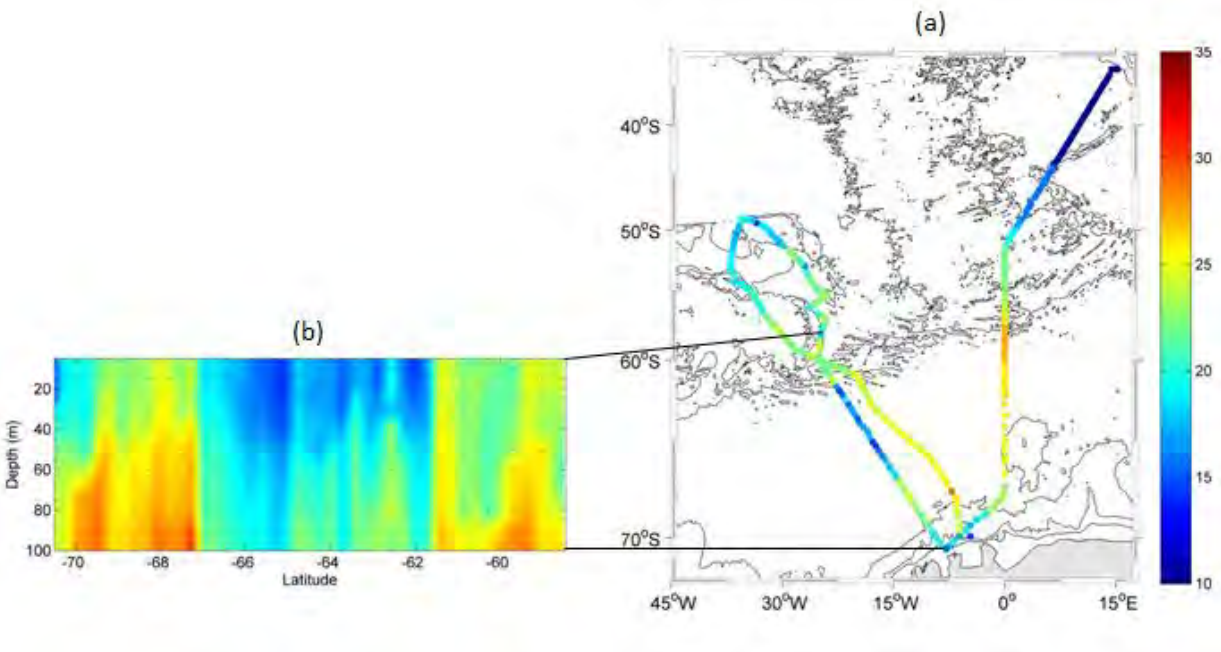

Figure 11: a) Surface distribution of $N0_3$ (µmol l^{-1}) for the north westward, south eastward and northward legs of SANAE 50 and b) vertical section of $N0_3$ from the CTD line during the south eastward leg.

3.1.3.2) Silicate

SiO_4 concentrations observed during SANAE 49 varied little between the north westward and south eastward legs (figure 12). Concentrations generally exceeded 40 µmol l^{-1}, with maximum concentrations (>70 µmol l^{-1}) evident below 350m between the SBdy and SACCF, as well as below 450m north of 55º S. Minimum values (5.45 µmol l^{-1}) were observed in the AASW near South Georgia on the north westward leg, steadily increasing with depth to 150m.

In surface waters between Antarctica and South Georgia, SiO_4 concentrations exceeded 70 µmol l^{-1} south of the SACCF (figure 13). Between this front, and South Georgia, concentrations decreased sharply to a minimum of 4.45 µmol l^{-1}. Along the south eastward leg of SANAE 49, maximum SiO_4 concentrations reached 150 µmol l^{-1} below 150m between 67º and 61.5º S.

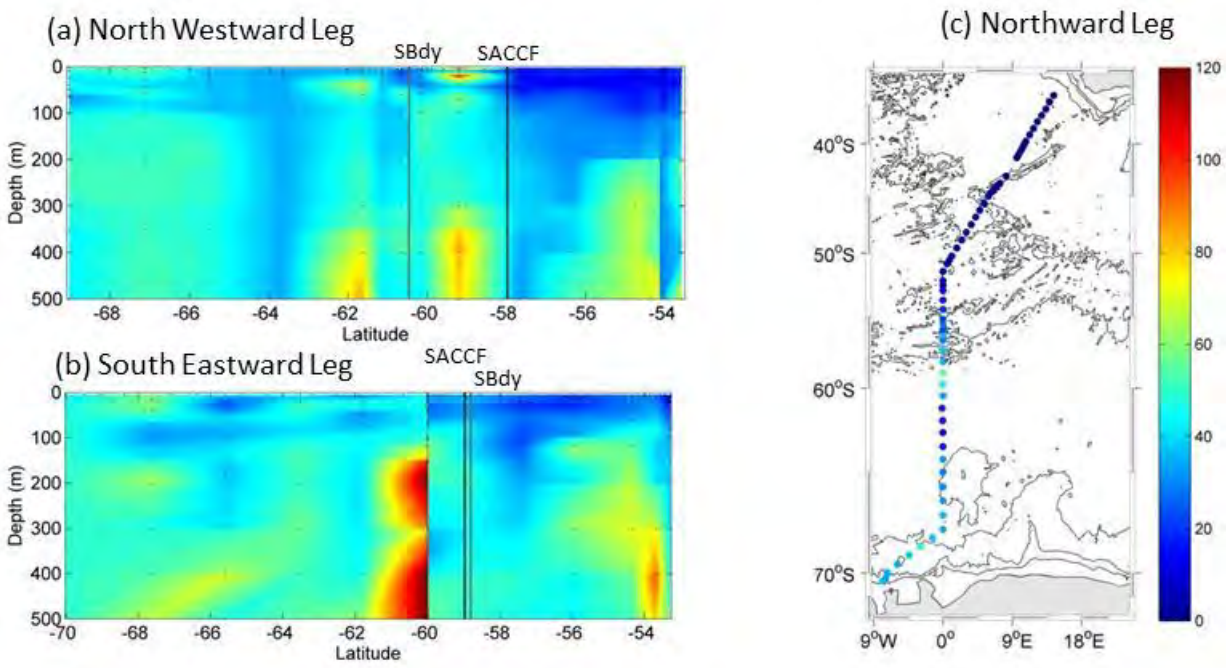

Figure 12: Vertical section showing SiO_4 (µmol l^{-1}) distributed on a) the north westward, b) the south eastward leg and c) the northward legs of SANAE 49. The SBdy and the SACCF are shown in (a) and (b) with a grey and black line respectively. The thin black line in (b) represents the region where more than one station occurred at 60º S on the south eastward leg.

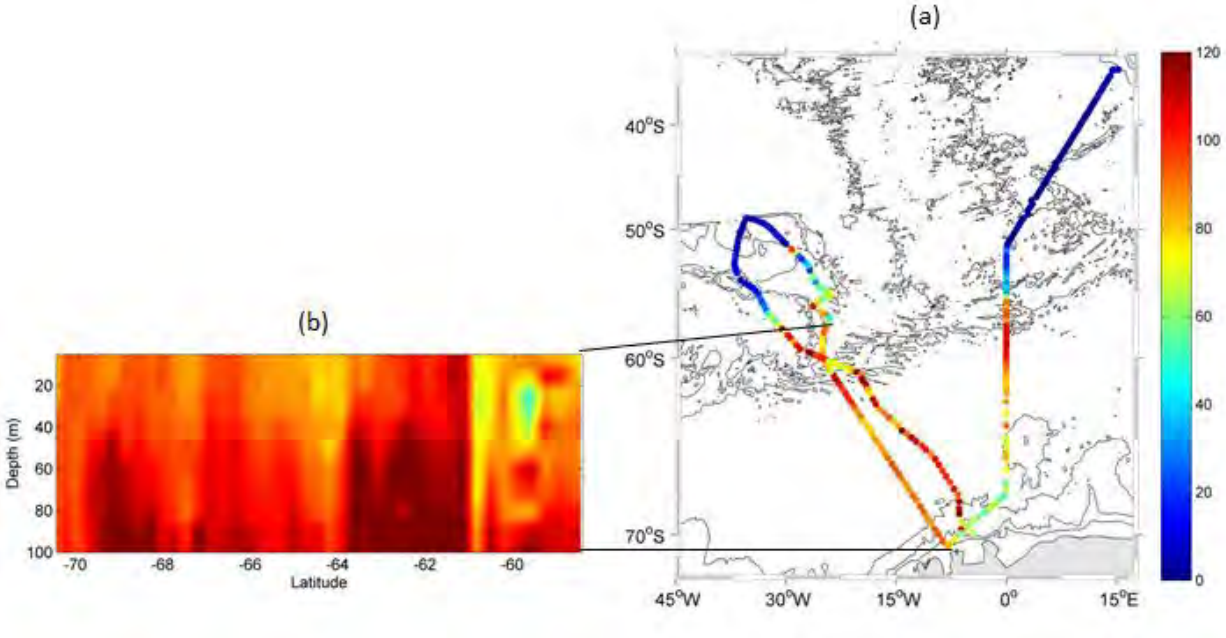

Figure 13: Surface distribution of SiO_4 (µmol l^{-1}) along SANAE 50's north westward, south eastward and northward legs. Vertical section of SiO_4 was obtained from the CTD line during the south eastward leg.

Low values of SiO_4 (<40 µmol l^{-1}) were found north of the APF on the northward legs of both SANAE 50 and SANAE 49 cruises, as well as north of the SACCF on the other legs (figures 13, 12).

3.1.4) Phytoplankton

3.1.4.1) Chlorophyll-a

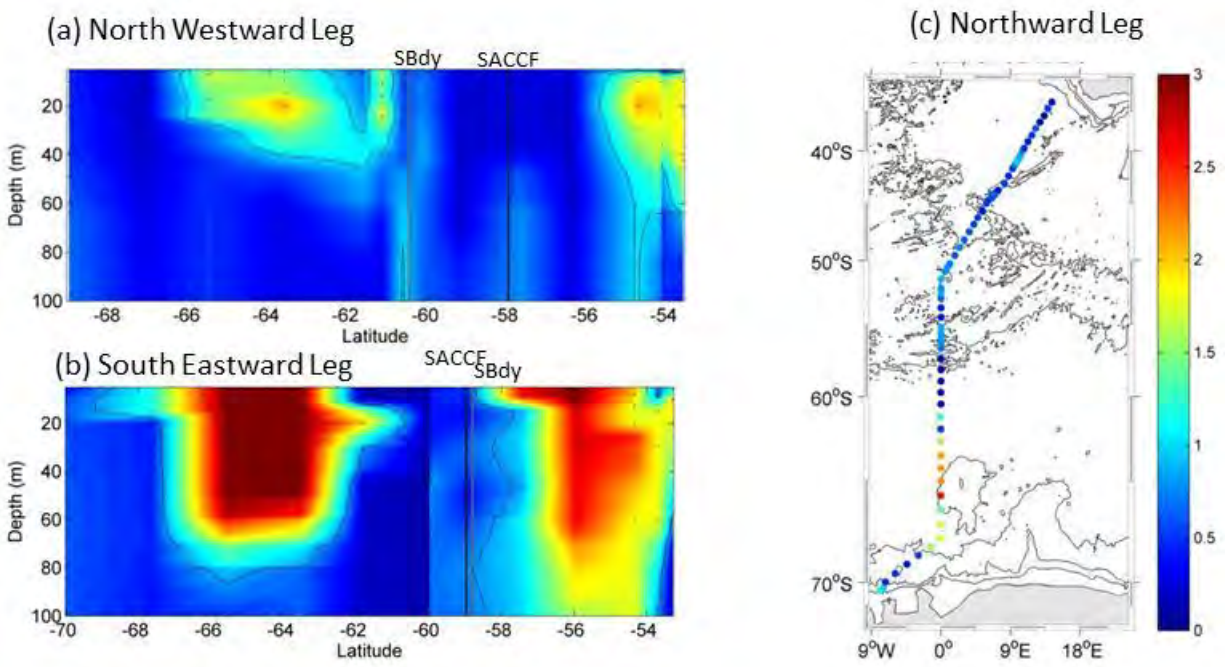

Figure 14: Vertical sections of chlorophyll (µg.l^{-1}) distribution on a) the north westward, b) the south eastward and c) the northward leg of SANAE 49. The SBdy and the SACCF are shown in (a) and (b) with a grey and black line respectively. The thin black line in (b) represents the region where more than one station occurred at 60º S on the south eastward leg.

Between Antarctica and South Georgia (SANAE 49) there were two main areas of moderate chl-a concentrations (>1 µg.l^{-1}) (figure 14). These blooms, although apparent on both legs, were deeper (>100m), with a higher chl-a maxima (2.5 – 3 µg.l^{-1}) on the south eastward leg. These blooms occurred in surface waters from 67º S to just South of 60º S and again near South Georgia. Chl-a concentrations (SANAE 50; figure 15) and (SANAE 49; figure 14) between Antarctica and South Georgia were not similar. Though, SANAE 50's south eastward leg revealed a chl-a bloom between 67º S and 62º S (similar in position to one of the SANAE 49 blooms), the north westward leg of SANAE 50 does not reveal a bloom in this position (figure 15). Both the north westward and south eastward legs of SANAE 50 see an increase in chl-a near South Georgia.

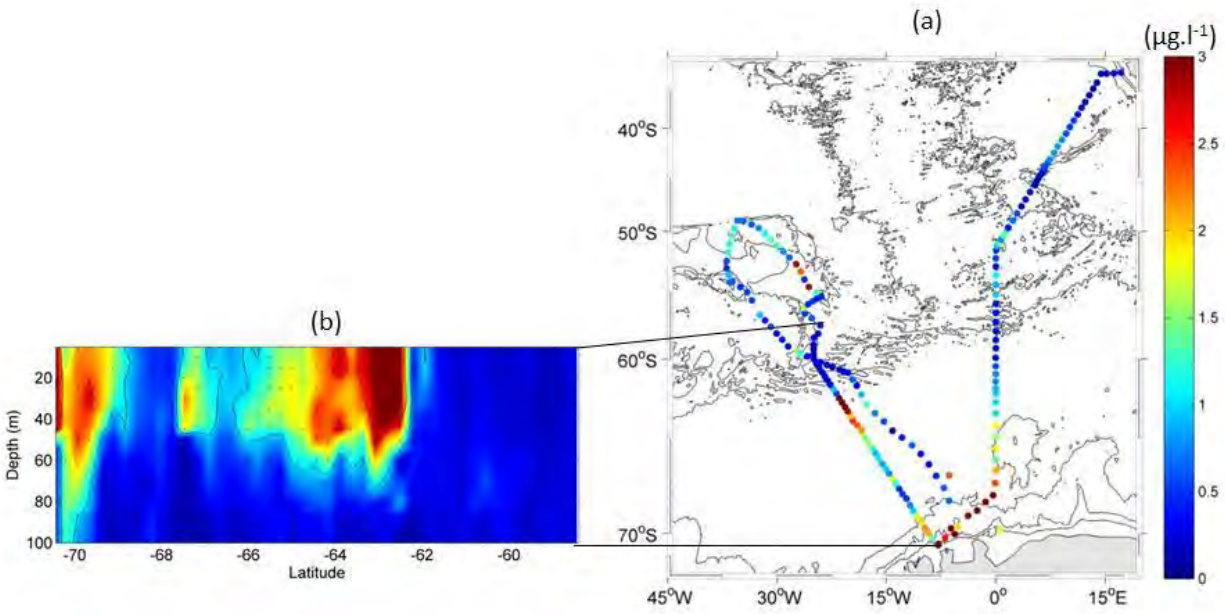

Figure 15: a) Surface distribution of chl-a (µg.l^{-1}) concentrations from SANAE 50's north westward, south eastward and northward legs. b) Vertical section of chl-a distribution from the CTD line on the south eastward leg of SANAE 50.

Along the northward legs of SANAE 49 (figure 14) and SANAE 50 cruises (figure 15), chl-a concentration decreased (from 2.57 to 0.03 µg.l^{-1} and from 3.65 to 0.26 µg.l^{-1} respectively) with distance away from Antarctica, but increased at each of the fronts.

3.1.4.2) Nitrogen uptake and f-ratio

The f-ratio is only available on the SANAE 49 cruise. On the north westward leg; low f-ratios (0.022 to 0.06) characterised deeper waters towards South Georgia, while the highest f-ratio (f = 0.37) present in AASW (>20m depth) near Antarctica (figure 16). On the south eastward leg, low (0.016 to 0.06) f-ratios characterised the water column between the SBdy and 65º S, with increasing f-ratios (up to 0.22) on either side.

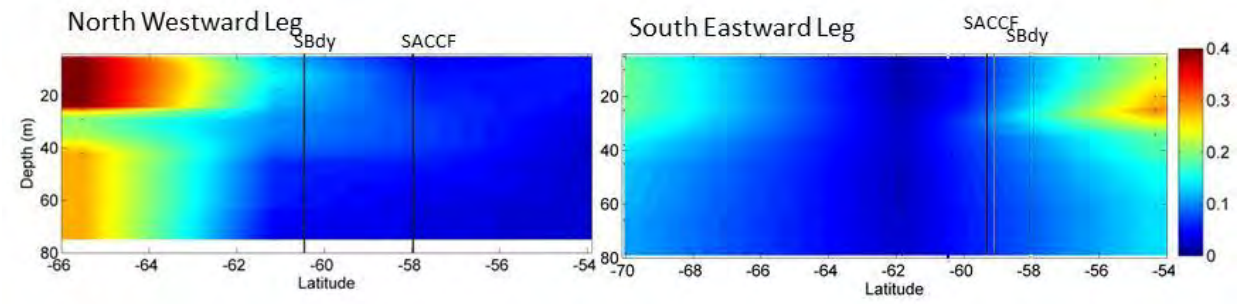

Figure 16: Vertical sections of f-ratios measured on the north westward (left) and south eastward (right) legs of SANAE 49. The SBdy and the SACCF are indicated using a grey and black lines respectively.

Table 2: f-ratio sensitivity test results, showing changes in f-ratio caused by a +/-10% variation in ambient NO_3

Station	latitude	Longitude	depth	Fratio			
				- 10% ambient NO3	ambient NO3	+ 10% ambient NO3	% difference in F ratio
BR-10	-65.52	-6.06	42	0.35	0.37	0.39	5%
BR-22	-61.15	-17.00	40	0.09	0.10	0.11	8%
BR-34	-57.68	-30.66	63	0.06	0.06	0.07	9%
BR-44	-54.14	-36.41	64	0.04	0.04	0.05	9%
BR-52	-54.34	-27.50	34	0.20	0.22	0.24	7%
BR-64	-60.00	-17.25	63	0.07	0.07	0.08	8%
BR-76	-61.83	-5.00	79	0.03	0.03	0.03	9%
BR-89	-70.04	-7.93	66	0.14	0.16	0.17	7%

Table 2 shows that a 10% variation in ambient NO_3 causes a less than 10% (5-9%) change in the f-ratio.

3.1.4.3) Phytoplankton Community Composition from HPLC

The community structure is reported here for dominant phytoplankton groups: i.e. those that represent more than 5% of the population on average. The data reveals only the north westward, south eastward (figure 17) legs of the SANAE 49 cruise. The data are unfortunately patchy due to loss of samples that were stored with the SANAE 50 samples, which were lost due to thawing.

Diatoms

Diatoms dominated much of the Southern Ocean between Antarctica and South Georgia, where they made up 80% of the populations.

Diatoms were abundant on both the north westward (45 - 88%) and south eastward (43 - 79%) legs from South Georgia to the SBdy (figure 17). Higher diatom abundance (73 - 60% and reaching 65% respectively) was evident closer to Antarctica. Relatively lower diatom abundances (>40%) characterised the open-ocean basin between the fronts, with a maximum (71%) just north of 64º S on the north westward leg.

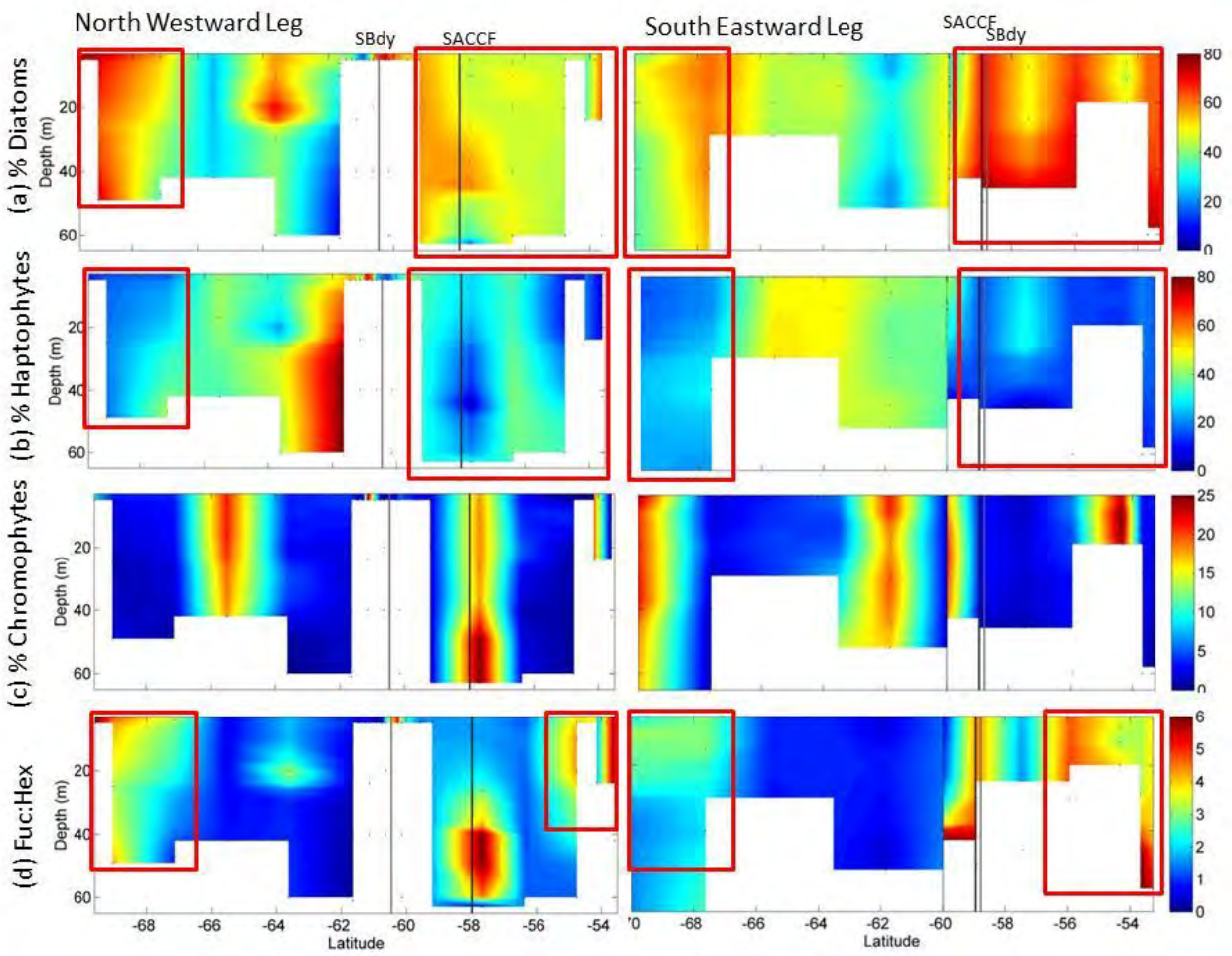

Figure 17: Vertical section of a) diatoms, b) haptophytes, c) chromophytes and d) Fuc:Hex from the north westward (left) and south eastward (right) legs of SANAE 49. The SBdy and the SACCF are indicated using a grey and black line respectively. The dotted line represents the region where more than one station occurred at 60º S on the south eastward leg. Red squares are used to highlight areas of interest.

Haptophytes

Inversely to diatoms, haptophytes were least abundant near South Georgia and Antarctica (<30%), with their highest abundances (53 - 88%) found in the open ocean south of the SBdy (figure 17), specifically on the north westward leg.

Chromophytes

Chromophytes made up a much smaller proportion (0.1 - 25%) of the phytoplankton community structure, compared to diatoms and haptophytes. This group rose in proportion close to Antarctica (reaching 25% on the south eastward leg only), South Georgia (20% and 25% for the north westward and south eastward legs respectively), on the SACCF (~20%), south of the SBdy (~20%) and in the case of the north westward leg, just north of 66º S (21%) (figure 17).

Fuc:Hex

The diatom to haptophyte ratio (Fuc:Hex [Fucoxanthin:19'-hexanoyloxyfucoxanthin]) rose close to South Georgia (reaching 8.8 and 11) and Antarctica (6.5 and 4.8) on both the north westward and south eastward legs respectively (figure 17), This increase in Fuc:Hex ratio extended further south (from South Georgia) on the south eastward leg, compared to the north westward leg. On the north westward leg, this ratio also increases in the subsurface waters just north of 64º S, and on the SACCF.

3.1.4.4) Phytoplankton photo-physiology (FRRf)

F_v/F_m

The photo-physiological health of phytoplankton in this study is represented by characteristic F_v/F_m and σ_{PSII} values, as shown in the SANAE 49 (figures 18 and 20 respectively) and SANAE 50 sections (figures 19 and 21).

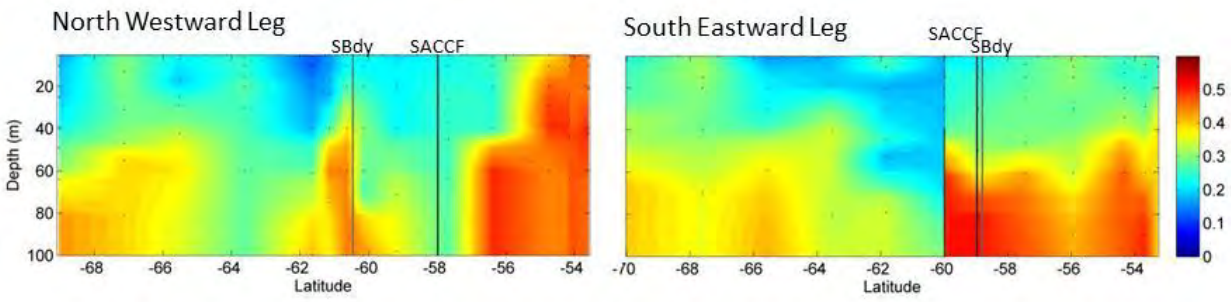

Figure 18: Vertical section of F_v/F_m values from the north westward (left) and south eastward (right) legs of SANAE 49. The SBdy and the SACCF are indicated using a grey and black lines respectively. The dotted line represents the region where more than one station occurred at 60º S on the south eastward leg.

On SANAE 49 the highest F_v/F_m values (0.50 ± 0.012) were found near South Georgia, on the south eastward leg (figure 18). The distribution of the F_v/F_m maxima (~0.45) around South Georgia differed between the south eastward and north westward legs. The north westward leg revealed that this maximum extended from South Georgia to just beyond 55º S, and throughout the water column to below 100m depth. On the south eastward leg, this maximum (~0.45) was present only below 50m, from South Georgia to 60º S. The F_v/F_m values along the north westward leg, near Antarctica, revealed a similar pattern to the south eastward leg, though with more moderate values (0.22 ± 0.017 - 0.43 ± 0.023) then the south eastward leg. Low F_v/F_m values (~0.12) were evident in the surface waters near Antarctica and in the middle of both legs. At about 60º S on the north westward leg, an increase in the F_v/F_m values (0.45 ± 0.02) in deeper waters was apparent.

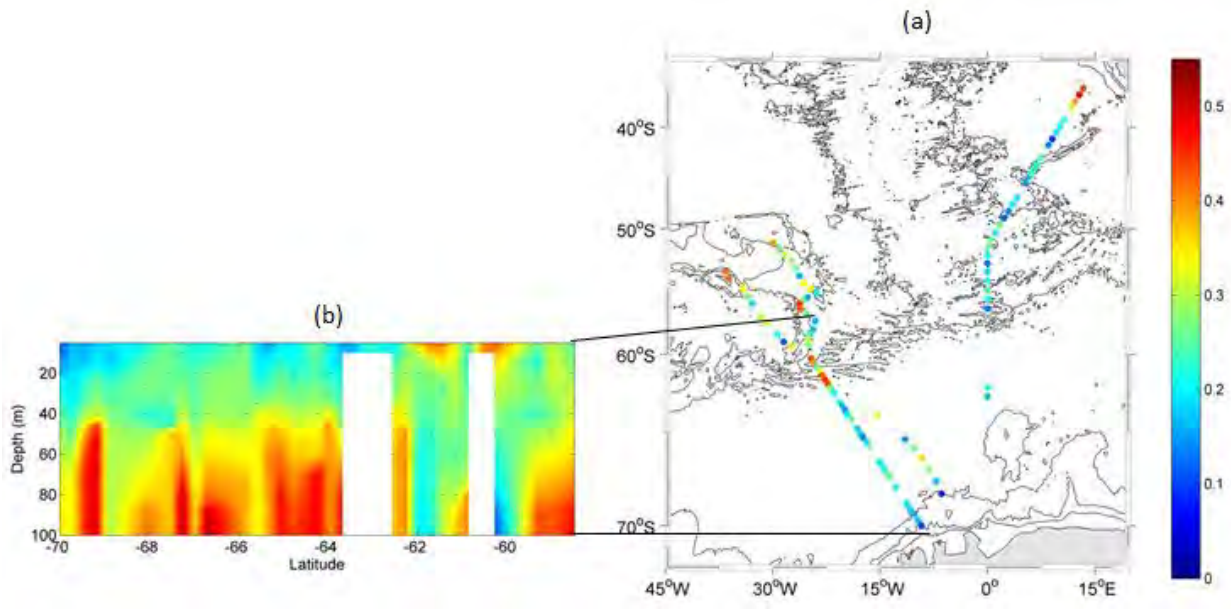

Figure 19: a) Surface distribution of F_v/F_m from SANAE 50's north westward, south eastward and northward legs. b) Vertical section of F_v/F_m from the CTD line of the south eastward leg.

The surface F_v/F_m values on SANAE 50 (figure 19) are continuously moderate to low (<0.2), with an exception of near South Africa (0.38 ± 0.063 - 0.49 ± 0.023), on the northward leg, around South Georgia (reaching 0.42 ± 0.007) on both the north westward and south eastward legs, as well as South of 60º S on the south eastward leg (reaching 0.43 ± 0.048) above topographical features, all of which show high F_v/F_m values. The deeper F_v/F_m values seen on the south eastward leg shows pulses of increased F_v/F_m values under 40m (>0.35) between 61º and 70º S.

σ PS II

On the north westward leg of SANAE 49 (figure 20), minimum σ_{PSII} values (152 ± 6.5 - 185 ± 7) were found near South Georgia where σ_{PSII} remained below 200 over the full 100m depth until ~55º S. Such minimum values were also evident in the surface waters between 65º S and 67º S and below 30m between 62º S and 63º S. Maximum values of σ_{PSII} (>260) were

found north of the SBdy until ~57º S; crossing both sides of the SACCF. These values were also present below 60m between 65º - 70º S, and in surface waters close to Antarctica and between 62º - 65º S.

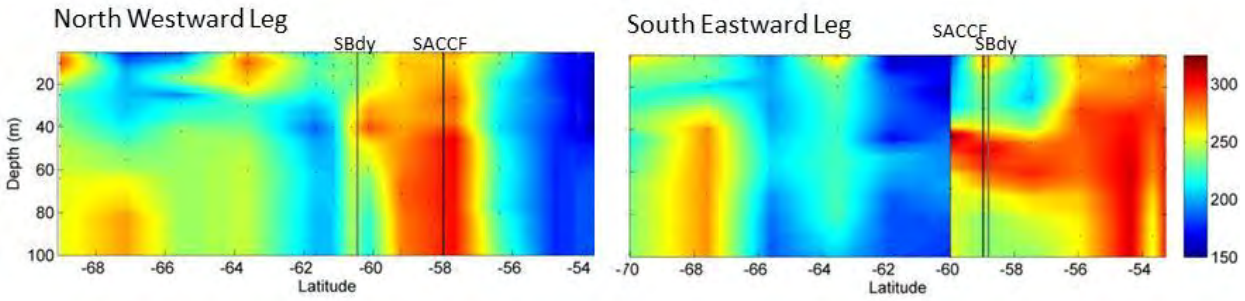

Figure 20: Vertical section of ó$_{PSII}$ from the north westward (left) and south eastward (right) legs of SANAE 49. The SBdy and the SACCF are indicated using grey and black lines respectively. The dotted line represents the region where more than one station occurred at 60º S on the south eastward leg.

On SANAE 49, the south eastward leg (figure 20), minimum values of σ_{PSII} (162 ± 38.2 - 200 ± 49) were evident in surface waters between 65º - 67º S, and at 60º S. Lowest values (156 ± 81 - 200 ± 49) were found at 50m depth, south of the SBdy. Maximum σ_{PSII} values (253 ± 17.6 - 308 ± 73.6) occurred closest to South Georgia and below 30m between 65º-70º S, as well as in surface waters near Antarctica and between 62º - 65º S.

There is less evidence of a pattern of σ_{PSII} from SANAE 50 (figure 21). σ_{PSII} Values varied between 102 ± 51.1 and 336 ± 17.1. On the northward leg, these surface values are low (<200) north of 50º S. In the depth profile on the south eastward leg, there is an overall increase in σ_{PSII} values as one moves south from ~63º S (~200 to ~300).

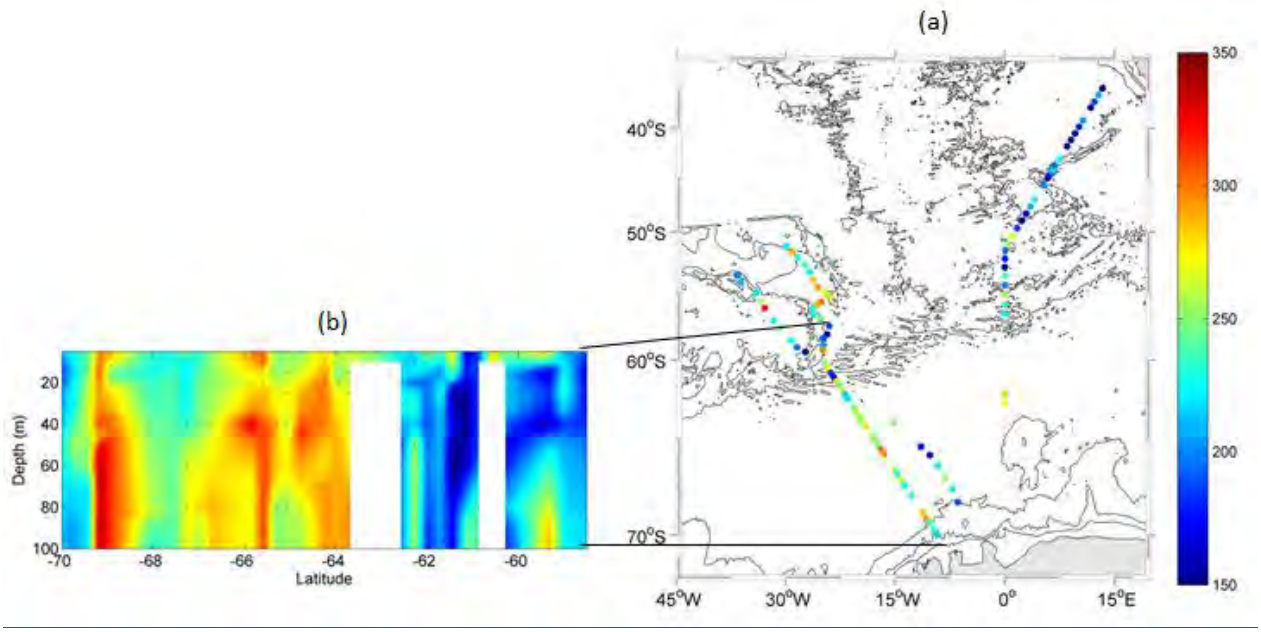

Figure 21: a) Surface distribution of σ_{PSII} from SANAE 50's north westward, south eastward and northward legs. b) Vertical section of $ó_{PSII}$ from the CTD part of the south eastward leg.

3.1.5) SiO_4:$N0_3$ Ratios

3.1.5.1) SiO_4:$N0_3$ Ratios: SANAE 49

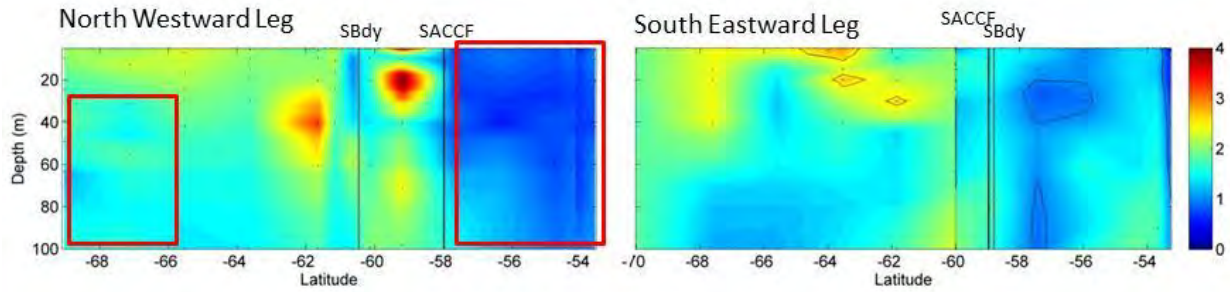

Figure 22: Vertical section of SiO_4:$N0_3$ ratios from the north westward (left) and south eastward (right) legs of SANAE 49. The SBdy and the SACCF are indicated using grey and black lines respectively. The dotted line represents the region where more than one station occurred at 60º S on the south eastward leg. Red squares are used to highlight areas of interest.

For SANAE 49, the combined north westward and south eastward legs (figures 22) reveal a distinct drop in SiO_4:NO_3 ratio (dropping below 1) around South Georgia.

3.1.5.2) SiO_4:$N0_3$ Ratios: SANAE 50

Table 3 Shows the SiO_4:NO_3 ratio, SiO_4 difference and NO_3 difference in different ocean regions (divided by fronts) in the different legs on SANAE 50

	SiO_4:NO_3				difference in SiO_4		Difference in NO_3	
Ocean Region	Southward leg	Northward leg	Northwestward leg	Southeastward leg	Southward and northward legs	Northwestward and southeastward legs	Southward and northward legs	Northwestward and southeastward legs
Between South Africa and northern STF	1.62	4.77	-	-	-0.75	-	1.17	-
Between northern STF and southern STF	0.39	0.38	-	-	0.38	-	0.87	-
Between southern STF and SAF	0.22	0.16	-	-	1.38	-	3.76	-
Between SAF and APF	0.39	0.12	-	-	5.12	-	2.19	-
Between APF and SACCF	1.55	0.50	0.25	0.32	25.48	-1.45	2.56	-0.76
Between SACCF and Sbdy	2.87	1.45	2.48	2.38	41.47	2.45	3.50	0.11
Between Sbdy and 69° S	4.21	3.65	3.96	4.40	30.71	10.54	4.31	4.83
Between 69° S and the iceshelf	6.01	3.28	4.30	4.52	31.59	2.24	-25.01	1.55

Combined north westward and south eastward legs of SANAE 50

There is a high (>1.5) SiO_4:NO_3 ratio throughout this region except around South Georgia (between the APF and SACCF) where the average SiO_4:NO_3 ratio for this region is 0.25 and 0.32 for the north westward and south eastward legs respectively.

The difference between the early north westward leg and the later south eastward leg's SiO_4 and NO_3 is positive in all regions expect around South Georgia (-1.45 μmol l^{-1} and -0.76 μmol l^{-1} for SiO_4 and NO_3 respectively).

Combined northward and southward legs of SANAE 50

There is a high (>1.5) SiO_4:NO_3 ratio between South Africa and the northern STF as well as south of the SACCF. Regions between the northern STF and APF have low (<1.5)

SiO_4:NO_3 ratio. In the region between the APF and SACCF, the ratio changed from a high (1.55) to a low (0.50) ratio between the southward and northward legs

The difference between the early southward leg and the later northward leg's SiO_4 and NO_3 is positive for all regions, except between South Africa and the northern STF for SiO_4 (-0.75 µmol l^{-1}), and south of 69º S for NO_3 (-25.01 µmol l^{-1}).

3.1.6) Statistical analyses

3.1.6.1) linear regression

To determine whether various factors that might be influence F_v/F_m and ó$_{PSII}$ values were significant, linear regressions were performed for a number of variables from the SANAE 49 cruise only, since this is the most complete data set. Two alternative linear regressions were run. The first (tests a and b) included the dominant phytoplankton groups that on average made up more than 5% of the population. The second (tests c and d) used the Fux:Hex ratio.

Test a)

$Y(F_v/F_m) = 3.385e+00 + (-1.175e-03)SiO_4 + (-9.648e-03)PO_4 + (6.800e-03)N0_3 +$
(4.049e-02)chlorophyll + (-6.515e-03)temperature + (-7.500e-02)salinity +
(-6.959e-02)oxygen + (-2.280e-02)fluorescence + (-2.604e-04) PAR +
(-8.572e-04)diatoms + (-2.174e-03)haptophytes + (-2.051e-03)chromophytes

P value <0.001 (chlorophyll, PAR)
P value <0.01 (SiO_4, oxygen, fluorescence)
P value <0.05(haptophytes)

Test b)

$Y(ó_{PSII}) = -2.001e+03 + (1.061e-01)SiO_4 + (2.089e+00)PO_4 + (-4.732e+00)N0_3 +$
(-1.858e+01)chlorophyll + (-2.241e+00)temperature + (7.177e+01)salinity +
(-2.120e+01)oxygen + (2.013e+01)fluorescence + (1.549e-02)PAR +
(1.176e+00)diatoms + (-8.329e-01)haptophytes + (1.567e+00)Chromophytes

P value <0.001 (fluorescence)

P value <0.01 (chlorophyll, salinity)

P value <0.05(NO_3, diatoms, chromophyte)

Test c)

$Y(F_v/F_m) = 5.020e+00 + (-1.041e-03)SiO_4 + (-6.409e-03)PO_4 + (8.141e-03)N0_3 +$
(3.330e-02)chlorophyll + (1.524e-03)temperature + (-1.230e-01)salinity +
(-9.384e-02)oxygen + (-2.005e-02)fluorescence + (2.615e-04)PAR +
(7.083e-03)Fuc:Hex

P value <0.0001 (Fuc:Hex)

P value <0.001 (oxygen, PAR)

P value <0.01 (chlorophyll, salinity)

P value <0.05(SiO_4, NO_3, fluorescence)

Test d)

$Y(ó_{PSII}) = -1.809e+03 + (-2.255e-01)SiO_4 + (9.016e+00)PO_4 + (-1.999e-01)N0_3 +$
(-1.804e+01)chlorophyll + (5.458e+00)temperature + (5.935e+01)salinity +
(6.992e-02)oxygen + (1.740e+01)fluorescence + (6.170e-02)PAR +
(3.266e+00)Fuc:Hex

P value <0.01 (fluorescence, Fuc:Hex)

P value <0.05(chlorophyll, salinity)

3.1.6.2) Specific parameter comparison

Specific parameter comparisons with F_v/F_m show a positive relationship with F_v/F_m and NO_3, PO_4, % diatoms, SiO_4:NO_3, while showing a negative relationship between F_v/F_m

and SiO_4, f-ratio (Figure 23). However, in this analysis, due to the complexity of the system, these trends have a very low gradient (R^2 ranges between 0.081 and 0.2055).

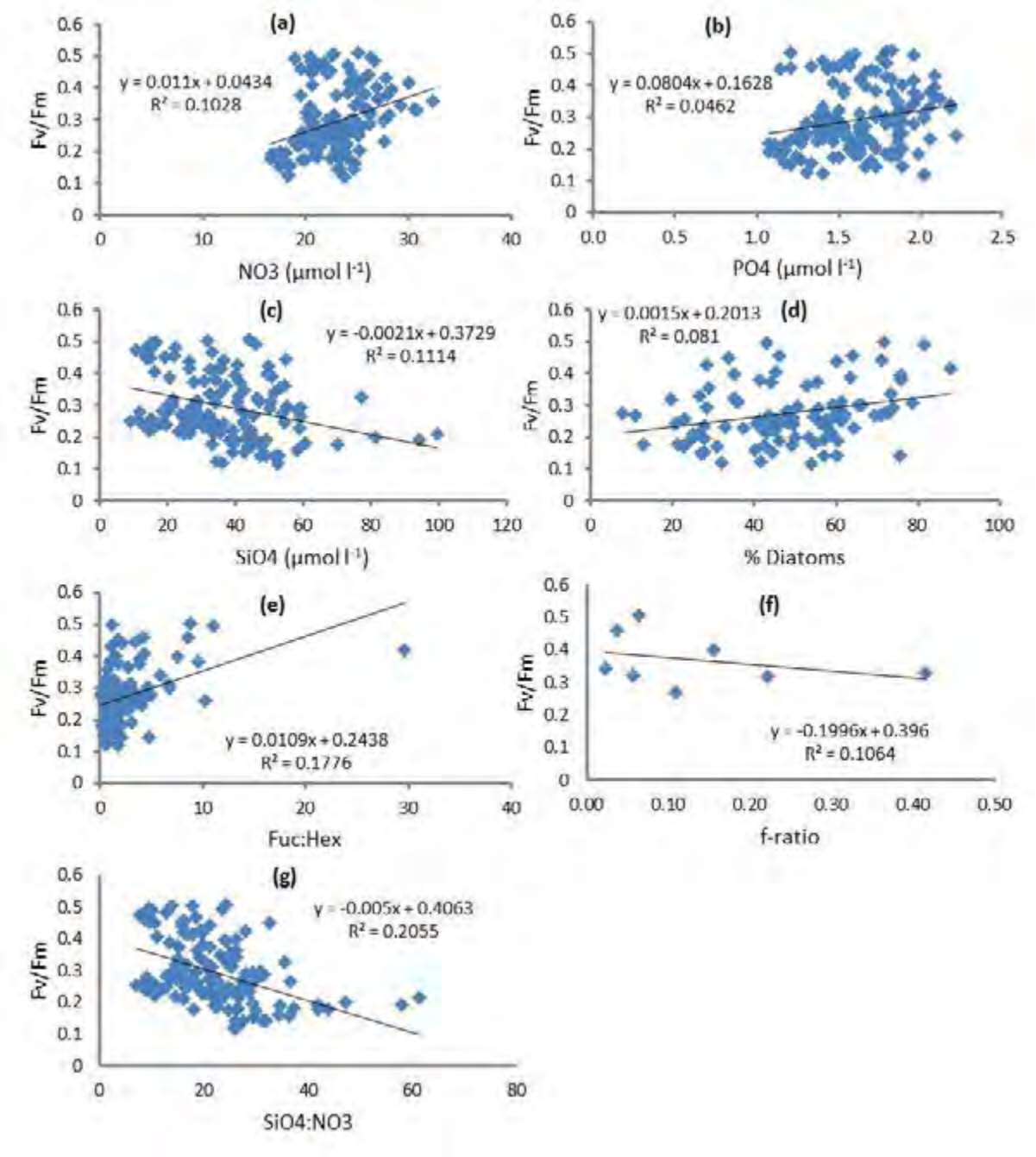

Figure 23: Graphs showing SANAE 49 F_v/F_m in relation to individual parameters namely: NO_3 (a), PO_4 (b), SiO_4 (c), % Diatoms (d), Fuc:hex ratio (e), f-ratio (f) and SiO_4:NO_3 (g).

SECTION 2: Bio-Assay Experiment Results

Due to logistical reasons each experiment was started on a different day, thus experiencing a range of conditions, reflecting both spatial and temporal variability within the Southern Ocean (table 4).

3.2.1) Initial conditions of bio-assay experiments

Table 4: The position and associated water mass for each on board Fe-light incubation experiment on SANAE 50. The positions for the 6 experiments are marked on figure 5.

Exp.	Sampling Date	Latidtue	Longitude	SST (°C)	Nitrate (uM)	Silicate (uM)	Phosphate (uM)	SiO_4:NO_3 for region	Chl-a (µg.l-1)	Comments
A	04-Jan	-64.021	-15.3282	-0.82	24.49	80.87	1.44	3.96	0.58 ± 0.014	North-Eastern leg, South of the southern boundary, still icebergs and growlers around
B	15-Jan	-62.276	-21.8786	-0.55	15.77	103.00	1.35	3.96	0.56 ± 0.093	South-Western leg, South of the southern boundary
C	19-Jan	-68.911	-11.2692	-0.30	22.02	92.60	1.57	4.40	1 ± 0.000	South-Western leg, icebergs, South of the Southern Boundary
D	26-Jan	-70.545	-7.867	0.28	17.76	81.69	1.35	4.52	1.93 ± 0.077	South of the polar circle, marginal ice zone. High productive area with a lot of top predators e.g. killer whales, minke whales, humpback whales and leopard seals
E	09-Feb	-55.962	0.0203	0.88	24.67	90.36	1.81	1.45	0.77 ± 0.028	Northward leg, between SBdy and SACCF, water blue, low productivity, miserable, cloudy weather. 1-3 m swell. Weather cleared a bit during the day. Whales and albatrosses sighted
F	11-Feb	-50.335	1.0675	6.79	19.00	0.29	1.02	0.12	1.28 ± 0.042	Northward leg, in the APZ, after the Polar Front. Highly productive warm waters

3.2.2) Physical changes experienced by Fe incubations

Table 5: Average (graphically depicted) sea temperature and PAR (ambient, high and low light bottles) for each Fe-light experiment on SANAE 50. Columns from left to right show: average, standard deviation and range. The logging of the data is explained in the methods section (page 41).

experiment	average sea temperature (°C)			average par (W/m2)			average par for high light (W/m2)			average par for low light (W/m2)		
A	1.3	(+/-1.6)	(-1.4-4.5)	449	(+/-534)	(0-3804)	224	(+/-267)	(0-19)	112	(+/-133)	(0-951)
B	-0.5	(+/-0.1)	(-1-0)	264	(+/-241)	(0-909)	132	(+/-120)	(0-454)	66	(+/-60)	(0-227)
C	0.1	(+/-0.5)	(-1.5-1.6)	1001	(+/-885)	(6-35670)	501	(+/-442)	(3-1783)	250	(+/-221)	(1-892)
D	0.1	(+/-0.4)	(-1.2-0.8)	971	(+/-783)	(16-2870)	486	(+/-391)	(8-1435)	243	(+/-196)	(4-717)
E	7.5	(+/-3.3)	(1.3-13)	478	(+/-678)	(0-3865)	239	(+/-339)	(0-1932)	119	(+/-169)	(0-966)
F	10.1	(+/-1.8)	(5.9-13.2)	560	(+/-772)	(0-3865)	280	(+/-386)	(0-1932)	140	(+/-193)	(0-9660

3.2.2.1) Sea temperature changes

Experiments E (7.5 ± 3.3 ºC) and F (10.1 ± 1.8 ºC) were characterised by the greatest average sea temperatures as well as the greatest ranges in temperature (1.3 - 13 ºC and 5.9 -

13.2 ºC respectively) the other four experiments had very low sea temperatures and ranges of: -1.4 ºC to 4.5 ºC for experiment A, -1 ºC to 0 ºC for experiment B, -1.5 ºC to 1.6 ºC for experiment C and -1.2 ºC to 0.8 ºC for experiment D (table 5).

3.2.2.2) PAR readings

Average PAR for 'high' and 'low' light incubations represented 50% and 25% of ambient irradiance respectively.

Experiment C experienced the highest average PAR of 1001 ± 885 $\mu E.m^{-2}.s^{-1}$ (table 5). Experiment D experienced 971 ± 783 $\mu E.m^{-2}.s^{-1}$; experiment A 449 ± 534 $\mu E.m^{-2}.s^{-1}$; experiment E 478 ± 678 $\mu E.m^{-2}.s^{-1}$ and F (560 ± 772 $\mu E.m^{-2}.s^{-1}$. Experiment B experienced notably lower irradiances 264 ± 772 $\mu E.m^{-2}.s^{-1}$ than any other experiment.

3.2.2.3) Summary of weather observations

As is clear from the PAR values, experiment A was overcast throughout the experiment except for the evening of the second day until 6am on the third day.

Experiment B experienced mostly overcast weather, except for 2 hours at 20:00 on the second day, and full sunshine on the last day.

Experiment C experienced mostly full sunshine except for day 1, which was overcast, with heavy clouds, rain, and snow.

Experiment D started off sunny, becoming overcast by 8am on day 1, but the dull weather cleared by the end of day 2, only to return in the latter half of day 3 with snow.

Experiment E and F remained overcast except for an hour or two of patchy sunshine every day.

3.2.3) Experiment results

3.2.3.1) Variation in physiological response time

Experiment A showed a change in the photo-physiological response from day 2 and 3 for $ó_{PSII}$ and F_v/F_m respectively (figure 24). Experiment B responded quickly from day 1 and also showed the greatest change. Photo-physiological responses for Experiments C, E and F also started on day 1, with experiment D starting at days 0 and 1 for F_v/F_m and $ó_{PSII}$ respectively.

3.2.3.2) Variation in ranges

Experiment B shows the greatest response to Fe alleviation (figure 24). This is evident especially through the F_v/F_m response. Experiment B began at a F_v/F_m value of 0.27 ± 0.000. By the end of day 5, the Fe addition bottles reached 0.47 ± 0.014 and 0.47 ± 0.016 for 50% and 25% light respectively, while the control bottles for 50% and 25% light were at 0.29 ± 0.049 and 0.28 ± 0.031 respectively.

.

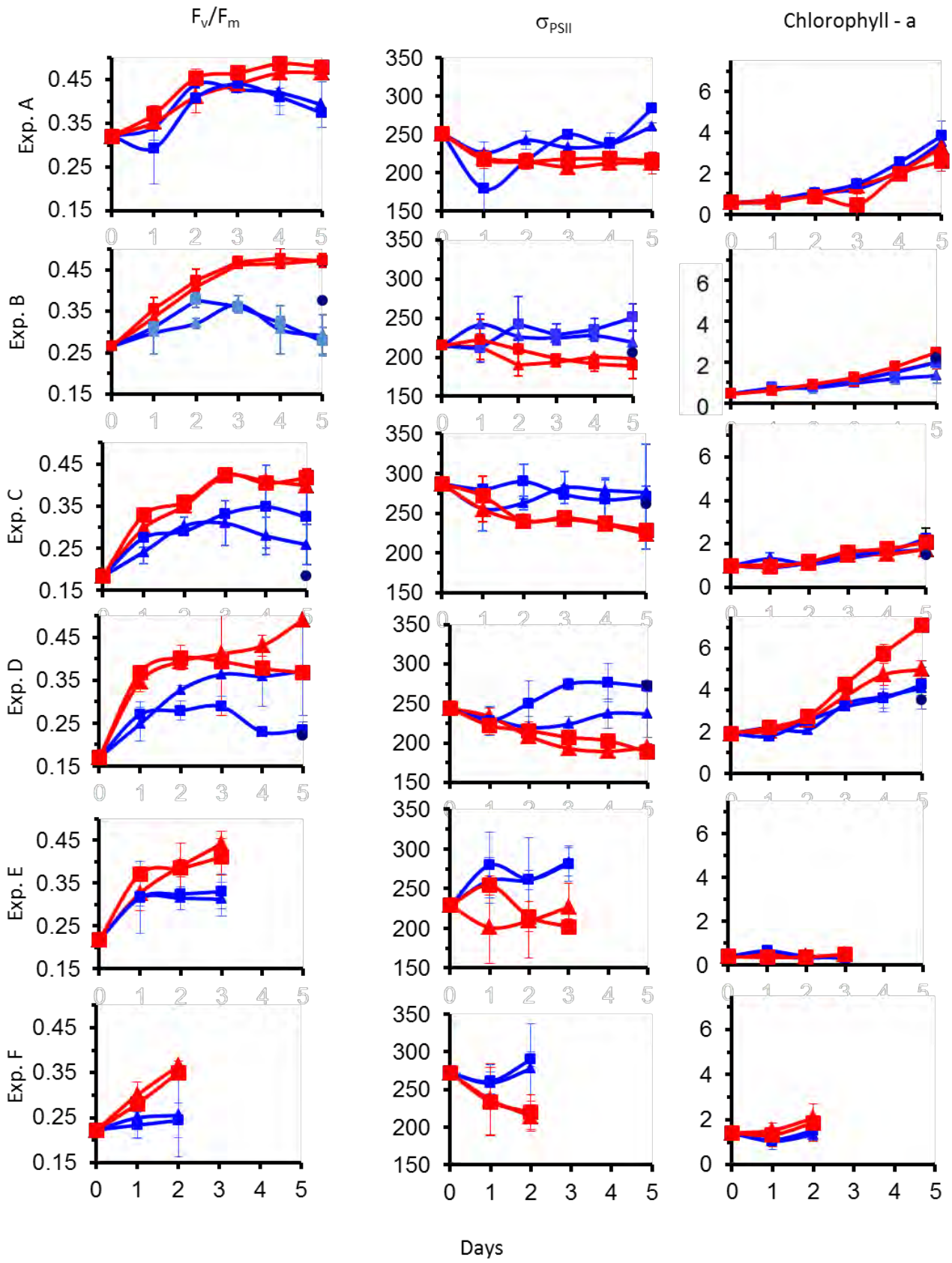

Figure 24: Averaged F_v/F_m (left), $ó_{PSII}$ (middle) and chl-a (right) results for Fe incubation experiments on SANAE 50. Red represents the Fe addition bottles. Blue represents the control bottles. A triangle and square represents 50% and 25% light respectively. Circles symbolise the overall control.

Despite huge variation in starting photosynthetic parameters, by day 5 (excluding experiments E and F, which didn't reach day 5) each experimental Fe addition bottles reached values ~0.4 and ~200 for F_v/F_m and $ó_{PSII}$ respectively, while the control bottles were below these values for F_v/F_m and above for $ó_{PSII}$.

3.2.3.3) FIRe

A paired-samples t-test was conducted to separately compare the F_v/F_m and $ó_{PSII}$ values under the following conditions:

1) All the control bottles + the Fe addition bottles

2) The control bottles + the Fe addition bottles at 50% irradiance

3) The control bottles + the Fe addition bottles at 25% irradiance

4) The control bottles at 50% irradiance and 25% light irradiance

5) The Fe addition bottles at 50% irradiance and 25% irradiance

6) The contamination control bottle and the control bottle at 50% irradiance (Experiments B, C and D only)

Summary: FRRf responses to Fe additions

All experiments showed an increase in F_v/F_m and a decrease in $ó_{PSII}$ for bottles with Fe additions (figure 24). The degree to which this occurred was highly variable.

Experiment B showed the greatest statistically significant response (table 6) to Fe alleviation with both F_v/F_m and $ó_{PSII}$ responding significantly under both high light (50%) and low light (25%) conditions ($P < 0.001$ for all). Experiment C showed a full response at high irradiance ($P = 0.0031$, and $P = 0.0005$ for F_v/F_m and $ó_{PSII}$ respectively), while experiments D

(P <0.001 for F_v/F_m and $ó_{PSII}$) and F (P =0.0288; P =0.0148 for F_v/F_m and $ó_{PSII}$ respectively) showed statistically significant responses at low irradiances.

Table 6: The F_v/F_m, $ó_{PSII}$ and chl-a results for all the Fe-light incubation experiments. X is used to show no significant difference

experiments	response measured	All the control bottles and all the Fe addition bottles	The control bottles and the Fe addition bottles at 50 % light levels	The control bottles and the Fe addition bottles at 25 % light levels	The control bottles at 50 % light levels and 25% light levels	The Fe addition bottles at 50 % light levels and 25% light levels
A	F_v/F_m	**Significant difference (p=0.0092)**	*x*	**Significant difference (p=0.0105)**	*x*	*x*
A	$ó_{PSII}$	**Significant difference (p=0.0064)**	**Significant difference (p=0.0003)**	*x*	*x*	*x*
A	Chlorophyll-a	x	x	*x*	*x*	*x*
B	F_v/F_m	**Significant difference (p=0.0000001)**	**Significant difference (p=0.00019)**	**significant difference (p=0.0003)**	*x*	*x*
B	$ó_{PSII}$	**Significant difference (p=0.0000000017)**	**Significant difference (p=0.0000008)**	**Significant difference (p=0.0001)**	*x*	*x*
B	Chlorophyll-a	x	x	x	*x*	*x*
C	F_v/F_m	**Significant difference (p=0.0003)**	**Significant difference (p=0.0031)**	*x*	*x*	*x*
C	$ó_{PSII}$	**Significant difference (p=0.00001)**	**Significant difference (p=0.0005)**	*x*	*x*	*x*
C	Chlorophyll-a	x	x	*x*	*x*	*x*
D	F_v/F_m	**Significant difference (p=0.0003)**	*x*	**Significant difference (p=0.0001)**	**Significant difference (p=0.0157)**	*x*
D	$ó_{PSII}$	**Significant difference (p=0.00000003)**	**Significant difference (p=0.0025)**	**Significant difference (p=0.0000005)**	**Significant difference (p=0.0007)**	*x*
D	Chlorophyll-a	**Significant difference (p=0.0193)**	x	**Significant difference (p=0.0411)**	x	*x*
E	F_v/F_m	**Significant difference (p=0.0181)**	*x*	*x*	*x*	*x*
E	$ó_{PSII}$	**Significant difference (p=0.00003)**	**Significant difference (p=0.0022)**	**Significant difference (p=0.0074)**	*x*	*x*
E	Chlorophyll-a	x	**Significant difference (p=0.0175)**	x	*x*	*x*
F	F_v/F_m	**Significant difference (p=0.0037)**	*x*	**Significant difference (p=0.0288)**	*x*	*x*
F	$ó_{PSII}$	**Significant difference (p=0.0034)**	*x*	**Significant difference (p=0.0148)**	*x*	*x*
F	Chlorophyll-a	**Significant difference (p=0.0190)**	**Significant difference (p=0.0092)**	x	*x*	*x*

Experiment C shows no significant statistical photo-physical response to Fe addition in low light levels; however a significant statistical photo-physical response was seen in high light conditions. Experiment F shows no significant statistical photo-physical response to Fe addition in high light levels; however a significant statistical photo-physical response was seen in low light conditions. In experiments A, D, E (high light) a significant difference between Fe supplemented bottles and controls without Fe was only shown by $ó_{PSII}$ (P =0.0003, P =0.0025, P =0.0022 for A, D and E respectively). Under low light in experiment

A, F_v/F_m responded significantly (P =0.0105) to Fe addition, while in experiment E, $ó_{PSII}$ responded significantly (P =0.0074) under low light to Fe alleviation.

Experiment D was the only experiment where the controls between light levels differed.

3.2.3.4) Chlorophyll-a

Similarly to the Fire data (section 3.1.1), a paired-samples t-test was conducted to separately compare chl-a under the same conditions.

Although there was an observable increase seen in chl-a concentrations in response to Fe additions (figure 24) in all experiments this was only significantly different from the controls in experiments D (P =0.041; 25% light), E (P =0.0175; 50% light) and F (P =0.0092; 50% light) (see table 6).

3.2.3.5) Nutrient concentrations

Unfortunately, the experimental nutrients values were incomprehensible and unrealistic (see appendix I for example), almost certainly due to poor on-board analyses combined with poor storage options (See appendix J for critique on these methods).

CHAPTER 4: DISCUSSION

Although the Southern Ocean is a HNLC ecosystem (Levitus *et al*., 1993; Sullivan *et al*., 1993; Moore and Abbott, 2000; Boyd *et al*., 2002; Seeyave et al., 2007), intense and sporadic chl-a blooms do occur (Arrigo *et al*., 2008) and their presence is controlled by the oceans physical and chemical environment. The open ocean north of the ice zone, away from fronts and shallow topography tends to have low primary production that has been attributed to Fe limitation (Sunda and Huntsman, 1997; Boyd *et al*., 2000; Sokolov and Rintoul, 2007). However blooms are known to form around frontal zones (Laubscher *et al*., 1993; Joubert *et al.,* 2011), sub-Antarctic islands (Blain *et al*., 2001; Seeyave *et al*., 2007) and in the marginal ice zone (Boyd, 2002; Dierssen *et al.,* 2002; Lannuzel *et al*., 2006).

Given the important contribution of these phytoplankton blooms to the Southern Ocean biological pump (Longhurst, 1991; Schlitzer, 2002), it is important for us to observe and characterise variability in both the physical mechanisms controlling primary production and the biological response to these forcing mechanisms.

The following section describes the physical and chemical environment encountered in the South Atlantic sector of the Southern Ocean in the austral summers of 2009 (SANAE 49) and 2010 (SANAE 50) together with the biological response in chlorophyll. In addition it makes inter-annual comparisons between the two years describing notable inter-annual variability in the physical and chemical environment as well as the biological response.

I: Physical, chemical and biological environment

4.1.1) Hydrography

Phytoplankton distribution, diversity, biomass and production depend on the physiological responses of phytoplankton to the often extreme conditions under which they live. The hydrography of the Southern Ocean is a key determinate of phytoplankton distribution via its effects on the light environment (through changes in the MLD) and the nutrient supply (through adjustments in stratification and mixing).

4.1.1.1) Hydrography between Antarctica and South Georgia

WW, the relatively homogeneous, subsurface temperature minimum layer (Park *et al.,* 1998), is evident on both cruises. This water originates from cooling in the previous winters mixed layer and is capped by seasonal warming and ice melt in the summer. UCDW and Lower Circumpolar Deep Water (LCDW) were present (below ~100m north of SACCF) in both years (figure 7 and 8). UCDW originates from the Indian and Pacific basin and is characterised by relatively warm, highly saline waters that are nutrient rich but low in oxygen (Callahan, 1972; Orsi *et al*., 1995; Veth *et al.,* 1997; Park *et al.,* 1998). Conversely, LCDW (below ~200m south of the SBdy) is nutrient poor and denser (figure 7 and 8); hence its position below UCDW.

4.1.1.2) Hydrography from Antarctica to Cape Town

The very distinctive temperature increase seen just south of South Africa is caused by the Agulhas Current, originating in the Indian Ocean. The warm (≥18ºC), salty (≥35.5 PSU), subtropical surface water of the Agulhas Current interacts with and warms the South Atlantic

through both anticyclonic ring (averaged 50 km wide, 50m deep) shedding from the Agulhas Retroflection Region and warm filaments of Agulhas Current Water (Gordon *et al.,* 1987; Lutjeharms and Cooper, 1996).

Temperatures decrease significantly as one moves south towards Antarctica. The deeper, colder, sinking WW can be seen in both years south of 50º S (figure 9).

4.1.1.3) Inter-annual variability in hydrography

Although frontal positions remained consistent within the property ranges given by Orsi *et al.,* (1995), some variability in position was observed between years. The SACCF moved from ~58º S to ~50º S from SANAE 49 to SANAE 50. The SBdy showed a slight northward movement between years moving from between ~59º S and ~60º S to ~57º S. On the northward leg, between the summers of 2009 (SANAE 49) and 2010 (SANAE 50) the STF and APF moved ~1º north, the SAF moved ~1º south, while the SACCF and SBdy moved <1º south and north respectively. As frontal regions are areas associated with increased chl-a (due to the upwelling of deep nutrient rich waters caused by diverging surface waters), slight movement of these fronts influences the distribution of chl-a blooms.

Changes in the MLD play a particularly important role in the Southern Ocean's biology due to its influence on the light environment that phytoplankton are exposed to. A deep mixed layer relative to the euphotic zone means that phytoplankton will be mixed outside of a favourable light environment, therefore negatively impacting photosynthesis. MLD's were deeper on the south eastward legs compared to the north westward legs of both SANAE 49 and 50. This is specifically noticeable south of the SBdy (figures 7 and 8).

Deeper MLD's later in the summer season are counter-intuitive given that MLD's are expected to shoal with seasonal warming. As such the deeper MLD's south of the SBdy on the south eastward legs are likely the result of localised wind events deepening the mixed layer.

4.1.1.4) Inter-annual variability in sea ice

As Southern Ocean blooms are tied to the timing between seasonal ice melt and available sunlight (Moore and Abbott, 2000), an overall comparison between the two years is useful. Melting ice is known to release Fe into surface waters (Dierssen *et al.,* 2002), additionally the increase in buoyancy from the input of fresh melt water leads to increased stratification in the water column, allowing the phytoplankton to experience favourable light conditions. These combined features allow both sufficient Fe and light needed for the formation of a phytoplankton bloom event. Sea surface conditions between the two consecutive summers were remarkably different, notably in terms of seasonal ice coverage. In 2009, extensive and thick ice was evident, while in 2010, sea-ice cover was minimal (table 1; NSIDC, 2012). This highlights inter-annual-variability, as frequently noted for example by Murphy *et al*., (1998) and Reid and Croxall (2001).

A consequence of variable sea ice cover is that the warm surface waters that were observed stretching southwards from South Georgia extended further south in 2010 (SANAE 50, figure 8) than they did in 2009 (SANAE 49, figure 7).

4.1.2) Nutrients

Nutrient concentrations are known to limit the growth of phytoplankton. This affects both the size (Sunda and Huntsman, 1995) and community structure (de Baar and Boyd, 2000; Smetacek *et al.,* 2004; Seeyave *et al.,* 2007) of the phytoplankton community. The most important limiting nutrients are Fe, NO_3 and SiO_4 (Boyd, 2002; Arrigo *et al*., 2008).

Fe is known to be limiting within the Southern Ocean, specifically in open ocean conditions north of the sea ice zone, away from fronts and continental land masses (Boyd *et al*., 2000; Sokolov and Rintoul, 2007). As the Fe data (responsibility of the CSIR and the University of Stellenbosch) remain unavailable at the time of writing, secondary indicators of Fe availability have been used.

Although all Southern Ocean waters are known to have high concentrations of NO_3 and PO_4, concentrations of SiO_4 are known to differ markedly from north to south. Subantarctic waters north of the Antarctic Polar Frontal (APF) have low SiO_4 concentrations (1 to 5 μmol l^{-1}), whereas high SiO_4 concentrations (> 60 μmol l^{-1}) are found south of the APF (Coale *et al*., 2004).

4.1.2.1) Nutrients between Antarctica and South Georgia

Neither NO_3 (>10 μmol l^{-1}) nor SiO_4 (>15 μmol l^{-1}) concentrations were limiting between Antarctica and South Georgia on either SANAE 49 or SANAE 50.

Both NO_3 and SiO_4 show an increase in concentrations with depth, and a decrease in concentration in the surface waters around South Georgia. This indicates the use of these

nutrients (by phytoplankton) in the surface waters, specifically around South Georgia (figures 10, 11, 12 and 13).

In increase in NO_3 concentrations is noted in the deeper waters between 62º S and 66º S on the south eastward leg of SANAE 49 (figure 10).

4.1.2.2) Nutrients from Antarctica to Cape Town

On both Antarctica to Cape Town transects neither NO_3 (>1 µmol l^{-1}) nor SiO_4 (>2 µmol l^{-1}) were limiting south of ~50º S (figure 10, 11, 12 and 13), however north of the APF (found at 50.08º S and 49.36º S on SANAE 49 and SANAE 50 respectively), SiO_4 concentrations dropped to below <2 µmol l^{-1} a concentration that is often considered limiting for diatom growth (Ragueneau *et al*., 2000; Peterson *et al*., 2005; Whitney *et al*., 2005). North of the northern STF at Northern STF ~39º S NO_3 concentrations fell to <1 µmol l^{-1}, limiting phytoplankton growth in these subtropical waters (e.g. Joubert *et al*., 2011).

4.1.2.3) Inter-annual variability in nutrients

Although, the relative geographic distribution of nutrients was similar for both SANAE 49 and 50, there were inter-annual differences between minima and maxima. On SANAE 49, the SiO_4 minimum was 0.09 µmol l^{-1} lower than on SANAE 50, whereas the NO_3 minimum was 0.36 µmol l^{-1} higher on SANAE 49. On SANAE 49, the SiO_4 maximum was 52.15 µmol l^{-1} lower than on SANAE 50, whereas the NO_3 maximum was 2.44 µmol l^{-1} higher on SANAE 49 (figures 10, 11, 12 and 13). Differences in nutrient concentrations can

be accounted for by natural variability and by differences in biological uptake and physical replenishment.

4.1.3) Chlorophyll-a

Chl-a is used as a proxy for phytoplankton biomass. As a complex interplay between nutrient availability and light controls the formation of chl-a blooms in the Southern Ocean (Raven, 1990; Sunda and Huntsman, 1997; Boyd *et al.,* 1999; Boyd, 2002; Hassler *et al.,* 2012), interpreting phytoplankton distribution in relation to the physical and chemical environment is key to understanding the mechanisms leading to phytoplankton adaptions and distributions in the oceans. This understanding becomes an imperative, as climate projections predict changes in the MLD and stratification, both of which influence nutrient and light availability (Greenblatt and Sarmiento, 2004).

4.1.3.1) Chlorophyll-a between Antarctica and South Georgia

There were two main areas containing chl-a blooms (here described as chl-a>1 $\mu g.l^{-1}$) between Antarctica and South Georgia (figure 14 and 15). These blooms occurred around South Georgia as well as between ~67º S and ~61º S. A third bloom was present in SANAE 50 at ~70º S (figure 15).

Both years saw an increase (reaching a maximum of 2.5 - 3 $\mu g.l^{-1}$ and 3.8 $\mu g.l^{-1}$ for 2009 and 2010 respectively) in chl-a associated with South Georgia (figure 14 and 15) which is likely due to natural Fe fertilization from shallow sediments associated with sub Antarctic islands (De Baar *et al*., 1995; Blain *et al*., 2001; Holeton *et al*., 2005; Seeyave *et al*., 2007) as

well as increased stratification due to increase buoyancy from fresh-water runoff (Joubert *et al*., 2011).

The blooms occurring between ~67º S and ~61º S are in the open ocean, largely away from divergent fronts. However in this region of marginal ice zone melting, which extends to ~55º S (at 10º E) in winter (NSIDC, 2012) is known to increase Fe in surface waters and improve light conditions through increased buoyancy (Joubert *et al*., 2011). This likely explains the presence of these blooms. In addition, during SANAE 49, it is noticeable that on the south eastward leg, the chl-a bloom at ~61º S (figure 14) corresponded with an increase in deeper NO_3 concentrations (figure 10). The deeper mixed layer on this return leg could account for mixing of this increased nutrient concentration in to the surface water, thus aiding this chl-a bloom.

4.1.3.2) Inter-annual variability in Chlorophyll-a

There were some substantial differences in the distribution and abundance of chl-a between 2009 (figure 14) and 2010 (figure 15). Although both years showed a general northward decrease in chl-a biomass between Antarctica and South Africa, this decrease differed slightly in both concentration (SANAE 49's maximum was higher than SANAE 50 by 0.68 $\mu g.l^{-1}$) and distribution of chl-a maxima. The distribution of the high chl-a region varied from 65.8º S to 57.5º S and from 70.6º S to 59.3º S for 2009 and 2010 respectively (figures 14 and 15). On SANAE 50, the maximum was higher (3.65 $\mu g.l^{-1}$) and further south (70.6º S) compared to SANAE 49 (2.57 $\mu g.l^{-1}$ at 65.8º S). A likely explanation of the more southward peak in chl-a on SANAE 50 was the ice conditions. SANAE 50 saw a smaller area

of sea ice cover (table 1) than during SANAE 49, thus allowing the formation of a more southerly bloom.

The chl-a blooms associated with South Georgia on the two years were different in that chl-a maxima were higher in 2010 (3.8 ug l^{-1}) than in 2009 (2.5-3.0 ug l^{-1}) (figure 15 and 14 respectively). Other differences include the notable lack of a bloom event on SANAE 50's north westward leg at 67º S and 62º S (figure 15). Chl-a blooms were evident at these positions on all three of the other transects (figures 14 and 15) namely SANAE 50's south eastward leg, as well as both of SANAE 49's legs to and from South Georgia. These differences could be due to a lack of a localised wind event on SANAE 50's north westward leg. In the Southern Ocean one expects the phytoplankton to bloom in spring with the release from light limitation (Venables and Moore, 2010), with these blooms decreasing in intensity as nutrients become limiting over summer. The deeper MLD's on the south eastward legs (of SANAE 49 and 50) compared to the north westward legs suggest increased wind events on the later south eastward legs that potentially mixed limiting nutrients into the surface waters accounting for the increase in Chl-a concentrations found later in the season.

II: Phytoplankton photo-physiology

Variability in FRRf values as a measure of physiological competency has been attributed to differences in phytoplankton community structure (Suggett *et al.,* 2004, 2009; Moore *et al.,* 2005), as well as light and Fe co-limitation (Greene *et al.,* 1991; Boyd and Abraham, 2001). Meanwhile macronutrient availability, temperature and salinity play lesser roles in regulating the FRRf response (Kolber *et al.,* 1988; Boyd and Abraham, 2001).

A low F_v/F_m and high σ_{PSII} reveals physiological stress brought on by environmental parameters, while the inverse reveals a healthy, efficient phytoplankton population (Holeton *et. al.,* 2005; Suggett *et al*., 2006; Moore *et al*., 2007b). This section focuses on discussing the photo-physiological "health" of phytoplankton based on FRRf measurements during SANAE 49 and 50 and assesses the environmental controls potentially accounting for differences in the measured photo-physiological responses.

4.2.1.1) Observed phytoplankton photo-physiology (FRRf)

Corresponding with past literature (Holeton *et al.,* 2005; Moore *et al*., 2007b), F_v/F_m and $ó_{PSII}$ values were the converse of each other (figures 18 and 20) throughout the summer of 2009. Over the summer of 2010, F_v/F_m and $ó_{PSII}$ values were largely the converse of each other (figures 19 and 21), with corresponding inverse values (of F_v/F_m and $ó_{PSII}$) north of 63º S (figure 19 b and 21 b), north of 40º S and around South Georgia (on the north westward leg) (figure 19 a and 21 a). During SANAE 49, there was however, one notable difference near South Georgia (on the south eastward leg), where the F_v/F_m values were high (reaching a maximum of ~0.45), indicating physiologically healthy cells, but $ó_{PSII}$ values were also unexpectedly high (253 ± 17.6 - 308 ± 73.6), rather than low as anticipated. This suggests that although the high F_v/F_m shows an increase in photosynthetic efficiency, part of the photosynthetic process is undergoing photosynthetic stress (high $ó_{PSII}$). Hence it is possible that the population in this region is undergoing change, either in photosynthetic health or in community structure. Considering the photosynthetic health, enough Fe could be allowing F_v/F_m to function efficiently, but with insufficient Fe for this to apply to $ó_{PSII}$ as well. However, considering that both parameters are an indication of the functioning of PS II, this explanation is unlikely. Alternatively, the low light, storm conditions that occurred during

this section of the transect supports the notion that though some Fe alleviation occurred, the phytoplankton were still struggling to function efficiently under low light conditions. Considering community structure, the data (figure 17) shows an increase in diatom dominance (from ± 45% to >60%, figure 17 a) as well as an increase in the diatom to haptophyte ratio (showing a move towards diatom dominance) on the south eastward leg around South Georgia (figure 17 d). This dominance corresponds with that found by Gibberd *et al*., (2013), who studied the same are, the previous year. It is possible that the changing phytoplankton community was receiving enough Fe to increase its photosynthetic efficiency through F_v/F_m and become a diatom dominated community, despite the still prevalent inefficiency in $ó_{PSII.}$

The phytoplankton photo-physiology FRRf parameters of F_v/F_m were remarkably similar between the austral summers of 2009 and 2010. High F_v/F_m (reaching a maximum of >0.4 for both years) characterised the region around South Georgia and South of 60º S, although highest F_v/F_m values were at depth in 2009, but on the surface in 2010. The moderate to low values (<0.2) in the remaining areas between Antarctica and South Georgia were also consistent for both years.

From these data, the areas of high photosynthetic efficiency are near South Georgia, in the deeper waters near Antarctica and to a lesser extent around the SBdy and SACCF. These are areas known for elevated Fe concentrations (Laubscher *et al*., 1993; Blain *et al*., 2001; Seeyave *et al*., 2007; Joubert *et al.,* 2011) and as such, Fe alleviation is thought to be the main driver of the high, efficient FRRf values found here. Conversely, the areas between these high photosynthetic efficiency regions are typically low in Fe as they are distant from fronts and shallow topography and terrestrial sources (Sunda and Huntsman, 1997; Boyd *et*

al., 2000; Sokolov and Rintoul, 2007) such that Fe limitation is the likely cause of low photosynthetic efficiency values found here.

4.2.2) Statistical evidence for controls on photo-physiology

To identify the major controlling factors behind the FRRf values, two main statistical tests were carried out to relate the photosynthetic parameters (F_v/F_m and σ_{PSII}) to environmental factors. These tests focused on the SANAE 49 (2009) cruise only due to the more complete nature of this data set, which included HPLC. The first test was a linear analysis that compared F_v/F_m and σ_{PSII} to a number of environmental factors (temperature, salinity, PAR, SiO_4, NO_3, oxygen) and phytoplankton indices (chl-a, fluorescence, community structure). The community structure was classified according to three main phytoplankton groups (diatoms, 49%; haptophytes, 29%; and chromophytes, 8%).

The following variables were all significantly related to values of F_v/F_m: chl-a and PAR ($P < 0.001$), SiO_4, oxygen and fluorescence ($P < 0.01$) and haptophytes ($P < 0.05$).

Whereas the following where all significantly related to $ó_{PSII:}$ Fluorescence ($P < 0.001$), chl-a and salinity ($P < 0.01$), NO_3, diatoms and chromophytes ($P < 0.05$).

In the second test, the community structure data was replaced with the Fuc:Hex ratio (as used by: Barlow *et al*., 1998; Smith and Asper, 2001; Hirata *et al.,* 2008; Feng *et al.,* 2010; Alderkamp *et al.,* 2012). Fuc:Hex ratio is used to determine the relative abundance of diatoms to *P. antarctica* within Antarctic phytoplankton populations (Alderkamp *et al.,* 2012). If the Fuc:Hex ratio increases, there are more diatoms relative to *P. antarctica* and

vice versa. The main known cause of a shift towards a diatom-dominated community is Fe alleviation (Boyd *et al*., 2000). Within Fe fertilised areas diatom growth can be further increased by increased light and SiO_4 concentrations (Boyd, 2002), as well as increased CO_2 concentrations (Tortell *et al*., 2008). Increased stratification of surface waters is also known to favour an increase in the Fuc:Hex ratio (Arrigo *et al*., 1999). Furthermore, an increase in diatoms relative to *P. antarctica* implies major changes in the heterotrophic community. This likely results in an increase in downward carbon fluxes due to an increase in the efficiency of the herbivorous food web, thus enhancing the export of CO_2 into the deeper ocean (Fonda Umani *et al*., 2002, 2005).

The community structure in this instance now gains the most significant influence; with F_v/F_m now significantly related to Fuc:Hex ($P < 0.0001$), oxygen and PAR ($P < 0.001$), chl-a and salinity ($P < 0.01$), SiO_4, NO_3 and fluorescence ($P < 0.05$).

The statistical relationship with $ó_{PSII}$ and community structure also improved as follows: Fuc:Hex and fluorescence ($P < 0.01$), chl-a and salinity ($P < 0.05$).

Though strongly significant relationships can be drawn between F_v/F_m and $ó_{PSII}$ in the linear regressions (section 3.1.6.2), the complexity of the South Ocean system, in relation to photosynthetic efficiency, is highlighted by Figure 23 where individual parameter comparison is inconclusive.

The results of the linear regression statistical tests are elaborated on in the following sections, explaining the role of the various environmental and biological factors influencing the statistical relationships between phytoplankton photo-physiology and the environment.

4.2.2.1) Fe availability as a driver of photo-physiology

Past literature shows that the most influential factors behind phytoplankton's photosynthetic efficiency are known to be Fe and taxonomic community structure (Suggett *et al.,* 2009). Unfortunately, the Fe data for this investigation is not available at this time, hence the interpretations presented here between photo-physiology and Fe are speculative, but based on published observations.

Indirect indicators for the presence of Fe in the HNLC waters of the Southern Ocean include: phytoplankton community structure and NO_3 uptake. Haptophyte dominance is found in areas of limiting Fe, while diatom dominated communities are found in regions of sufficient Fe (Sakshaug *et al*., 1991; Laubscher *et al*., 1993; de Baar *et al*., 1995; Smetacek *et al*., 1997; Boyd, 2002; Gibberd *et al*., 2913). In addition, f-ratios typically increase with increasing Fe availability (Lucas *et al.,* 2007) due to the high Fe demand of NO_3 reduction (Lucas, 2009). Conversely, where Fe is limited, NO_3 uptake and its intracellular reduction to NH_4 via the Fe dependent enzymes nitrate and nitrite reductase is compromised (Lehninger, 1975), resulting in low f-ratios (<0.2) and low specific uptake rates (VNO_3) despite high ambient NO_3 concentrations (Lucas *et al*., 2007).

NO_3 uptake in the Southern Ocean may also be inferred by changes in the SiO_4:NO_3 ratios. If the SiO_4:NO_3 ratio becomes high (>1.5), there is little SiO_4 removed relative to NO_3. This occurs in Fe limiting regions. On the other hand, increased uptake rates of SiO_4 to an equal uptake rate of SiO_4 and NO_3 in the presence of sufficient Fe can shift the ambient SiO_4:NO_3 ratios towards a low ratio of 1.1. Although not conclusive, increased concentrations of NO_3 and SiO_4 in surface waters can imply upwelling of deeper nutrient rich

waters with similarly increased Fe concentrations. Such combined upwelling of Fe and other macronutrients has been found off Peru (Bruland *et al*., 2005).

Following this argument, on the south eastward leg from 58º S to 54º S (figure 16) high f-ratios (up to 0.22) suggests the presence of Fe associated with South Georgia. Similarly, Fe limitation is thought to account for the low f-ratios (<0.06) found in the middle of the ocean away from known Fe sources (Boyd *et al*., 2000; Sokolov and Rintoul, 2007). On the north westward leg from 66º S to 62º S high f-ratios (reaching 0.37) similarly reveal a likely Fe source in surface waters off Antarctica. Fe enrichment in these waters is known to occur through upwelling of Fe rich water along the continental margin (Lannuzel *et al*., 2006) that is enriched by glacial scouring of underlying rocks (Dierssen *et al.,* 2002) and by accumulation from atmospheric deposition of dust that is released into the surface ocean during ice melt (Dierssen *et al.,* 2002; Lannuzel *et al*., 2006). F-ratios decreased with depth, most notably below 30m on the north westward leg, nearing South Georgia (figure 16). This finding of low f-ratios at depth can be explained by light limitation rather than Fe limitation, as NO_3 uptake is energy expensive and has a high light demand (as seen by the Michaelis-Menten equation [MacIsaac and Dugdale, 1972; Kudela *et al*., 1997]). Rather than low Fe concentrations, low f-ratios found near South Georgia likely reveal phytoplankton's preference for reduced nitrogen in the form of NH_4 (Eppley and Peterso, 1979; Lucas *et al*., 2007; Joubert *et al*., 2011), which is often abundant in surface waters of subantarctic archipelago's due to high annual rainfall transporting terrestrial sources offshore (Ismail, 1990).

As f-ratios are dependent on ambient NO_3 data, it should be remembered here that the SANAE 49 NO_3 data underwent a correction. However, table 2 reveal that a 10% change in

ambient NO_3 leads to a 5-9% change in f-ratio. This shows a low sensitivity to variation in NO_3.

Increases in NO_3 concentrations (figure 10) corresponded with increases in F_v/F_m (figure 18), specifically near South Georgia, implying that upwelled waters are enriched by both NO_3 and Fe (Hiscock, 2004), where elevated F_v/F_m values are likely due to enhanced Fe availability (Suggett *et al.,* 2009). Similar results were found in a study by Fung *et al,.* (2000) and Pollard *et al.,* (2009) where Fe was made available to phytoplankton around Crozet, from a shallow sedimentary source and from island runoff, resulting in high values of F_v/F_m, characteristic of Fe-replete cells (Suggett *et al.,* 2009). This conclusion is statistically supported by the significant positive correlation between NO_3 and F_v/F_m in test c (methods section 3.1.5) ($P < 0.05$) and the significant negative correlation between NO_3 and $ó_{PSII}$ in tests b ($P < 0.05$). These observations suggest a benthic or sedimentary source of Fe into surface waters around South Georgia, as with the Crozet Islands (Pollard *et al*., 2009; Venables and Moore, 2010). Increased NO_3 concentrations (figure 10) corresponding with increases in F_v/F_m (figure 18) were also noted below 40m around the SBdy on both legs where frontal upwelling is expected to increase Fe supply to surface waters (Laubscher *et al*., 1993; Joubert *et al.,* 2011), Similarly, near Antarctica photo-physiological responses were improved at depth where F_v/F_m increased suggest upwelling of Fe along the continental shelf.

The presence of Fe downstream of South Georgia and adjacent to Antarctica is also indicated through relative SiO_4 depletion (which implies active diatom growth) and community structure adjustments to a diatom dominated community (figure 17). Diatoms thrive in Fe alleviated waters (Coale *et al.,* 1996; de Baar and Boyd, 2000) and correspond with the drawdown of SiO_4 (Coale *et al.,* 1996). In the Southern Ocean, between Antarctica

and South Georgia, SiO_4 is never limiting (Timmermans, 2004 and figure 12), and so not expected to negatively control diatom growth. However, low SiO_4 concentrations (5.45 µmol l¯) in surface waters downstream of South Georgia (figure 12) statistically correlate negatively ($P < 0.01$ and < 0.05 for tests a and c respectively) with high F_v/F_m, (figure 18) and positively with low $ó_{PSII}$ (figure 20). This indicates that where F_v/F_m values were high SiO_4 concentrations were lowered, such that an Fe-replete diatom community was responsible for the reduction in SiO_4 concentrations. Community structure data and *in situ* SiO_4:NO_3 ratios further support this argument with diatoms dominating the community structure close to Antarctica and near South Georgia (figure 17), while lower SiO_4:NO_3 ratios (figure 22) found in surface waters around South Georgia support either a terrestrial runoff source of Fe or upwelling very close to the island that supports diatom growth. Similarly, the lower SiO_4:NO_3 ratios in deeper waters off Antarctica support Fe upwelling in this region. Though unusual to have enhanced diatom growth at depth, SANAE 49 HPLC data (figure 17) shows it can occur off South Georgia. Higher SiO_4:NO_3 removal ratios that depart from 1:1 towards 3:1 or more, as one moves away from South Georgia and Antarctica into open waters, implies increased Fe-limitation of diatom growth as well as a shift towards NO_3 uptake by phytoplankton other than diatoms. A similar scenario was observed in studies around the Crozet Islands (Moore *et al.,* 2007a, 2007b).

4.2.2.2) Community structure as a driver of photo-physiology

The development of different phytoplankton under various environmental conditions ensures adaptation, through evolution, of taxa. As different taxa are exposed to different yearly light and nutrient conditions, their photo-physiology will vary. This section looks at the community structure (though HPLC data), and the influence it has on the photosynthetic parameters over the summer of 2009.

It has already been shown that the ratio of diatoms to haptophytes significantly ($P < 0.0001$) controls F_v/F_m, where the presence of actively growing diatoms elevate F_v/F_m, and less significantly ($P < 0.01$) $ó_{PSII}$ values.

Individually the three predominant phytoplankton groups (diatoms, haptophytes and chromophytes) have a less significant effect on the photosynthetic parameters compared to the Fuc:Hex ratio. An increase in haptophytes sees a significant decrease ($P < 0.05$) in F_v/F_m, while an increase in diatoms and chromophyte both see a slight significant (both $P < 0.05$) increase in $ó_{PSII.}$

These statistical results show that when looking at photo-physiology and community structure; it is the population as a whole (seen by Fuc:Hex ratio) which is important in influencing the photosynthetic efficiency, rather than the individual phytoplankton groups.

The best-known haptophytes are coccolithophores and *Phaeocystis* species. Coccolithophores, with their calcareous 'liths', are key particulate inorganic carbon (PIC) exporters in the biological pump, despite CO_2 being released to the atmosphere during the process of $CaCO_3$ formation, (Poulton *et al*., 2007). Coccolithophores tend to occupy the open ocean basins north of the APF, in warmer temperatures and lower calcite saturation states (Poulton *et al*., 2007, 2010). *Phaeocystis* species occurs in the open ocean basins south of the APF where low SiO_4 concentrations limit diatom growth, with the exception of the Ross Sea, where the *Phaeocystis's* efficient photo-physiology allows an early spring bloom (Arrigo *et al*., 1999; Boyd, 2002). *Phaeocystis* species are also dominant in the Atlantic section of the Southern Ocean near the ice shelf (Gibberd *et al.,* 2013). Diatoms are found in

Fe alleviated area such as around fronts and islands (Sakshaug *et al*., 1991; Laubscher *et al*., 1993; de Baar *et al*., 1995; Smetacek *et al*., 1997; Boyd, 2002; Gibberd *et al*., 2013). Diatoms, with their silica ballast, are also important exporters of carbon through the biological pump. Diatoms and *Phaeocystis* species are often the dominant phytoplankton taxa in Southern Ocean waters (Arrigo *et al*., 1999; Boyd, 2002; Poulton *et al*., 2007; Hassler *et al.,* 2012). Chromophytes on the other hand are scarce in the Southern Ocean relative to diatoms and haptophytes and are more usually dominated by brown seaweeds (Jeffrey *et al.,* 1997).

The simplified statement that diatoms dominate around South Georgia and adjacent to Antarctica, while haptophytes occupy in the open ocean basins, can be explained through the Fe hypothesis. This hypothesis states that the physiological nature of phytoplankton and the environment in which they live will determine their distribution. The Fe hypothesis, first proposed by Martin *et al.,* in 1990, explains the dominance of smaller pico- and nano phytoplankton (Gervais *et al.,* 2002) such as haptophytes in Fe limited seas. Unlike larger phytoplankton (e.g. large diatoms), smaller species have high surface to volume ratios facilitating the uptake of Fe at low concentrations (Sunda and Huntsman, 1995). Smaller species, with lower overall demands for Fe, are likely to have higher photosynthetic efficiency under low Fe conditions, compared to larger phytoplankton, which cannot function optimally under the same low Fe conditions. When an area is freed from Fe limitation the community structure changes, becoming dominated by larger phytoplankton species such as diatoms (de Baar and Boyd, 2000; Smetacek *et al.,* 2004; Seeyave *et al.,* 2007). Apart from increased growth rates in Fe-replete waters, larger phytoplankton are less prone to grazing pressure (Hoffmann *et al.,* 2006), so emerge as a dominant group. Herbivorous mesozooplankton that feed on large cells including large diatoms have a relatively long

generation time and therefore cannot control a fast growing phytoplankton biomass where doubling times are measured in hours rather than days. On the other hand, microzooplankton have a short generation time, and so are able to control the biomass of smaller phytoplankton species (Coale *et al.,* 1996).

Unlike the other diatom patches near South Georgia and the Antarctic continent mentioned earlier, which all corresponded with high F_v/F_m values, a more unusual diatom patch was encountered just north of 64º S (figure 17) where F_v/F_m values were relatively low (~0.3) (figure 18). A possible explanation for the low photo-physiological efficiency of this particular patch of diatoms is that it developed previously due to an input of Fe into the system, which has now been exhausted. At low Fe concentrations the diatoms start becoming less photosynthetically efficient (Greene *et al*., 1991), but have not yet decreased in dominance. The weakening of this populations photosynthetic efficiency will likely result in a decrease in their dominance, and a shift towards a smaller phytoplankton population that is more efficient at taking up Fe at lower concentrations such that the F_v/F_m values will once again increase, though this is not yet apparent in this patch. Hence, phytoplankton efficiency increases in response to both Fe alleviation and an associated shift in community structure; however the photosynthetic parameters indicate the health of the population rather than its population dynamics.

4.2.2.3) Other factors influencing F_v/F_m and $ó_{PSII}$

Chlorophyll-a

Chl-a concentration exhibits a significant positive correlation with F_v/F_m ($P < 0.001$, < 0.01 for tests a and c respectively) and a significant negative correlation with $ó_{PSII}$ ($P < 0.01$, < 0.05 for linear regressions tests b, and d respectively). This is hardly surprising for two reasons. Firstly, high chl-a concentrations imply fast growth rates of phytoplankton, such that biomass is accumulating despite predation pressure from zooplankton (Fielding *et al.,* 2007). This would not occur in an environment that was limited by either Fe or light. Secondly, although this is chl-a specific, where there is more chlorophyll present per phytoplankton cell, the more effective it will be at photosynthesis, thus reflecting higher F_v/F_m values and lower $ó_{PSII}$ values. Similar results have been recorded in a number of Fe addition bio-assay experiments where both chl-a concentrations and F_v/F_m values are shown to increase in response to Fe addition while $ó_{PSII}$ decreases (Moore *et al.,* 2007a, 2007b).

PAR and fluorescence

The Southern Ocean is often considered to be light limited (Hiscock, 2004), either due to low ambient PAR or to deep MLD's. Light is a requirement for photosynthesis, such that F_v/F_m is driven by a changing light field which is particularly significant in the often light limited Southern Ocean (Sunda and Huntsman, 1997; Lindley and Barber, 1998; Timmermans *et al.,* 2001; Moore *et al.,* 2007a, 2007b). Evolutionary trends indicate that different phytoplankton groups can be found at different light depths. Between these groups, the arrangement of pigments housed within the light-harvesting antennae will vary greatly

(MacIntyre *et al.,* 2002; Johnsen and Sakshaug, 2007), leading to differences in both PS II light-harvesting potential and efficiency (Lutz *et al.,* 2001). This, along with the fact that the number of photochemically competent reaction centres can vary as a function of irradiance (Neale, 1987; Long *et al.,* 1994; Vassiliev *et al.,* 1994; Babin *et al.,* 1996) ensures that F_v/F_m and $ó_{PSII}$ values vary with PAR and fluorescence (Suggett *et al.,* 2009), as seen by the statistical analyses.

III: Nutrient ratios and phytoplankton community structure

Nutrient inputs through ocean circulation, and winter mixing resets the Southern Oceans nutrient concentrations annually. Therefore seasonal changes in the nutrient ratios reflect nutrient uptake by the phytoplankton community structure that forms. However, the relationship between the source, use and therefore concentration of nutrients and the community structure of phytoplankton is complex. A diatom dominated community takes up SiO_3 and NO_3 and leaves behind a characteristically low SiO_4:NO_3 ratio (<1.5). However when Fe is limiting, haptophytes dominate the community such that the SiO_4:NO_3 uptake ratio increases, leaving a trace in the ratio SiO_4:NO_3 left behind (Takeda 1998). Fe availability also drives SiO_3 and NO_3 removal by individual species, with a limitation of Fe limiting NO_3 removal and enhancing the uptake of SiO_4 per unit of NO_3.

Concerns over the quality of the SANAE 49 nutrient data (Section 2.4.3), undermine the confidence of the following discussion concerning the SANAE 29 nutrient ratio's and community structure. However, this lack of confidence does not apply regarding the SANAE 50 data sets.

4.3.1) SANAE 49: Nutrient ratio's and Community Structure

The NO_3:PO_4 ratio bore no relationship to the community structure using HPLC, in contrast with Arrigo *et al.,* (1999) who showed that the NO_3:PO_4 draw-down ratio was twice as high for *Phaeocystis antarctica* (19.2 ± 0.61) than for diatoms (9.69 ± 0.33). The SiO_4:NO_3 removal ratio does however reflect community composition, in that low SiO_4:NO_3 ratios (figure 22) coincide with diatom dominated communities (figure 17). This confirms Holeton's *et al.,* (2005) finding that variation in SiO_4 concentrations can indicate the presence of diatoms. In waters between Antarctica and South Georgia, a high SiO_4:NO_3 ratio was linked with high haptophyte and low diatom concentrations, as well as low Fuc:Hex values.

4.3.2) SANAE 50: Nutrient ratio's and Community Structure

The low SiO_4:NO_3 drawdown ratio's (table 3) found north of the SACCF, around South Georgia (0.25 and 0.32 for the north westward and south eastward legs respectively) reveal a diatom dominated community in this region. This finding is supported by Gibbert *et al*., (2013). The dominance of diatoms can be explained by the presence of Fe (diatom dominated communities are found in areas of sufficient Fe [Sakshaug *et al*., 1991; Laubscher *et al*., 1993; de Baar *et al*., 1995; Smetacek *et al*., 1997; Boyd, 2002]). A 1:1 removal ratio indicates that both nutrients have been taken up by the phytoplankton in a 1:1 molar ratio (Brzezinski, 1985), implying Fe-availability.

Between South Africa and Antarctica, the regions between the northern STF and APF all reveal a low (<1.5) SiO_4:NO_3 removal ratio (table 3), suggesting a diatom dominated

community. These regions are all narrow frontal regions, which accounts for the diatom dominance which this ratio reveals (Laubscher *et al*., 1993; Joubert *et al.,* 2011).

Between Antarctica and South Georgia, the moderately high (<1.5) SiO_4:NO_3 removal ratio's found south of the SACCF (table 3) reveal a high removal of NO_3 relative to SiO_4. This suggests haptophyte-dominated community and associated iron limitation in this region. The high (>1.5) SiO_4:NO_3 ratio between South Africa and the northern STF reveals a haptophyte dominated community within this region, this finding is supported by Gibbert *et al*., 2013.

The changing removal ratios from a low (1.6) to a high (4.8) between South Africa and the northern STF reveal a shift to a more haptophyte dominated community here. While the inverse is seen between the APF and the iceshelf revealing a shift in community structure (between the southern and northward legs), with increasing diatom numbers, resulting in an outright shift to diatom dominance on the northward leg between the APF and the SBdy.

The positive differences in SiO_4 and NO_3 between the earlier north westward and south eastward legs reveal a continued drawdown of both these nutrients in these regions. The negative differences in SiO_4 (-1.45 μmol l^{-1}) and NO_3 (-0.76 μmol l^{-1}) between the earlier north westward and south eastward legs (around South Georgia) reveals an introduction of SiO_4 into the region (probably through upwelling, which may indicate Fe upwelling in the region as well), together with a tendency for phytoplankton to use nitrogen in the form of NH_4 rather than NO_3. Similarly, the negative difference (-0.75 μmol l^{-1}) in SiO_4 between the southward and northward legs, north of the northern STF also reveals an input of SiO_4 into the system around South Africa. While the negative difference in NO_3 (-25.01 μmol l^{-1})

between the southward and northward legs south of 69º S show a preference for the phytoplankton to use NH_4 or nitrogen assimilation at the ice shelf.

IV: Experimental Fe incubation results during SANAE 50

4.4.1) Overall control and contamination of experiments

The form of Fe added in these experiments was $FeSO_4$; chosen for two reasons: Firstly, through the atmospheric deposition of dust, it is believed that Fe is transported between systems in the form of $FeSO_4$ (Zhuang and Duce, 1993). Secondly, IronEx2 clearly shows that any changes brought about by the addition of acidic $FeSO_4$, is due to the Fe, not the sulphate or miniscule changes in pH (Coale *et al.,* 1996). Hence, changes brought about in phytoplankton production can be attributed to the Fe only.

Three of the experiments (B, C and D) contained overall controls (figure 24). These were bottles at 50% light that remained closed for the duration of the experiment, any difference between this bottle, and the 5th day 50% control bottles highlights any sub sampling contamination in the experimental bottles. Experiment D reveals no differences in F_v/F_m or $ó_{PSII}$ between the overall control and 50% control bottles on the 5th day, thus showing no contamination during subsampling in this experiment. Experiment C shows that the overall control (0.18) has a lower F_v/F_m value than the 5th day 50% control (0.26 ± 0.048), revealing that there was probably slight contamination during the removal of sub-samples, and that the Fe fertilization has a greater effect than shown in this study (this contamination signal is not evident in $ó_{PSII}$, suggesting that the contamination is only slight). Experiment B shows the F_v/F_m for the overall control (0.38) to be higher than the 5th day 50% control (0.29

± 0.049) (no difference in $ó_{PSII}$), suggesting that sub sampling saw the contamination with a substance that had a negative effect on the phytoplankton. Over all, there was little (experiment B and C) or no (experiment D) contamination during subsampling during this study.

4.4.2) Introduction to experiments:

The SOIREE (Boyd and Abraham, 2001) and CROZEX (Moore *et al.,* 2007a, 2007b) Fe fertilization experiments clearly revealed an increase in photosynthetic efficiency of the phytoplankton (through an increase in F_v/F_m values and a decrease in $ó_{PSII}$ values), an increase in chl-a concentrations, a decrease in NO_3 concentration, and an increase in CO_2 drawdown. However the degree to which the efficiency is increased as well as the magnitude of the resulting Chl-a increase is still a matter of discussion. In this investigation, the Fe alleviation incubations were conducted in varying areas of the Southern Ocean south of Africa, under varying initial conditions. The experiments clearly show an increase in the photo-physiological health of phytoplankton, as previously shown (Boyd and Abraham, 2001; Moore *et al.,* 2007b). The variation seen in the photophysical efficiencies response to Fe addition between experiments, and the factors behind it, are discussed below.

4.4.3) Relationship of photo-physiology to Fe alleviation

All the experiments show a statistically significant increase in photosynthetic ability for both, or, either F_v/F_m and $ó_{PSII}$ when Fe is added (figure 24 and table 6). Thus, when Fe is added in the Southern Ocean, the photosynthetic efficiency of phytoplankton increases, however, the degree of this changes, and the response time varies.

The variation observed between experiments, despite an overall positive response to Fe alleviation, is consistent with the results of Moore *et al.,* (2007b). The differences they observed were accounted for by variability in initial community structure, stage of the bloom and availability of Fe and possibly silicic acid prior to manipulation (Moore *et al.,* 2007a).

In this study, Experiment B, performed south of the SBdy in ice-free conditions (table 4), shows the most statistically significant changes in photosynthetic efficiency. The addition of Fe caused an increase in efficiency in both F_v/F_m and $ó_{PSII}$ at low light (F_v/F_m increased from 0.27 ± 0.000 to 0.47 ± 0.016 and $ó_{PSII}$ decreased from 214 ± 0.0 to 189 ± 15.9 [while the controls ended after five days at 251 ± 16.9 and 0.28 ± 0.031 for F_v/F_m and $ó_{PSII}$ respectively]). This improvement in efficiency was also seen at high light levels (where F_v/F_m increased from 0.27 ± 0.000 to 0.47 ± 0.014 and $ó_{PSII}$ decreased from 214 ± 0.0 to 198 ± 6.1 [while the controls ended after five days at 0.29 ± 0.049 and 219 ± 13.5 for F_v/F_m and $ó_{PSII}$ respectively]). Although there is no statistical difference between the Fe addition bottles at 50% and 25% light, the clear statistical differences (figure 24 and table 6) between the Fe supplemented bottles and control bottles without Fe shows that Fe additions improved photosynthetic efficiency in all regions sampled in the Southern Ocean and consequently that primary production in these regions is Fe limited.

Experiment D, conducted at the ice shelf (table 5), was the only site that showed a statistical difference (final difference at day 5: 0.14 and 34 for F_v/F_m and $ó_{PSII}$ respectively) in photophysical responses in the control bottles without Fe alleviation at the two different light levels (table 6). This difference in the importance of light levels diminishes under Fe alleviation. As at 50% light (Fe addition), only $ó_{PSII}$ remains significant (P =0.0025), while at 25% light under Fe alleviation both the photophysical (P value for F_v/F_m and $ó_{PSII}$ is 0.0001

and 0.0000005 respectively) and chlorophyll (P =0.041) response improved significantly. Thus, at the iceshelf, Fe significantly changes the ability of phytoplankton to photosynthesis efficiently at depth where light is limited.

For experiments C (conducted south of the SBdy, in the presence of icebergs, table 4) and F (conducted in the Antarctic Polar Zone [APZ], table 4), both physiological indices (F_v/F_m and $ó_{PSII}$) responded to Fe alleviation, however this positive response occurred at only one light depth but not the other. For experiment C, Fe alleviation elevated the physiological response at 50% light, whereas in Experiment F, Fe alleviation elevated the physiological response at 25%. These results suggest that the response to light and Fe co-limitation is not entirely predictable and almost certainly complicated by the taxonomic composition of the community, which is adapted to the *in situ* light environments (see also Moore *et al.,* 2007a, 2007b). Complications introduced by the taxonomic composition of the community is discussed under the next section (Fe alleviation and chlorophyll response).

Again as Moore *et al.,* (2007a, 2007b) noted, responses in the incubation experiments showed variability from day zero to 1-2 days that were independent of initial weather conditions or the previous light history (PAR) experienced by the phytoplankton. Since sampling of the experiments was done at night, potential 'light-shock' effects can be disregarded. Temperature does not significantly alter photo-physiological responses either, as shown by the statistical analyses in Chapter three (Section 3.1.5). Variability in F_v/F_m and $ó_{PSII}$ between experiments was almost certainly due to different taxa, as previously noted. Changes in F_v/F_m and $ó_{PSII}$ responded relatively quickly, but changes in biomass and nutrient take longer.

4.4.4) Fe alleviation and chlorophyll response

Past literature (Boyd and Abraham, 2001; Moore *et al.,* 2007b) clearly indicates that Fe alleviation, whether natural or artificial causes a chl-a bloom that occurs after the PS II and PS I responses. Chl-a concentrations increased during all treatments in all experiments, in the Fe-supplemented bottles, but also in the controls. However, a statistically significant difference between the Fe addition and controls was only evident in three of the experiments in this investigation (experiment D, E and F).

In experiment D (conducted at the ice shelf, table 4) the chl-a in the 25% Fe alleviated bottles was higher (7.1 $\mu g.l^{-1} \pm 0.32$) than in the controls (4.3 $\mu g.l^{-1} \pm 0.54$) (there was an overall significant difference [p =0.02] between all the Fe bottles and all the controls). Similarly for experiment E (conducted between the SBdy and SACCF, table 4) chl-a in the 50% Fe alleviated bottles was (0.49 $\mu g.l^{-1} \pm 0.04$) versus the controls (0.42 $\mu g.l^{-1} \pm 0.04$) and in experiment F (conducted in the APZ, table 4) chl-a in the 50% Fe alleviated bottles was (2.1 $\mu g.l^{-1} \pm 0.05$) versus the controls (1.3 $\mu g.l^{-1} \pm 0.24$). Experiment F also showed an overall significant difference [p =0.02] between all the Fe bottles and all the controls. These results indicate that in three of the experiments Fe addition led to a significant increase in chl-a (relative to the non Fe controls) which is likely a direct result of enhanced productivity via increased photosynthetic efficiency in the Fe addition bottles.

FRRf can be interpreted in relation to community structure (Suggett *et al.,* 2004, 2009; Moore *et al.,* 2005) rather than photosynthetic efficiency affected by nutrient stress (Kolber *et al.,* 1988; Greene *et al.,* 1991; Boyd and Abraham, 2001). This could be used to further explain the lack of a significant chl-a increase in Fe alleviated incubations. Rather than an increase of the photosynthetic efficiency of the phytoplankton species present, the

FRRf values could show a changing community structure in response to Fe alleviation. However, a study of the controlling factors of F_v/F_m and σ_{PSII} (Section 2 of this discussion) reveal that the changes in FRRf parameters are more likely to be related to Fe related physiological changes then a community structure shift.

The lack of any statistically significant chl-a response in the remaining three experiments (A, B and C) may be explained by two different possibilities. Firstly the original community structure of the phytoplankton and secondly by bottle effects.

4.4.4.1) Community structure and Fe alleviation

The influence of community structure on Fe fertilization and resulting chl-a blooms is based on evolutionary theory. Different oceanic regions are subject to different conditions in which phytoplankton need to adapt and thrive, resulting in differing community structures throughout the world's oceans. As phytoplankton species have adapted to different conditions, they will respond differently to changes in their environment. The community structure for these incubations was gained through the nutrient data (Section 3 of this discussion) and backed up by past published research.

Experiment's A, B and C all began with high SiO_4:NO_3 ratio's (>1.5) found in the waters between Antarctica and South Georgia (before the SACCF). These experiments were thus most likely initiated in haptophyte-dominated communities of the Fe-limited open ocean.

Conversely, experiments D, E and F are all considered to be initiated in a community where diatoms were prevalent. Low SiO_4:NO_3 ratios of experiment E and F were 1.45 and

0.12 respectively revealing a diatom dominated community. Diatoms are known to be prevalent in the high Fe waters of the marginal ice zone of Experiment D (Laubscher *et al*., 1993; de Baar *et al*., 1995; de Baar and Boyd, 2000; Boyd, 2002; Dierssen *et al.,* 2002; Lannuzel *et al*., 2006). Despite the high SiO_4:NO_3 ratios found at this station, Ceinwen Smith, working on microscopy data, confirmed a haptophyte dominated community, but with the presence of the chain forming *Chaetoceros* diatoms (personal communication), the finding of a haptophyte dominated community in this marginal ice zone is further confirmed for the late summer of 2009 by Gibberd *et al*., (2013).

It is significant that the three experiments which developed statistically significant increases in chl-a all began in either diatom dominated (experiment E and F) communities or in communities containing large chain forming diatoms (experiment D). Diatoms have a faster growth rate than the herbivorous mesozooplankton that prey on them. As such they are able to escape grazing pressure allowing an increase in population abundance and the statistically significant increase in measured chl-a. Conversely, experiments A, B and C began in smaller haptophyte dominated communities, where an increase in Fe probably led to an increase in production (as witnessed by the increase in photosynthetic parameters). However, the microzooplankton which graze on small haptophytes and other small taxa have a short generation time that is more evenly matched by their haptophyte prey, such that they were able to control net community growth, so preventing an increase in observed chl-a biomass (Coale *et al.,* 1996).

4.4.4.6) Bottle effects

A second theory states that bottle effects could be the reason for a lack of distinct chl-a increase when there is a clear and positive physiological response. Closed systems can create bottle effects that bias the results, through potentially unrealistic ecosystem dynamics due to the loss of grazers and advective processes. Grazing rates increase with increasing biomass accumulation, thus it is expected that grazing would lower the chl-a accumulation in the Fe addition bottles. This, along with the slight contamination seen at the beginning of the experiments (which increases the response in the control bottles), would remove or lower the statistically significant difference between Fe addition bottles and their controls. However, one would expect such an effect to be experienced by all the experiments (Cullen *et al.,* 1992; Geider and Laroche, 1994; Moore *et al.,* 2007a).

V: Conclusions

Between the two years of study, the chemical and physical environment of the South Atlantic sector of the Southern Ocean varied little. Variation in the intensity and distribution of the chl-a blooms is explained through variation in fronts, localised wind events and ice coverage between the two summers. Compared with the open ocean, the photosynthetic health of phytoplankton increases remarkably throughout the water column near South Georgia, and to a lesser degree, near Antarctica. Secondary indicators of the presence of Fe, all individually suggest Fe alleviation in these regions. Phytoplankton efficiency increases in response to both Fe alleviation and an associated shift in community structure; however the photosynthetic parameters indicate the health of the population rather than its population dynamics.

Increased Fe leads to an increase in the physiological efficiency of phytoplankton in the Southern Ocean and where diatoms were present, lead to an increase in chl-a biomass. This proves that the majority of the Southern Ocean is Fe limited, and that an increase in Fe would lead to an increase in photosynthetic efficiency, but not necessarily biomass or carbon export.

Given the anticipated changes in light and Fe availability to the Southern Ocean (Sarmiento *et al*., 1998; Boyd, 2002; Hillel and Rosenzweig, 2002; Greenblatt and Sarmiento, 2004), due to climate change, and the important role the Southern Ocean plays in alleviating atmospheric increases in CO_2 through the biological carbon pump (Volk and Hoffert, 1985; Longhurst, 1991; Schlitzer, 2002; Falkowski and Raven, 2007), assessing phytoplankton responses to Fe and light co-limitation is important. This research provides us with a better understanding of the nuances of the response of the Southern Oceans phytoplankton physiology and community structure to Fe and light variability and the impact this has on the potential for carbon export.

Appendixes

List of Appendix's

Appendix A: A T-S plot of all the CTD stations on a) the north westward leg and b) the south eastward leg of SANAE 49 used to determine the position of the water masses.

Appendix B: MATLAB code by Dr Brian Hopkinson, a model determining F_v/F_m and σ_{PSII} values.

Appendix C: MATLAB code by Dr Mark Moore, a model determining F_v/F_m and σ_{PSII} values.

Appendix D: Graphs depicting a) the northward leg of NO_3 for SANAE 48, 49 and the adjusted NO_3 values for SANAE 49, b) The northward leg of PO_4 for SANAE 48 and 49, and c) the NO_3:PO_4 ratio for the northward leg of SANAE 49.

Appendix E: Graph showing the NO_3:PO_4 ratios from SANAE 48 and SANAE 49 used to correct the NO_4 data on the northward leg.

Appendix F: Pigments to species table.

Appendix G: Code used for statistical analysis in R regarding the influences on F_v/F_m and σ_{PSII}.

Appendix H: Weather observations during experiments.

Appendix I: The nutrient results of experiment B.

Appendix J: Critique and recommendations on the bio-assay nutrient methods

Appendix A: A T-S plot of all the CTD stations on a) the north westward leg and b) the south eastward leg of SANAE 49 used to determine the position of the water masses.

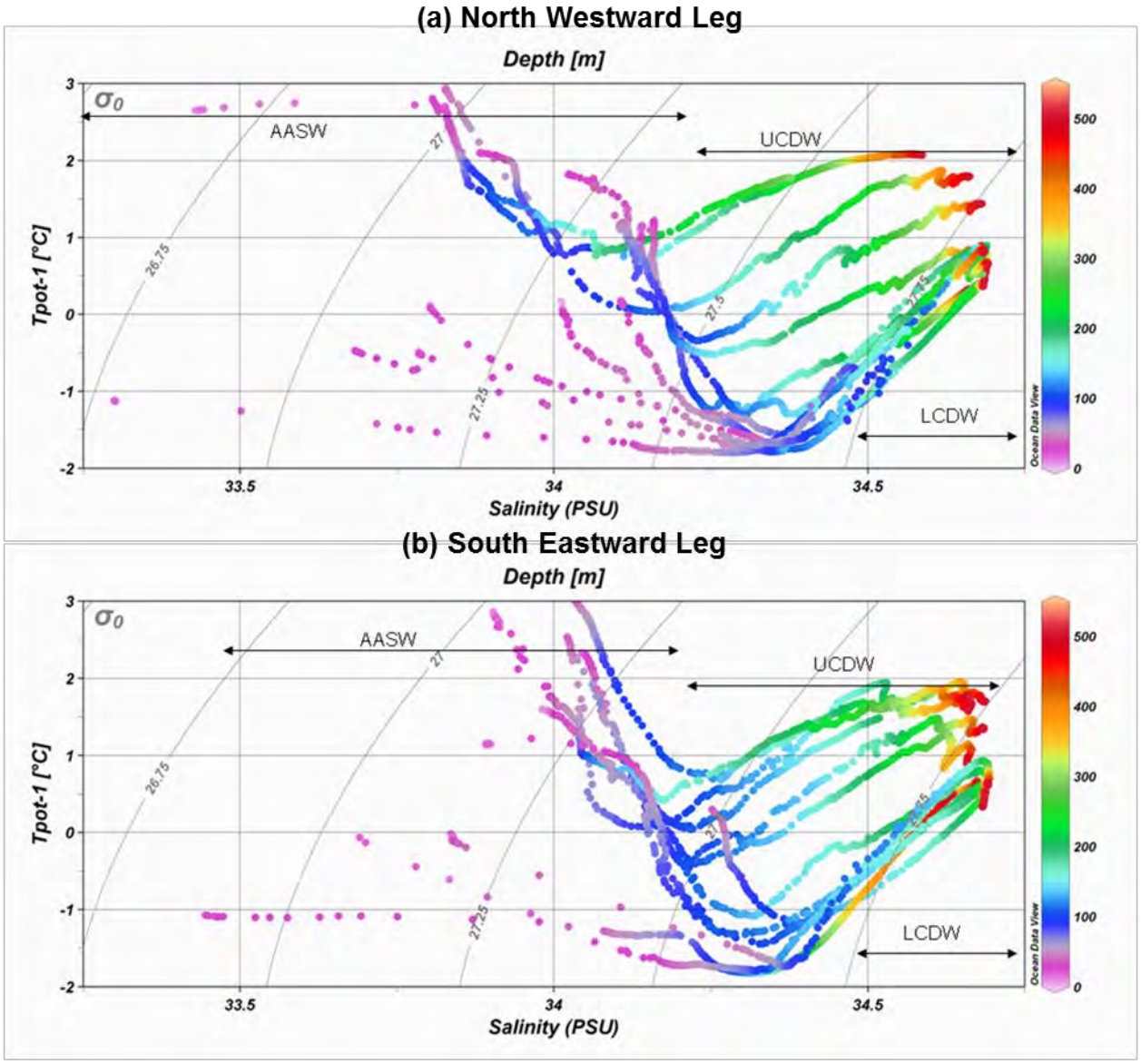

Appendix B: MATLAB code by Dr Brian Hopkinson, a model determining F_v/F_m and σ_{PSII} values.

```
files = dir ('BR*.*')
for i = 1 : numel(files)
    infile = files(i).name;
    fid = fopen (infile);
    for  j = 1:3
        waste = fgetl(fid);
    end
    line = fgetl(fid);
    gain = sscanf(line(6:9), '%i');

    blanks = dir('ABL*.*');
    for x = 1 : numel(blanks)
        test = blanks(x).name;
        fidblank = fopen (test);
        for  j = 1:3
          waste = fgetl(fidblank);
        end
        line = fgetl(fidblank);
        blankgain = sscanf(line(6:9), '%i');
        if gain == blankgain
            blank = blanks(x).name;
        end
        fclose(fidblank);
    end
    fclose(fid);
    outfile = 'output.txt';
    iter = 1;
    test_firefit(infile, blank, outfile, iter);
    infile
    blank
    pause

end
function paramsfit = test_firefit(infile, blank, outfile, iter)
%first need to open file and read header.
%now get data.
%infile = 'V1P27_1.000';
%blank = 'LP2400.blk';
%outfile = 'output.out';
%iter = 1;
disp(infile);
doplots = 0;
%infile = 'INC1_T0.000';
%blank = 'INC1_T0B.000';
%outfile = 'INC1_T0.pro';

fid = fopen(infile,'r');
frewind(fid);

%read in relevant information from header
for i = 1:6                             %discard first 6 header lines
waste = fgetl(fid);
end;

line = fgetl(fid);
STS_num = sscanf(line(14:16), '%i');  %number of samples in single turnover
saturation
line = fgetl(fid);
```

```
STR_num = sscanf(line(19:21), '%i');    % number of samples in ST relaxation
line = fgetl(fid);                       %discard STRI
line = fgetl(fid);                       %discard MTF duration
line = fgetl(fid);
MTS_num = sscanf(line(19:21), '%i');    % number of samples in MT saturation
line = fgetl(fid);
MTR_num = sscanf(line(19:21), '%i');     %number of samples in MT relaxation

for i = 1:3
waste = fgetl(fid);                     % discard addtional lines
end;

line = fgetl(fid);
PARint = sscanf(line(18:23), '%f');      % input PAR intensity for P vs E
curves

line = fgetl(fid);
if line(1) == 'C'
       lskip=4;
   end
if line(1) == 'N'
        lskip = 7;
    end

for i = 1:lskip  %need to discard different number of lines depending on
whether this is a standard sample or part of PvE curve
    waste = fgetl(fid);
end;

%read in sample file
%read in single turnover saturation

data = fscanf(fid,'%f %f %f %f',[4 inf]);
data = data';
STSsamp = round(data(1:STS_num,1))';
STS_t = data(1:STS_num,2)';
STS_ex = data(1:STS_num,3)';
STS_fl = data(1:STS_num,4)';

 %read in ST relaxation
STRsamp = round(data(STS_num+1:STS_num+STR_num,1))';
STR_t = data(STS_num+1:STS_num+STR_num,2)';
STR_ex = data(STS_num+1:STS_num+STR_num,3)';
STR_fl = data(STS_num+1:STS_num+STR_num,4)';

N = STS_num+STR_num;
 %read in multi-turnover saturation
MTSsamp = round(data(N+1:N+MTS_num,1))';
MTS_t = data(N+1:N+MTS_num,2)';
MTS_ex = data(N+1:N+MTS_num,3)';
MTS_fl = data(N+1:N+MTS_num,4)';

N = N+MTS_num;

 %read in multi-turnover relaxation
MTRsamp = round(data(N+1:N+MTR_num,1))';
MTR_t = data(N+1:N+MTR_num,2)';
MTR_ex = data(N+1:N+MTR_num,3)';
MTR_fl = data(N+1:N+MTR_num,4)';

fclose(fid);
```

```
clear data;
%read in blank file

fib = fopen(blank,'r');
frewind(fib);

for i = 1:16
    line = fgetl(fib);
end;

line = fgetl(fib);
if line(1) == 'C'
       lskip=4;
   end
if line(1) == 'N'
        lskip = 7;
    end

for i = 1:lskip  %need to discard different number of lines depending on
whether this is a standard sample or part of PvE curve
    waste = fgetl(fib);
end;

data = fscanf(fib,'%f %f %f %f',[4 inf]);
data = data';
STSsampb = round(data(1:STS_num,1))';
STS_tb = data(1:STS_num,2)';
STS_exb = data(1:STS_num,3)';
STS_flb = data(1:STS_num,4)';

 %read in ST relaxation
STRsampb = round(data(STS_num+1:STS_num+STR_num,1))';
STR_tb = data(STS_num+1:STS_num+STR_num,2)';
STR_exb = data(STS_num+1:STS_num+STR_num,3)';
STR_flb = data(STS_num+1:STS_num+STR_num,4)';

N = STS_num+STR_num;
 %read in multi-turnover saturation
MTSsampb = round(data(N+1:N+MTS_num,1))';
MTS_tb = data(N+1:N+MTS_num,2)';
MTS_exb = data(N+1:N+MTS_num,3)';
MTS_flb = data(N+1:N+MTS_num,4)';

N = N+MTS_num;

 %read in multi-turnover relaxation
MTRsampb = round(data(N+1:N+MTR_num,1))';
MTR_tb = data(N+1:N+MTR_num,2)';
MTR_exb = data(N+1:N+MTR_num,3)';
MTR_flb = data(N+1:N+MTR_num,4)';;

%subtract blank from sample
STS_fl = STS_fl - STS_flb;
STR_fl = STR_fl - STR_flb;
MTS_fl = MTS_fl - MTS_flb;
MTR_fl = MTR_fl - MTR_flb;

%fits single turnover saturation
%define irradiance applied in saturation phase
skip = 2 ;                          %samples to skip at start of STS phase
```

```
    irrad = 47248;                    %irradiance in uEi/m2/sec, from
calibration sheet
    irrad = irrad * 1E-6 *6.02E23;    %irradiance in quanta/m2/sec
    STStint = 1E-6;                   %'flashlet' duration in sec, or time
of light application between sampling (light is on constantly)
    sigscale = 1e-20;                  % sigma in m2/quanta
    pulse = irrad * STStint * sigscale;

    for i = 1:STS_num,
        pfd(i) = pulse;
    end;

    STS_fl2 = STS_fl(skip+1: STS_num);
    STSparams = [STS_num skip];

%make initial guesses
fog = mean(STS_fl(3:5));
fmg = mean(STS_fl(STS_num - 4:STS_num));
sigg = 1000;                                    % 1e-20 m2/quanta, see
scaling of pfd above
pg = 0.6;

x0 = [fog, fmg, sigg, pg];

%set search bounds
ming = [fog*0.5, fmg*0.5, 10, 0];               %set lower bounds for fo,
fm, sig, p
maxg = [fog*1.5, fmg*1.5, 2500, 1];             %set upper bounds for fo,
fm, sig, p

%STSfitted = STSfit(x0, pfd, STSparams);

%plot(STS_t(skip+1:STS_num),STSfitted,STS_t,STS_fl,'r');

%set options for lsqcurvefit
      opts = optimset('lsqcurvefit');
      opts = optimset(opts,'Display','off');
      opts = optimset(opts,'MaxIter',4000);
      opts = optimset(opts,'Diagnostics','off');
      opts = optimset(opts,'MaxFunEvals',24000);
      opts = optimset(opts,'TolFun',1e-9);
      %opts = optimset(opts,'TolX',[0.001 0.001 0.1 0.01]);

[xfit, resnorm, residual, exitflag, output] = lsqcurvefit('STSfit', x0,pfd,
STS_fl2, ming, maxg, opts, STSparams);
%lsqcurvefit setup
%[x,resnorm,residual,exitflag,output] =
lsqcurvefit(fun,x0,xdata,ydata,lb,ub,options)

fvfm = (xfit(2)-xfit(1))/xfit(2);

STSbestfit = STSfit(xfit, pfd, STSparams);

if doplots == 1,
    figure(iter);   %open new figure window for each iteration of the
firefit program
    subplot(2,2,1);

plot(STS_t(skip+1:STS_num),STSbestfit,STS_t(skip+1:STS_num),STS_fl2,'r'),
title(strcat(infile,' STS'));
end;
```

```
%fit single turnover relaxation data, oxidation of Qa
fo = mean(STR_fl(STR_num - 3: STR_num));
fm = mean(STR_fl(1:2));
params =[fo fm];
tau0 = 4000;                                %oxidation timescale of Qa in us
taumin = 10;                                %minimum tau 10 us
taumax = 100000;                            %maximum tau 100 ms

[taufit, resnorm, residual, exitflag, output] = lsqcurvefit('STRfit',
tau0,STR_t, STR_fl,taumin, taumax,opts, params);
STRbestfit = STRfit(taufit, STR_t, params);

if doplots == 1,
subplot(2,2,2);
plot(log(STR_t), STRbestfit, log(STR_t), STR_fl, 'r'), title('STR');
end;

%fit multi turnover saturation data
%divide up MT phase into chunks, average, and chose max of these

nblocks = fix(MTS_num / 20);        %break into blocks of 20 samples,
leaving off trailing samples after final block of 20;

for i = 1:nblocks,
    Blockavg(i) = mean(MTS_fl(1 + 20*(i-1):20*i));
end;
fmMT = max(Blockavg);

if doplots == 1,
subplot(2,2,3);
plot(MTS_t,MTS_fl), title('MTS');
end;

%fit relaxation phase after multi turnover saturation, oxidation of PQ
pool.

foMT = mean(MTR_fl(MTR_num - 3: MTR_num));
fmMT = mean(MTR_fl(1:3));
paramsMTR = [foMT fmMT];
tauPQ_0 = 20000;          % oxidation time of PQ in us, guess 20 ms
tauPQ_min = 1000;         % minimum oxidation time 1 ms
tauPQ_max = 200000;       % maximum oxidation time 200 ms

[tauPQ_fit, resnorm, residual, exitflag, output] = lsqcurvefit('MTRfit',
tauPQ_0, MTR_t, MTR_fl,tauPQ_min, tauPQ_max, opts, paramsMTR);
MTRbestfit = MTRfit(tauPQ_fit, MTR_t, paramsMTR);

if doplots == 1,
subplot(2,2,4);
plot(log(MTR_t), MTRbestfit, log(MTR_t), MTR_fl, 'r'), title('MTR');
end;

%export to an outfile
first = exist(outfile);                     %test if the outfile has
already been created and written to
if first == 0,                               %for the first time write
header and data to file
    fid = fopen(outfile, 'w');
    fprintf(fid,'sample \t fo \t fm \t fv/fm \t sig \t p \t tauQa \t fmMT
\t tauPQ \t PAR \n');
```

```
    fprintf(fid,'%s \t %5.2f \t %5.2f \t %1.3f \t %6.2f \t %2.2f \t %6.2f
\t %5.2f \t %6.2f \t %6.2f',infile, xfit(1), xfit(2), fvfm, xfit(3),
xfit(4),...
    taufit, fmMT, tauPQ_fit, PARint);
    fprintf(fid,'\n');
else                                        %after first access just write
data
    fid = fopen(outfile,'a');
    fprintf(fid,'%s \t %5.2f \t %5.2f \t %1.3f \t %6.2f \t %2.2f \t %6.2f
\t %5.2f \t %6.2f \t %6.2f',infile, xfit(1), xfit(2),fvfm, xfit(3),
xfit(4),...
    taufit, fmMT, tauPQ_fit, PARint);
    fprintf(fid,'\n');
end

fclose(fid);

paramsfit = [xfit(1) xfit(2) xfit(3) xfit(4) taufit fmMT tauPQ_fit PARint];

return;
```

Appendix C: MATLAB code by Dr Mark Moore, a model determining F_v/F_m and σ_{PSII} values.

```
% This code fits variable fluorescence data from the Satlantic FIRe
% instrument to the model of Kolber et al. 1998

% Version V3 disregards the first 3 micro seconds of data from the ST
% saturation phase

% IMPORTANT NOTE! The Connectivity value recovered when disregarding the
% first 3 micro seconds is likely to be inaccurate

% Mark Moore 14th May 2007. Version V3 revised 21 June 2007

clear all;
close all;

LED_intensity = 31000; % muMol m-2 s-1 % Must be set for absolute values of
sigPSII

% Request input files
in_file = input('Enter raw data file name (excluding extensions): ','s');

d = dir([in_file '.0*']); % Look for all files of correct format. This
should be changed if the are >100 files!

for filecount = 1:length(d)

    fid = fopen(d(filecount).name,'r'); % Open this file
    frewind(fid);

    f=find(d(filecount).name=='.');
    outfile = ([d(filecount).name(1:f-1),'proc']); % Define name of output
file
    textoutfile = ([d(filecount).name(1:f-1),'proc.txt']); % Define name of
output file

    record_no = 0;
```

```
    % ====================== Read in header information, PAR etc.
==============

    line = fgets(fid);  % Read in headers
    line = fgets(fid);  % This line is the time
    time_secs(filecount) = str2num(line(end-9:end));
    line = fgets(fid);  % Read in headers: LED
    line = fgets(fid);  % Read in headers: Gain
    Gain = str2num(line(6:9));
    line = fgets(fid);  % Read in headers: Sample delay
    line = fgets(fid);  % Read in headers: Number of samples

       line = fgets(fid);, STF = str2num(line(end-4:end));  % Duration of
ST saturation sequence
       line = fgets(fid);, STRP = str2num(line(end-4:end)); % Number of
points in ST relaxation sequence
       line = fgets(fid);, STRI = str2num(line(end-4:end)); % Interval
between first ST relaxation measurement
       line = fgets(fid);                                   % MTF lenght
(ms)
       line = fgets(fid);, MTF = str2num(line(end-4:end));  % Number of
points in MT saturation sequence
       line = fgets(fid);, MTRP = str2num(line(end-4:end)); % Number of
points in MT relaxation sequence
       line = fgets(fid);, MTRI = str2num(line(end-4:end)); % Interval
between first MT relaxation measurement
       line = fgets(fid);
       line = fgets(fid);

       if line(end-4:end-2) == 'Off' % Read in the PAR data iff Actinic
source was used
           PAR(filecount) = 0;
          for i = 1:5
           line = fgets(fid);
          end
       else if line(end-4:end-2) == ' On'
             line = fgets(fid);
             f=find(line==':');
             PAR(filecount) = str2num(line(f+1:end));
                for i = 1:8
                    line = fgets(fid);
                end
           end
       end

    %
==========================================================================

    % ======= Read in Data
=================================================

    while (feof(fid) == 0)     % while not end of input file.....

           line = fgets(fid);       % start loading data
           line = str2num(line);
           record_no = record_no + 1;
           Time(record_no) = line(2); % in microseconds
           Ex(record_no) = line(3);
           Yield(record_no) = line(4);
    end % loading data
```

```
    %
================================================================================

    % Correct yields to absolute values

    if Gain == 2200
        Yield = Yield./283;
    end
    if Gain == 2000
        Yield = Yield./195;
    end
    if Gain == 1800
        Yield = Yield./123;
    end
    if Gain == 1600
        Yield = Yield./78.3;
    end
    if Gain == 1400
        Yield = Yield./50;
    end

    Yield_STS = Yield(1:STF); % Break records into separate phases
    Yield_STR = Yield(STF+1:STF+STRP);
    Yield_MTS = Yield(STF+STRP+1:STF+STRP+MTF);
    Yield_MTR = Yield(STF+STRP+MTF+1:STF+STRP+MTF+MTRP);

    Time_STS = Time(1:STF);
    Time_STR = Time(STF+1:STF+STRP)-Time(STF);
    Time_MTS = Time(STF+STRP+1:STF+STRP+MTF);
    Time_MTR = Time(STF+STRP+MTF+1:STF+STRP+MTF+MTRP);

    Yield_STS_no3 = Yield_STS(4:end); % Reduced ST section ignoring first 3
micro secs

    %
================================================================================

    % ================== Perform fitting
====================================

    PFD_STS = ones(size(Time_STS)).*LED_intensity.*6.023e23/1e32;
    PFD_STS_no3 = [sum(PFD_STS(1:4)) PFD_STS(5:end)]; % Reduced PFD for ST
section ignoring first 3 micro secs

    sparams_saturate = [Yield_STS(1) Yield_STS(end) 300 0.5]; % Set initial
guesses for relaxation parameter fits
    sparams_relax_ST = [200 2000 20000 0.3 0.3 0.3 Yield_STR(end)
Yield_STR(1)]; % Set initial guesses for relaxation parameter fits
    sparams_relax_MT = [2000 20000 200000 0.3 0.3 0.3 Yield_MTR(end)
Yield_MTR(1)]; % Set initial guesses for relaxation parameter fits

    [f,sfitparams_STS,kvg,iter,corp,covp_exp,covr,stdresid,Z,r2]=...

nlleasqr(PFD_STS_no3',Yield_STS_no3',sparams_saturate,'Saturation_function'
); % Perform fitting for STS kinetic
    [f,sfitparams_STS_nop,kvg,iter,corp,covp_nop,covr,stdresid,Z,r2]=...
```

```
nlleasqr(PFD_STS_no3',Yield_STS_no3',sparams_saturate(1:3),'Saturation_func
tion_nop'); % Perform fitting for STS kinetic without p

    [f,sfitparams_STR,kvg,iter,corp,covp_exp,covr,stdresid,Z,r2]=...

nlleasqr(Time_STR',Yield_STR',sparams_relax_ST,'Relaxation_function'); %
Perform fitting for STR kinetic
    [f,sfitparams_MTR,kvg,iter,corp,covp_exp,covr,stdresid,Z,r2]=...

nlleasqr(Time_MTR',Yield_MTR',sparams_relax_MT,'Relaxation_function'); %
Perform fitting for MTR kinetic

    Fm_MT(filecount) = max(Yield_MTS);

    % pause

    % ======= Copy outputs from fitting routine into vectors
==================

    Fo_nop(filecount)  = sfitparams_STS_nop(1);
    Fm_nop(filecount)  = sfitparams_STS_nop(2);
    Sig_nop(filecount) = sfitparams_STS_nop(3);
    Fo(filecount)      = sfitparams_STS(1);
    Fm(filecount)      = sfitparams_STS(2);
    Sig(filecount)     = sfitparams_STS(3);
    p(filecount)       = sfitparams_STS(4);

    erFo_nop(filecount) = covp_nop(1,1)^0.5;
    erFm_nop(filecount) = covp_nop(2,2)^0.5;

    per_erFo_nop(filecount) = 100.*erFo_nop(filecount)/Fo_nop(filecount);
    per_erFm_nop(filecount) = 100.*erFm_nop(filecount)/Fm_nop(filecount);

    tau1_ST(filecount) = sfitparams_STR(1);
    tau2_ST(filecount) = sfitparams_STR(2);
    tau3_ST(filecount) = sfitparams_STR(3);
    alpha1_ST(filecount) = sfitparams_STR(4);
    alpha2_ST(filecount) = sfitparams_STR(5);
    alpha3_ST(filecount) = sfitparams_STR(6);
    Fo_relax_ST(filecount) = sfitparams_STR(7);
    Fm_relax_ST(filecount) = sfitparams_STR(8);

    tau1_MT(filecount) = sfitparams_MTR(1);
    tau2_MT(filecount) = sfitparams_MTR(2);
    tau3_MT(filecount) = sfitparams_MTR(3);
    alpha1_MT(filecount) = sfitparams_MTR(4);
    alpha2_MT(filecount) = sfitparams_MTR(5);
    alpha3_MT(filecount) = sfitparams_MTR(6);
    Fo_relax_MT(filecount) = sfitparams_MTR(7);
    Fm_relax_MT(filecount) = sfitparams_MTR(8);
    Average_F(filecount) = mean(Yield(2:STF));
    Fo_rough(filecount) = mean(Yield(3:6));
    Fm_rough(filecount) = mean(Yield(STF-2:STF));
    GAIN(filecount) = Gain;

    % ==== This is an attempt to calculate rate of PQ pool reduction,
    % ==== dosn't work very well yet!
```

```
%    Delta_Fm_ST_MT(filecount) = Fm_MT(filecount) - Fm_nop(filecount);
%    T_half_ST_MT(filecount) = min(Time_MTS(find(Yield_MTS >=
(Fm_nop(filecount) + Fm_MT(filecount))./2)));

    % ====== Plot fits =====

    clf;
    subplot(311), plot(Yield,'r','LineWidth',2)
    xlabel('Meaurement no.')
    ylabel('F (a.u.)')

    out = Saturation_function_nop(PFD_STS_no3, sfitparams_STS_nop); %
Predicted fit for single turnover relaxation
    outp = Saturation_function(PFD_STS_no3, sfitparams_STS); % Predicted
fit for single turnover relaxation with p
    subplot(323), plot(out,'b','LineWidth',3)
    hold on,
    plot(outp,'g','LineWidth',3)
    % plot(Yield_STS,'ok','MarkerFaceColor',[0.7 0.7 0.7],'MarkerSize',4)
    plot([1:length(Yield_STS)-
3],Yield_STS_no3,'ok','MarkerFaceColor','w','MarkerSize',4)
    xlabel('Meaurement no.')
    ylabel('F (a.u.)')

    out = Relaxation_function(Time_STR, sfitparams_STR); % Predicted fit
for single turnover relaxation
    subplot(324), semilogx(Time_STR,out,'r','LineWidth',3)
    hold on,
plot(Time_STR,Yield_STR,'ok','MarkerFaceColor','w','MarkerSize',4)
    xlim([10 5e6])
    xlabel('Time (\mus)')
    ylabel('F (a.u.)')

    subplot(325), plot(Time_MTS,Yield_MTS,'b')
    hold on
    plot(Time_MTS,ones(size(Time_MTS)).*Fm_nop(filecount),'k:')
    plot(Time_MTS,ones(size(Time_MTS)).*Fo_nop(filecount),'k:')
    plot(Time_MTS,ones(size(Time_MTS)).*Fm_MT(filecount),'k:')
 %
plot(Time_MTS,ones(size(Time_MTS)).*(Fm_nop(filecount)+Delta_Fm_ST_MT(filec
ount)./2),'r:')
 %   plot(T_half_ST_MT(filecount).*ones(1,2),[Fo_nop(filecount)
Fm_nop(filecount)+Delta_Fm_ST_MT(filecount)./2],'r:')
    out = Relaxation_function(Time_MTR, sfitparams_MTR); % Predicted fit
for single turnover relaxation
    xlabel('Time (\mus)')
    ylabel('F (a.u.)')

    subplot(326), semilogx(Time_MTR,out,'r','LineWidth',3)
    hold on,
plot(Time_MTR,Yield_MTR,'ok','MarkerFaceColor','w','MarkerSize',4)
    xlim([10 5e6])
    xlabel('Time (\mus)')
    ylabel('F (a.u.)')
    pause%(0.01);

    % ======================

    fclose(fid);                    % close this input file
```

```
    % ====== Save the evaluted parameters to the ouput file

    eval(['save ', outfile,' PAR Fo_nop Fm_nop per_erFo_nop per_erFm_nop
Sig_nop Fo Fm Sig p tau1_ST tau2_ST tau3_ST alpha1_ST alpha2_ST alpha3_ST
tau1_ST tau2_ST tau3_ST alpha1_MT alpha2_MT alpha3_MT Fm_MT Fo_relax_ST
Fm_relax_ST Fo_relax_MT Fm_relax_MT Average_F'])


end % of all files for this filename

alpha_sum_ST = alpha1_ST + alpha2_ST + alpha3_ST; % Check whether sum of
alpha terms equals 1
alpha_sum_MT = alpha1_MT + alpha2_MT + alpha3_MT; % Check whether sum of
alpha terms equals 1

% out = [Fo_nop(2:2:end)' Fm_nop(2:2:end)' Fm_MT(2:2:end)' Fo_nop(1:2:end)'
Fm_nop(1:2:end)' Fm_MT(1:2:end)'] % For copying to text/excel
out = [Average_F' Fo_nop' Fm_nop' per_erFo_nop' per_erFm_nop' Fo_rough'
Fm_rough' Fm_MT' Sig_nop' tau1_ST' tau2_ST' tau3_ST' alpha1_ST' alpha2_ST'
alpha3_ST' tau1_ST' tau2_ST' tau3_ST' alpha1_MT' alpha2_MT' alpha3_MT']; %
For writing to text out file

fid = fopen(textoutfile,'w');
fprintf(fid,' AvgF Fo Fm ErrorFo ErrorFm Fo_rough Fm_rough FmMT SigmaPSII
tau1_ST tau2_ST tau3_ST alpha1_ST alpha2_ST alpha3_ST tau1_MT tau2_MT
tau3_MT alpha1_MT alpha2_MT alpha3_MT\n');
fprintf(fid,'%6.3f %6.3f %6.3f %6.3f %6.3f %6.3f %6.3f %6.3f %6.2f %6.3f
%6.3f %6.3f %6.3f %6.3f %6.3f %6.3f %6.3f %6.3f %6.3f %6.3f %6.3f\n',out');
fclose(fid);
```

nlleasqr

```
function
[f,p,kvg,iter,corp,covp,covr,stdresid,Z,r2]=nlleasqr(x,y,pin,func,stol,nite
r,wt,dp,dfdp,options)

%function[f,p,kvg,iter,corp,covp,covr,stdresid,Z,r2]=
%                   nlleasqr(x,y,pin,{func,stol,niter,wt,dp,dfdp,options})
%
% Version 3.beta
% Levenberg-Marquardt nonlinear regression of f(x,p) to y(x), where:
% x=vec or mat of indep variables, 1 row/observation: x=[x0 x1....xm]
% y=vec of obs values, same no. of rows as x.
% wt=vec(dim=1 or length(x)) of statistical weights.  These should be set
%   to be proportional to (sqrts of var(y))^-1; (That is, the covaraince
%   matrix of the data is assumed to be proportional to diagonal with
diagonal
%   equal to (wt.^2)^-1.  The constant of proportionality will be
estimated.),
%   default=1.
% pin=vector of initial parameters to be adjusted by leasqr.
% dp=fractional incr of p for numerical partials,default=
.001*ones(size(pin))
%   dp(j)>0 means central differences.
%   dp(j)<0 means one-sided differences.
% Note: dp(j)=0 holds p(j) fixed i.e. leasqr wont change initial guess:
pin(j)
% func=name of function in quotes,of the form y=f(x,p)
```

```
% dfdp=name of partials M-file in quotes default is prt=dfdp(x,f,p,dp,func)
% stol=scalar tolerances on fractional improvement in ss,default stol=.0001
% niter=scalar max no. of iterations, default = 20
% options=matrix of n rows (same number of rows as pin) containing
%   column 1: desired fractional precision in parameter estimates.
%     Iterations are terminated if change in parameter vector (chg) on two
%     consecutive iterations is less than their corresponding elements
%     in options(:,1).  [ie. all(abs(chg*current parm est) < options(:,1))
%      on two consecutive iterations.], default = zeros().
%   column 2: maximum fractional step change in parameter vector.
%     Fractional change in elements of parameter vector is constrained to
be
%     at most options(:,2) between sucessive iterations.
%     [ie. abs(chg(i))=abs(min([chg(i) options(i,2)*current param
estimate])).],
%     default = Inf*ones().
%
%          OUTPUT VARIABLES
% f=vec function values computed in function func.
% p=vec trial or final parameters. i.e, the solution.
% kvg=scalar: =1 if convergence, =0 otherwise.
% iter=scalar no. of interations used.
% corp= correlation matrix for parameters
% covp= covariance matrix of the parameters
% covr = diag(covariance matrix of the residuals)
% stdresid= standardized residuals
% Z= matrix that defines confidence region
% r2= coefficient of multiple determination

%  {}= optional parameters
% ss=scalar sum of squares=sum-over-i(wt(i)*(y(i)-f(i)))^2.

% All Zero guesses not acceptable
% Richard I. Shrager (301)-496-1122
% Modified by A.Jutan (519)-679-2111
% Modified by Ray Muzic 14-Jul-1992
%       1) add maxstep feature for limiting changes in parameter estimates
%          at each step.
%       2) remove forced columnization of x (x=x(:)) at beginning. x could
be
%          a matrix with the ith row of containing values of the
%          independent variables at the ith observation.
%       3) add verbose option
%       4) add optional return arguments covp, stdresid, chi2
%       5) revise estimates of corp, stdev
% Modified by Ray Muzic 11-Oct-1992
%       1) revise estimate of Vy.  remove chi2, add Z as return values
% Modified by Ray Muzic 7-Jan-1994
%       1) Replace ones(x) with a construct that is compatible with
versions
%          newer and older than v 4.1.
%       2) Added global declaration of verbose (needed for newer than v4.x)
%       3) Replace return value var, the variance of the residuals with
covr,
%          the covariance matrix of the residuals.
%       4) Introduce options as 10th input argument.  Include
%          convergence criteria and maxstep in it.
%       5) Correct calculation of xtx which affects coveraince estimate.
%       6) Eliminate stdev (estimate of standard deviation of parameter
%          estimates) from the return values.  The covp is a much more
```

```
%          meaningful expression of precision because it specifies a
confidence
%          region in contrast to a confidence interval..  If needed,
however,
%          stdev may be calculated as stdev=sqrt(diag(covp)).
%       7) Change the order of the return values to a more logical order.
%       8) Change to more efficent algorithm of Bard for selecting epsL.
%
% Refrences:
% Bard, Nonlinear Parameter Estimation, Academic Press, 1974.
% Draper and Smith, Applied Regression Analysis, John Wiley and Sons, 1981.
%
%set default args

% argument processing
%

plotcmd='plot(x(:,1),y,''o'',x(:,1),f,''+''); shg';
if (sscanf(version,'%f') >= 4),
  global verbose
  plotcmd='plot(x(:,1),y,''o'',x(:,1),f,''+''); figure(gcf)';
end;

if(exist('verbose')~=1), verbose=0; end;
if (nargin <= 8), dfdp='dfdp'; end;
if (nargin <= 7), dp=.001*(pin*0+1); end; %DT
if (nargin <= 6), wt=1.0; end;
if (nargin <= 5), niter=20; end;
if (nargin <= 4), stol=.0001; end;
%

y=y(:); wt=wt(:); pin=pin(:); dp=dp(:); %change all vectors to columns
% check data vectors- same length?
m=length(y); n=length(pin); p=pin;[m1,m2]=size(x);
if m1~=m ,error('input(x)/output(y) data must have same number of rows ')
,end;

if (nargin <= 9),
  options=[zeros(n,1) Inf*ones(n,1)];
  nor = n; noc = 2;
else
  [nor noc]=size(options);
  if (nor ~= n),
    error('options and parameter matrices must have same number of rows'),
  end;
  if (noc ~= 2),
    options=[options(noc,1) Inf*ones(noc,1)];
  end;
end;
pprec=options(:,1);
maxstep=options(:,2);
%

% set up for iterations
%
f=feval(func,x,p); fbest=f; pbest=p;
r=wt.*(y-f);
sbest=r'*r;
nrm=zeros(n,1);
chgprev=Inf*ones(n,1);
```

```
kvg=0;
epsLlast=1;
epstab=[.1 1 1e2 1e4 1e6];

% do iterations
%
for iter=1:niter,
  pprev=pbest;
  prt=feval(dfdp,x,fbest,pprev,dp,func);
  r=wt.*(y-fbest);
  sprev=sbest;
  sgoal=(1-stol)*sprev;
  for j=1:n,
    if dp(j)==0,
      nrm(j)=0;
    else
      prt(:,j)=wt.*prt(:,j);
      nrm(j)=prt(:,j)'*prt(:,j);
      if nrm(j)>0,
        nrm(j)=1/sqrt(nrm(j));
      end;
    end
    prt(:,j)=nrm(j)*prt(:,j);
  end;
  [prt,s,v]=svd(prt,0);
  s=diag(s);
  g=prt'*r;
  for jjj=1:length(epstab),
    epsL = max(epsLlast*epstab(jjj),1e-7);
    se=sqrt((s.*s)+epsL);
    gse=g./se;
    chg=((v*gse).*nrm);
%   check the change constraints and apply as necessary
    ochg=chg;
    for iii=1:n,
      if (maxstep(iii)==Inf), break; end;
      chg(iii)=max(chg(iii),-abs(maxstep(iii)*pprev(iii)));
      chg(iii)=min(chg(iii),abs(maxstep(iii)*pprev(iii)));
    end;
    if (verbose & any(ochg ~= chg)),
      disp(['Change in parameter(s): ' ...
         sprintf('%d ',find(ochg ~= chg)) 'were constrained']);
    end;
    aprec=abs(pprec.*pbest);       %---
    if (any(abs(chg) > 0.1*aprec)),%---  % only worth evaluating function
if
      p=chg+pprev;                        % there is some non-miniscule
change
      f=feval(func,x,p);
      r=wt.*(y-f);
      ss=r'*r;
      if ss<sbest,
        pbest=p;
        fbest=f;
        sbest=ss;
      end;
      if ss<=sgoal,
        break;
      end;
    end;                           %---
  end;
```

```
  epsLlast = epsL;
  if (verbose),
    eval(plotcmd);
  end;
  if ss<eps,
    break;
  end
  aprec=abs(pprec.*pbest);
%  [aprec chg chgprev]
  if (all(abs(chg) < aprec) & all(abs(chgprev) < aprec)),
    kvg=1;
    if (verbose),
      fprintf('Parameter changes converged to specified precision\n');
    end;
    break;
  else
    chgprev=chg;
  end;
  if ss>sgoal,
    break;
  end;
end;

% set return values
%
p=pbest;
f=fbest;
ss=sbest;
kvg=((sbest>sgoal)|(sbest<=eps)|kvg);
if kvg ~= 1 , disp(' CONVERGENCE NOT ACHIEVED! '), end;

% CALC VARIANCE COV MATRIX AND CORRELATION MATRIX OF PARAMETERS
% re-evaluate the Jacobian at optimal values
jac=feval(dfdp,x,f,p,dp,func);
msk = dp ~= 0;
n = sum(msk);           % reduce n to equal number of estimated parameters
jac = jac(:, msk);      % use only fitted parameters

%% following section is Ray Muzic's estimate for covariance and correlation
%% assuming covariance of data is a diagonal matrix proportional to
%% diag(1/wt.^2).
%% cov matrix of data est. from Bard Eq. 7-5-13, and Row 1 Table 5.1

Qinv=diag(wt.*wt);
Q=diag((0*wt+1)./(wt.^2));
%[nrw ncw]=size(wt);
%Q=ones(nrw,ncw)./wt; Q=diag(Q.*Q);
resid=y-f;                                      %un-weighted residuals
covr=resid'*Qinv*resid*Q/(m-n);                   %covariance of residuals
Vy=1/(1-n/m)*covr;  % Eq. 7-13-22, Bard           %covariance of the data
covr=diag(covr);                                  %for compact storage
Z=((m-n)*jac'*Qinv*jac)/(n*resid'*Qinv*resid);
stdresid=resid./sqrt(diag(Vy));

jtgjinv=inv(jac'*Qinv*jac);
covp=jtgjinv*jac'*Qinv*Vy*Qinv*jac*jtgjinv; % Eq. 7-5-13, Bard %cov of parm
est
for k=1:n,
  for j=k:n,
    corp(k,j)=covp(k,j)/sqrt(abs(covp(k,k)*covp(j,j)));
```

```
    corp(j,k)=corp(k,j);
  end;
end;

%%% alt. est. of cov. mat. of parm.:(Delforge, Circulation, 82:1494-1504,
1990
%%disp('Alternate estimate of cov. of param. est.')
%%acovp=resid'*Qinv*resid/(m-n)*jtgjinv

%Calculate R^2 (Ref Draper & Smith p.46)
%
r=corrcoef(y,f);
r2=r(1,2).^2;

% if someone has asked for it, let them have it
%
if (verbose),
  eval(plotcmd);
  disp(' Least Squares Estimates of Parameters')
  disp(p')
  disp(' Correlation matrix of parameters estimated')
  disp(corp)
  disp('Covariance matriix of Residuals  ' )
  disp(covr)
  disp( 'Correlation Coefficient R^2')
  disp(r2)
  sprintf('95%% conf region: F(0.05)(%.0f,%.0f)>=
delta_pvec''*Z*delta_pvec',n,m-n)
  Z
end;

% A modified version of Levenberg-Marquardt
% Non-Linear Regression program previously submitted by R.Schrager.
% This version corrects an error in that version and also provides
% an easier to use version with automatic numerical calculation of
% the Jacobian Matrix. In addition, this version calculates statistics
% such as correlation, etc....
%
% Version 3 Notes
% Errors in the original version submitted by Shrager (now called version
1)
% and the improved version of Jutan (now called version 2) have been
corrected.
% Additional features, statisitcal tests, and documentation have also been
% included along with an example of usage.  BEWARE: Some the the input and
% output arguments were changed from the previous version.
%
%     Ray Muzic     rfm2@ds2.uh.cwru.edu
%     Arthur Jutan  jutan@charon.engga.uwo.ca
```

Saturation_function

```
% FRRF Saturation curve for FIRe_processing (see Kolber et al. 1998)

function out = Saturation_function(pfd,params);

fo = params(1);
fm = params(2);
```

```
sig = params(3);
p = params(4);

out = zeros(1,length(pfd));
c = zeros(1,length(pfd));

c(1) = pfd(1) * sig;
for i = 2:length(out),
  c(i) = c(i-1) + pfd(i) * sig * (1 - c(i-1))/(1 - p * c(i-1));
end;

out = fo + (fm - fo)*c*(1-p)./(1-c*p) ;

out = out';
```

dfdp

```
function prt=dfdp(x,f,p,dp,func)
% numerical partial derivatives (Jacobian) df/dp for use with leasqr
% --------INPUT VARIABLES---------
% x=vec or matrix of indep var(used as arg to func) x=[x0 x1 ....]
% f=func(x,p) vector initialsed by user before each call to dfdp
% p= vec of current parameter values
% dp= fractional increment of p for numerical derivatives
%      dp(j)>0 central differences calculated
%      dp(j)<0 one sided differences calculated
%      dp(j)=0 sets corresponding partials to zero; i.e. holds p(j) fixed
% func=string naming the function (.m) file
%       e.g. to calc Jacobian for funcion expsum
prt=dfdp(x,f,p,dp,'expsum')
%----------OUTPUT VARIABLES-------
% prt= Jacobian Matrix prt(i,j)=df(i)/dp(j)
%===============================
m=length(x);n=length(p);      %dimensions
ps=p; prt=zeros(m,n);del=zeros(n,1);          % initialise Jacobian to Zero
for j=1:n
      del(j)=dp(j) .*p(j);    %cal delx=fract(dp)*param value(p)
            if p(j)==0
            del(j)=dp(j);     %if param=0 delx=fraction
            end
      p(j)=ps(j) + del(j);
      if del(j)~=0, f1=feval(func,x,p);
            if dp(j) < 0, prt(:,j)=(f1-f)./del(j);
            else
            p(j)=ps(j)- del(j);
            prt(:,j)=(f1-feval(func,x,p))./(2 .*del(j));
            end
      end
      p(j)=ps(j);       %restore p(j)
end
return
```

Saturation –function_nop

```
% FRRF Saturation curve for FIRe_processing (see Kolber et al. 1998)

function out = Saturation_function_nop(pfd,params);

  fo = params(1);
```

```
  fm = params(2);
  sig = params(3);

  out = fo + (fm - fo)*(1 - exp( -sig * cumsum(pfd))) ;
```

Relaxation_function

```
function out = Relaxation_function(Time_Relax, params)

tau1 = params(1);
tau2 = params(2);
tau3 = params(3);
alpha1 = params(4);
alpha2 = params(5);
alpha3 = params(6);
fo_relax = params(7);
fm_relax = params(8);

% the simple triple exponential model
out = fo_relax + (fm_relax-fo_relax).*(...
    alpha1*exp(-Time_Relax/tau1) + alpha2*exp(-Time_Relax/tau2) +
alpha3*exp(-Time_Relax/tau3) ) ;
```

Appendix D: Graphs depicting a) the northward leg of NO_3 for SANAE 48, 49 and the adjusted NO_3 values for SANAE 49, b) The northward leg of PO_4 for SANAE 48 and 49. and c) the NO_3:PO_4 ratio for the northward leg of SANAE 49.

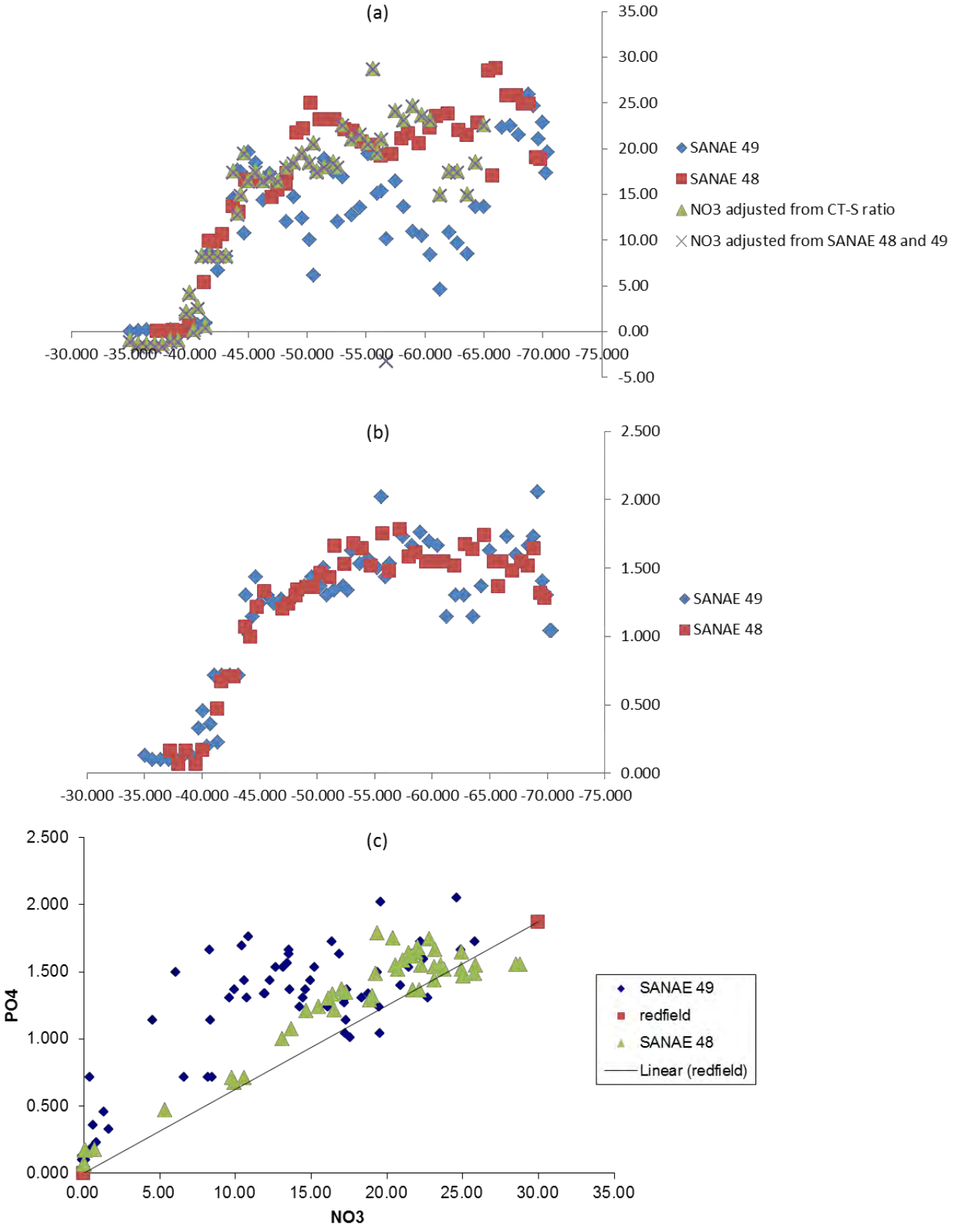

Appendix E: Graph showing the NO_3:PO_4 ratios from SANAE 48 and SANAE 49 used to correct the NO_4 data on the northward leg.

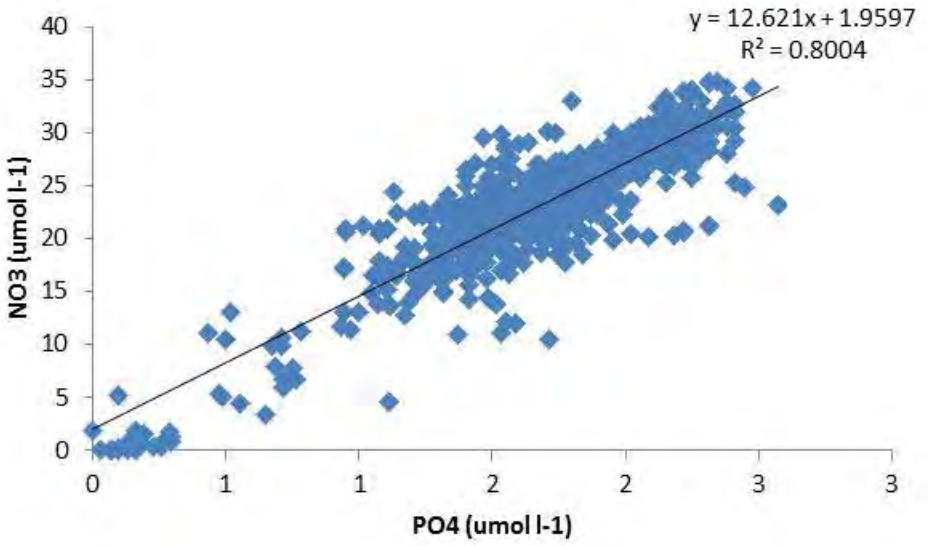

Appendix F: Pigments to species table.

Wright and Jeffery 2006; Jeffery *et al*, 1997	
Pigment	Significants
Chlorophyll *c* 3	Haptophytes types 4-8 (including coccolithophorids (Type 6), Chrysochromulina sp. (Type 7) and Phaeocystis sp. (Type 8))
Chlorophyll *c* 2	Chromophyte algae, brown seaweed
Peridinin	Type 1 Dinoflagellates
19'-Butanoyloxyfucoxanthin	some Haptophytes, marine chrysophytes and three dinoflaggellate species
Fucoxanthin	Unique marker for diatoms, also present in haptophytes, chrysophytes, raphidaphytes, bolidaphytes and some dinoflagellates
19'-hexanoyloxyfucoxanthin	Haptophytes such as *Phaeocystis* spp
Violaxanthin	higher plants
Alloxanthin	Cryptophytes
Zeaxanthin	notably represent cynobacteria, also present in low concentrations in prochlorophytes, chlrorophytes, prasinophytes, eulenophytes, chrysphytes, raphidophytes and eustigmoterphytes
Chlorophyll *b*	distinguishes 'green algae' (chlorophytes, prasinophytes, euglenophytes and green dinoflagellates). Use relastive ratio with lutein to determine which
Lutein	Lutein : Chlorophyll *b* for Chlorophytes ans type 1 Prasinophytes. (Lut: Chl b = 0.30-1.77, 0-0.18 respectively)
Divinyl chlorophyll	*Prochlorococcus marinus*

Appendix G: Code used for statistical analysis in R regarding the influences on F_v/F_m and σ_{PSII}

```
####  first try


data=read.csv("E://Rplaywithsilicate//ALLDATAwithsilicate6.csv",header=TRUE)

attach(data)

data=data[1:175,]

data


Fv.Fm.average


model3=lm(Fv.Fm.average~SiO4+PO4+N03+Chlorophyll+Temperature+Salinity+Oxygen+Fluorescence+PAR)

model3

summary(model3)


model4=lm(Sigma.average~SiO4+PO4+N03+Chlorophyll+Temperature+Salinity+Oxygen+Fluorescence+PAR)

model4

summary(model4)


#### depth data devision


depth1=data[1:30,]

end
```

Appendix H: Weather observations during experiments.

day	time	Experiment A	Experiment B	Experiment C	Experiment D	Experiment E	Experiment F
0	20:00			**Just starting to become sunny**	**sunny, beautiful- lots of wildlife-mike, killer whales, humpbacks and leopard seals**	.	
	22:00					**overcast**	
	00.00	**cloudy**				dark, overcast	
	04.00			Full sunshine, beautiful!		dark, cloudy & misty	**high productivity-0.8, started raining just after station**
	06.00			sunshine		getting light on horizon, cloudy, mist cleared	light, 6.5'C! (Toasty!), high cloud, light rain.
	08.00			sunshine	miserable, overcatse day	cloudy, clearer	conditions becoming warmer, light cloud cover, drizzle
	10.00	overcast		sunshine	miserable, overcatse day	cloudy	warm
	12.00	overcast	Little windy, dark, cold. Chl-a up to 1.5 on flourometer! Huge bloom.	sunshine	miserable, overcatse day	misty, calm	cloudy
	14.00	Overcast, cold		cloudy	miserable, overcatse day	calm, misty	sunny
	16.00	Ice, Overcast, cold	Light, a little windy, overcast. Massive bloom. Water green.	miserable day with heavy cloud, wind, snow	miserable, overcatse day		sunny
	18.00	Inrease in ice, cold, overcast		miserable day with heavy cloud, wind, snow	miserable, overcatse day	misty, raining	clear, sunny
1	20.00	Exciting ice, cold, overcast	Cloudy, windy, light swell	miserable day with heavy cloud, wind, snow	miserable, overcatse day	misty, calm	partly cloudy, dark, spitting rain
	22.00	No ice. Overcase		miserable day with heavy cloud, wind, snow	miserable, overcatse day	nearly dark, overcast, misty	dark, overcast
	00.00	*Start of weddel. ACC front	Overcast, windy	miserable day with heavy cloud, wind, snow	miserable, overcatse day	dark, increasing resolution	**it was dark**
	02.00	**Weddel- ACC front. Rapid increase in Temp and decrease in CO2**		miserable day with heavy cloud, wind, snow	miserable, overcatse day	**Warm & dark**	clear with very bright stars
	04.00	Windy		miserable day with heavy cloud, wind, snow	miserable, overcatse day	warm, dark, with cool fluorescence We have crossed the APF	sun rising, Jupiter shining bright, Scorpios showing her tail
	06.00	Stormy, snowing,almost white out		miserable day with heavy cloud, wind, snow	miserable, overcatse day	high productivity-0.8, started raining just after station	overcast, temperature dropped
	08.00	Stormy, sleet		miserable day with heavy cloud, wind, snow		light, 6.5'C! (Toasty!), high cloud, light rain.	sunny
	10.00	stormy		miserable day with heavy cloud, wind, snow		conditions becoming warmer, light cloud cover, drizzle	misty
	12.00	Cold, stormy		miserable day with heavy cloud, wind, snow		warm	cloudy, windy
	14.00			miserable day with heavy cloud, wind, snow		cloudy	raining, overcast
	16.00	Cold	Overcast, windy	cloudy		sunny	
	18.00			cloudy		sunny	
2	20.00		Sun shining, wind, swell, white horses	beautiful sunny night	a little cloudy	clear, sunny	dark, windy, productivity increasing, on the STF??
	22.00	Overcast		sunny		partly cloudy, dark, spitting rain	
	00.00	Dark	Cloudy, wind, dusk light	sunny		dark, overcast	**windy, a sky full of sparkles**
	02.00	**cold, windy, dark**		sunny		**it was dark**	6m swell, dark, windy, sparkling ocean, flew clouds
	04.00	Oercast, light sleet and wind.	Cloudy, getting light	sunny		clear with very bright stars	getting light, windy, partly cloudy
	06.00			sunny		sun rising, Jupiter shining bright, Scorpios showing her tail	cloudy,3m swell, white horses cantering
	08.00	Wind perfect for upwelling. Productivity apparently low according to Luke	Cloudy, calm	sunny		overcast, temperature dropped	sunny
	10.00			sunny		sunny	sunny
	12.00		Calm, clear	sunny		misty	sunny
	14.00			sunny		cloudy, windy	sunny, calm
	16.00	Overcast, windy	Clear	sunny		raining, overcast	clear, warm
	20.00	Sunshine, white horses. Lots of birds	Cloudy, calm	sunny	sunny, clear, beautiful, cold		dark!, warm

3	22.00			sunny		dark, windy, productivity increasing, on the STF??	
	00.00	Clearing		sunny			
	02.00	**Clear, clouds on horison, windy**	Cloudy, calmish, a little wind	sunny		**windy, a sky full of sparkles**	
	04.00		Cloudy, calm. Icebergs again!	sunny		6m swell, dark, windy, sparkling ocean, flew clouds	
	06.00	Overcast, cold, misty		sunny		getting light, windy, partly cloudy	
	08.00	Overcast, cold.	Calm, cloudy, icebergs	sunny	weather starting to turn, ice on deck	cloudy,3m swell, white horses cantering	
	12.00	Overcast, cold, windy	Calm, overcast	sunny		sunny	
	16.00	Overcast, cold, windy	Overcast	sunny		sunny, calm	
	18.00			sunny		clear, warm	
	20.00		Cloudy	sunny	overcast, snowing		
4	22.00	Cloud cover, still light		sunny	overcast, snowing		
	00.00	Cloud cover, dark	Bloom present, cloudy, swell dropping	sunny	overcast, snowing		
	02.00	**Dark, cloud**		sunny	overcast, snowing		
	04.00		Cloudy, calm, light wind	sunny	overcast, snowing		
	06.00			sunny	overcast, snowing		
	08.00		Cloudy	sunny	overcast, snowing		
	12.00		Overcast	sunny	overcast, snowing		
	14.00			sunny	overcast, snowing		
	16.00	Taken as leaving South Georgia. Cloudy & Hailing		sunny	overcast, snowing		
	18.00			sunny	overcast, snowing		
	20.00	Overcast.	Just starting to become sunny	sunny	snowing, overcast		
5	22.00	Overccast, dark, cold		sunny			
	02.00	**overcast, cold, rainy**	**Full sunshine, beautiful!**	sunny			
	04.00			sunny			
	06.00			sunny			
	08.00			sunny			

Appendix I: The nutrient results of experiment B.

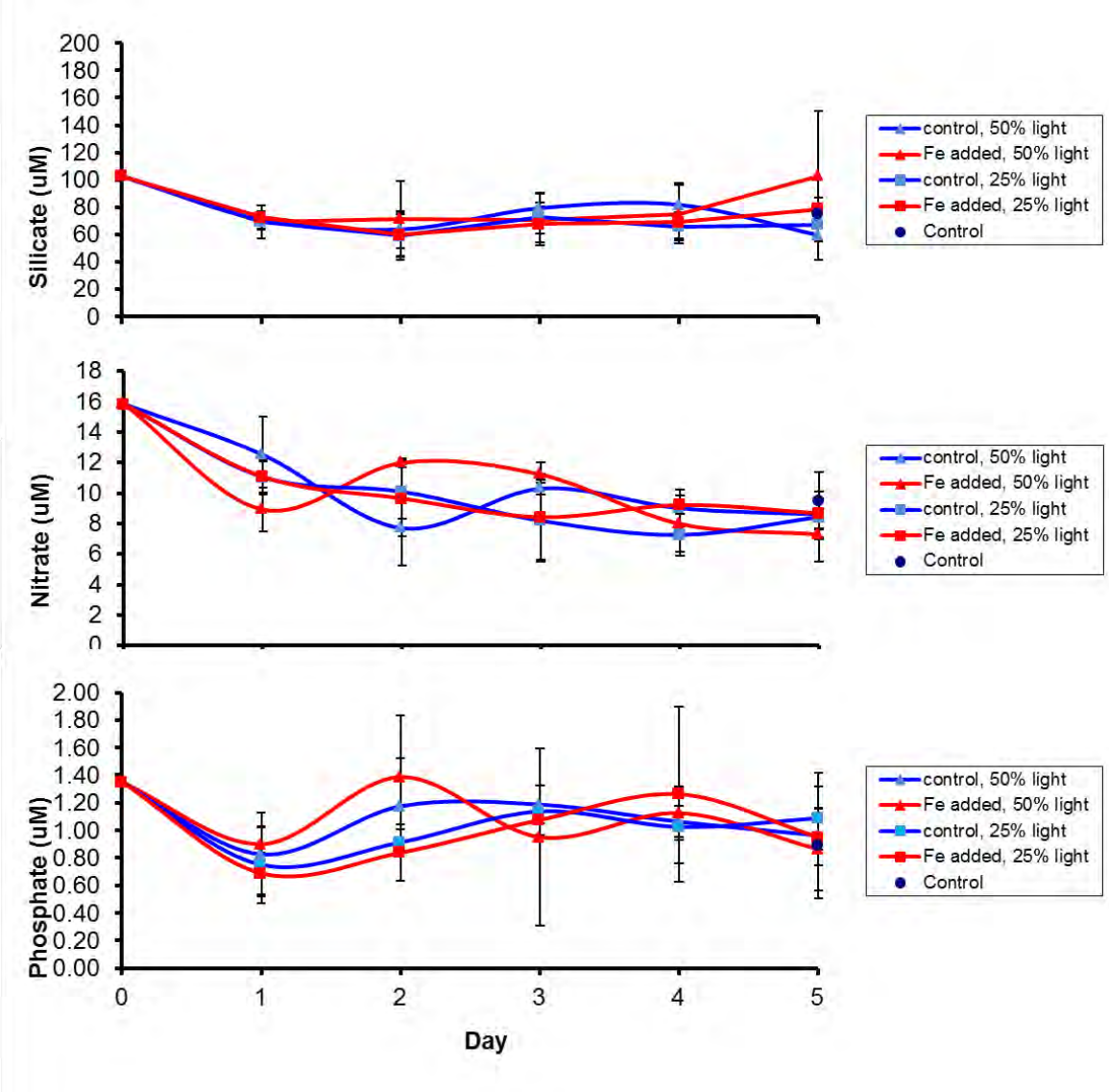

Appendix J: Critique and recommendations on the bio-assay nutrient methods

Critique

Phosphate

Variation with PO_4 can be explained by the lack of chloroform treatment before freezing. Without this treatment marked changes in the level of inorganic PO_4 can occur (Gilmartin, 1967). These changes may be seen through increases due to 'bacterial or enzymatic decomposition of organic phosphorus' or decreases from either the 'utilization by growing bacteria and plankton or by adsorption on detritus or sample bottle walls, or both' (Gilmartin, 1967). Furthermore, analysis of frozen PO_4 data should occur within 4 months of collection to prevent the steady decrease in concentration (Clementson and Wayte, 1992) that occurs after this time. The experimental data from SANAE 50 began to be analysed after 6 months due to available laboratory and personal time of the person charged with analysing these nutrients.

Silicate

Variation with SiO_4 can be explained through two experimental errors that occurred in the process. One being a straight experimental error of on board filtering of all samples through a Whatman GF/F (made intrinsically of SiO_4). This could unexpectedly raise sample values depending on the amount of SiO_4 transferred from the filter. Secondly, Zhange and Ortner (1998) discovered that the thawing process of water samples is important in the recovery of the intrinsic value of SiO_4. Their recommendations, four days thawing in a 4ºC freezer, for the 100% recovery of SiO_4 was not followed. This could lead to lower values of SiO_4.

Nitrate

With regard to the NO_3 data, consultation with various international experts both at NOC and in South Africa, confirm that sometimes this just happens with frozen samples. The length of time for sample storage (6 months – year) was probably a largely contributing factor (Kremling and Wenck, 1986).

Recommendations

Though straight freezing and thawing is fine in oligotrophic regions (Dore *et al.,* 1996), the results of this experiment along with experiences of a similar nature by other scientists suggest that it is not sufficient in the Southern Ocean. Hence I recommend that the processes recommended by Zhange and Ortner (1998) and Gilmartin (1967) and for SiO_4 and PO_4 respectively should be investigated and implemented in future cruises of this nature. If possible nutrients should be run on board the ship to prevent these complications. If this is not possible then they should be run immediately upon return to land.

Reference list

ALDERKAMP, A., KULK, G., BUMA, A.G.J., VISSER, R.J.W., VAN DIJKEN, G.L. er al., 2012. The effect of iron limitation on the photophysiology of *Phaeocystis antarctica* (prymnesiophyceae) and *Fragilariopsis cylindrus* (bacillariophyceae) under dynamic irradiance. *Jouranal of Phycology* **48**: 45-59

ARCHER, D. 2009. The long Thaw: How humans are changing the next 100,000 years of Earth's climate. Princeton University Press, United States of America

ARRIGO, K.R., ROBINSON, D.H., WORTHEN, D.L., DUNBAR, R.B., DITULLIO, G.R., *et al.,* 1999. Phytoplankton Community Structure and the Drawdown of Nutrients and CO_2 in the Southern Ocean. *Science* **283** (5400):365-367

ARRIGO, K.R., VAN DIJKEN, G.L. and BUSHINSKY, S. 2008. Primary production in the Southern Ocean, 1997-2006. *Journal of Geophysical Research* **113**: 27

AUMONT, O., BOPP, L. and SCHULZ, M. 2008. What does temporal variability in aeolian dust deposition contribute to sea-surface iron and chlorophyll distributions? *Geophysical Research Letters* **35**, L07607, [doi:10.1029/2007GL031131]

BABIN, M., MOREL, A., CLAUSTRE, H., BRICAUD, A., KOLBERT, Z. and FALKOWSKIT, P.G. 1996. Nitrogen- and irradiance dependent variations of the maximum quantum yield of carbon fixation in eutrophic, mesotrophic and oligotrophic marine systems. *Deep-Sea Research I: Oceanography Research Paper* **43** (8):1241-1272

BARLOW, R.G., CUMMINGS, D.G. and GIBB, S.W. 1997. Improved resolution of mono- and divinyl chlorophylls a and b and zeaxanthin and lutein in phytoplankton extracts using reverse phase C-8 HPLC. *Marine Ecology Progress Series* **161**: 303-307

BARLOW, R.G., MANTOURA, R.F.C., CUMMINGS, D.G., POND, D.W. and HARRIS, R.P. 1998. Evolution of phytoplankton pigments in mesocosm experiments. *Estuarine, Coastal and Shelf Science* **46** (Supplement A): 15-22

BARNOLA, J. M., RAYNAUD, D., KOROTKEVICH, Y. S. and LORIUS, C. 1987. Vostok ice cores provides 160,000-year record of atmospheric CO_2. *Nature* **329**: 408-414

BEHRENFELD, M.J., BALE, A., KOLBER, Z., AIKEN, J. and FALKOWSKI, P. 1996. Confirmation of iron limitation of phytoplankton photosynthesis in the equatorial Pacific Ocean. *Nature* **383**: 508-511

BERGER, W.H. and WEFER, G. 1991. Productivity of the glacial ocean: Discussion of the iron hypothesis. *Limnology and Oceanography* **36** (8): 1899-1918

BLAIN, S., TREGUER, P., BELVISO, S., BUCCIARELLI, E., DENIS, M., *et al.,* 2001. A biogeochemical study of the island mass effect in the context of the iron hypothesis: Kerguelen Islands, Southern Ocean. *Deep-Sea Research I: Oceanography Research Paper* **48**: 163-187

BLAIN, S., QUEGUINER, B., ARMANDI, L., BELVISO, S., BOMBLED, B., *et al.,* 2007. Effect of natural iron fertilization on carbon sequestration in the Southern Ocean. *Nature* **446,** [doi:10.1038/nature05700]

BLAIN, S., SARTHOU, G. and LAAN, P. 2008. Distribution of dissolved iron during the natural iron-fertilization experiment KEOPS (Kerguelen Plateau, Southern Ocean. *Deep-Sea Research II: Topical Studies in Oceanography* **55**: 594-605

BOND, W.J. and MIDGLEY, .G.F. 2000. A proposed CO_2-controlled mechanism of woody plant invasion in grasslands and savannas. *Global Change Biology* **6**: 865-869

BOND, T., and SUN, H. 2005. Can reducing black carbon emissions counteract global warming? *Environmental Science and Technology* **39**(16): 5921-5926

BOPP, L., MONFRAY, P., AUMONT, O., DUFRESNE, J. L., LE TREUT, H., *et al.,* 2001. Potential impact of climate change on marine export production. *Global Biogeochemical Cycles* **15**(1): 81−99, [doi:10.1029/1999GB001256]

BOYD, P.W. 2002. Review: Environmental factors controlling phytoplankton processes in the Southern Ocean. *Journal of Phycology* **38**: 844-861

BOYD, P. W. and ABRAHAM, E.R. 2001. Iron-mediated changes in phytoplankton photosynthetic competence during Soiree. *Deep-Sea Research II: Topical Studies in Oceanography* **48**: 2529-2550

BOYD, P.W and LAW, C.S. 2001. The Southern Ocean Iron RElease Experiment (SOIREE) introduction and summary. *Deep-Sea Research II: Topical Studies in Oceanography* **48**: 2425-2438

BOYD, P., LAROCHE, J., GALL, M., FREW, R. and MCKAY, R. M. L. 1999. Role of iron, light and silicate in controlling algal biomass in Subantarctic waters S.E. of New Zealand. *Journal of Geophysical Research* **104**: 13395-408

BOYD, P.W., WATSON, A.J., LAW, C.S., ABRAHAM, E.R., TRULL, T., *et al.,* 2000. A mesoscale phytoplankton bloom in the polar Southern Ocean stimulated by iron fertilization. *Nature* **407**: 695-702

BOYD, I.L., STANILAND, I.J. and MARTIN, A.R. 2002. Distribution of foraging by female Antarctic fur seals. *Marine Ecology. Progress Series* **242**: 285-294

BOYD, P.W., JICKELLS, T., LAW, C.S., BLAIN, S., BOYLE, E.A., *et al.,* 2007. Mesoscale iron enrichment experiments 1993 – 2005: Synthesis and future directions. *Science* **315**: 612-617

BRIFFA, K.R., JONES, P.D., SCHWEINGRUBER, F.H. and OSBORN, T.J. 1998. On Northern Hemisphere summer temperature over the past 600 years. *Nature* **393**: 450

BROECKER, W. S. 1991. The great ocean conveyor. *Oceanography* **4** (2): 79-89

BROECKER, W.S. 2000. Abrupt climate change: causal constraints provided by the paleoclimate record. *Earth-Science Review* **51**: 137-154

BRULAND, K.W., RUE, E.L., SMITH, G.J., DITULLIO, G.R. 2005. Iron, macronutrients and diatom blooms in the Peru upwelling regime: brown and blue waters of Peru. *Marine Chemistry* **93**: 81-103

BRZEZINSKI, M.A. 1985. The Si:C:N ratio of marine diatoms: interspecific variability and the effect of some environmental variables. *Journal of Phycology* **21**: 347-357

CALDEIRA, K. and DUFFY, P.B. 2000. The role of the Southern Ocean in uptake and storage of anthropogenic carbon dioxide. *Science* **287**: 620-622

CALLAHAN, J,E. 1972. The structure and circulation of deep water in the Antarctic. *Deep Sea Research and Oceanographic Abstracts* **19**: 563-575

CAMPBELL, N.A. and REECE, J.B. 2005. Biology (Seventh Edition). Pearson/Benjamin Cummings, Cape Town

CANADELL, J.G., LE QUERE, C., RAUPACH, M.R., FIELD, C.B., BUITENHUIS, E.T., *et al.,* 2007. Contributions to accelerating atmospheric CO_2 growth from economic activity, carbon intensity, and efficiency of natural sinks. *Proceedings of the National Academy of science of the United States of America* **104**: 18866-18870

CARPENTER, J.H. 1965. The Chesapeake Bay Institute technique for the Winkler dissolved oxygen method. *Limnology and Oceanography* **10**: 141-143

CHISHOLM, S.W. and MOREL, F.M.M. 1991. What controls phytoplankton production in nutrient-rich areas of the open sea? *Limnology and Oceanography* Special Issue **36**: 1507

CHISHOLM, S.W., FALKOWSKI, P.G. and CULLEN, J.J. 2001. Dis-crediting Ocean Fertilization. *Science* **294**: 309-310

CLEMENTSON, L.A. and WAYTE, S.E. 1992. The effect of frozen storage of open-ocean seawater samples on the concentration of dissolved phosphate and nitrate. *Water research* **26**(9): 1171-1176

COALE, K.H., JOHNSON, K.S., FITZWATER, S.E., GORDON, R.M., TANNER, S., *et al.,* 1996. A massive phytoplankton bloom induced by an ecosystem-scale iron fertilization experiment in the equatorial Pacific Ocean. *Nature* **383**: 495-501

COALE, K.H., JOHNSON, K.S., CHAVEZ, F.P., BUESSELER, K.O., BARBER, R.T., *et al*., 2004. Southern Ocean iron enrichment experiment: carbon cycling in high- and low- Si waters. *Science* **304**: 408-414

COCHLAN, W.P., HEMDON, J. and KUDELA, R.M. 2008. Inorganic and organic nitrogen uptake by the toxigenic diatom Pseudo-nitzschia australis (Bacillariophyceae). *Harmful Algae* **8**: 111-118

COX, P. M., BETTS, R. A., JONES, C. D., SPALL, S. A., and TOTTERDELL, I. J. 2000. Acceleration of global warming due to carbon‐cycle feedbacks in a coupled climate model. *Nature* **408**(6809): 184–187, [doi:10.1038/35041539]

CROWLEY, T.J. 2000. Causes of climate change over the past 1000 years. *Science* **289**: 270

CROWLEY, T.J. and KIM, K-Y. 1993. Towards development of a strategy for determining the origin of decadal-centennial scale climate variability. *Quaternary Science Reviews* **12**: 375-385

CROWLEY, T. J. and KIM, K-Y. 1999. Modeling the forced response to climate change over the last six centuries. *Geophysical Research Letters* **26**: 1901-1904

CUBASCH, U., VOSS, R., HEGERL, G.C., WASZKEWITZ, J. and CROWLEY, T.J. 1997. Simulation of the influence of solar radiation variations on the global climate with an ocean-atmosphere general circulation model. *Climate Dynamics* **13** (11): 757-767

CULLEN, J.J. 1991. Hypotheses to explain high-nutrient conditions in the open sea. *Limnology and Oceanography* **36** (8): 1578-1599

CULLEN, J.J., YANG, X. and MACINTYRE, H.L. 1992. Nutrient limitation of marine photosynthesis. P.G. Falkowski, A. Woodhead, (editors). Primary Productivity and Biogeochemical Cycles in the sea, Plenum, New York pp. 69-88

CUTNELL and JOHNSON. 2007. Physics (seventh edition). John Wiley and Sons, Inc. United States of America

CUYPERS, D., DAUWE, T. and VANGOIDSENHOVEN, M. 2011. REDD+ in the Cancun Agreement. An analysis from the front line. Working paper. Be-REDDi. NUMBER 1

DAMON, P.E. and PERISTYKH, A.N. 1999. Solar cycle length and 20th century Northern Hemisphere warming: revisited. *Geophysical Research Letters* **26**(16): 2469-72

DE BAAR, H. J. W., and BOYD, P. W. 2000. The role of iron in plankton ecology and carbon dioxide transfer of the global oceans. R.B. Hanson, H.W. Ducklow, and J.G. Field (editors). *The Dynamic Ocean Carbon Cycle: A Midterm Synthesis of the Joint Global Ocean Flux Study.* Cambridge University Press, Cambridge pp 61-140

DE BAAR, H.J.W., DE JONG, J.T.M., BAKKER, D.C.E., LOSCHER, B.M., VETH, C., *et al.,* 1995. Importance of iron for plankton blooms and carbon dioxide drawdown in the Southern Ocean. *Nature* **373**: 412-415

DE BAAR, H.J.W., VAN LEEUWE, M.A., SCHAREK, R., GOEYENS, L., BAKKER, K.M.J. and FRITSCHE, P. 1997. Nutrient anomalies in Fragilariopsis kerguelensis blooms, iron deficiency and the nitrate/phosphate ratio (A.C. redfield) of the Antarctic Ocean. *Deep Sea Research Part II: Topical Studies in oceanography* **44**: 229-260

DE BAAR, H.J.W., BOYD, P.W., COALE, K.H., LANDRY, M.R., TSUDA, A., *et al.,* 2005. Synthesis of iron fertilisation experiments: from the Iron Age in the age of enlightenment. *Journal of Geophysical Research (Oceans)* **110** (C9)

DIERSSEN, H.M., SMITH, R.C. and VERNET, M. 2002. Glacial meltwater dynamics in coastal waters west of the Antarctic peninsula. *Proceedings of the National Academy of Sciences of the United States of America* **99** (4): 1790-1795

DUCE, R.A. and TINDALE, N.W. 1991. Atmospheric transport of iron and its deposition in the ocean. *Limnology and Oceanography* **36** (8): 1715-1726

DUGDALE, R.C. and GOERING, J.J. 1967. Uptake of new and regenerated forms of nitrogen in primary productivity. *Limnology and Oceanography* **12**: 196-206

EPPLEY, R.W. and PETERSON, B.J. 1979. Particulate organic matter flux and planktonic new production in the deep ocean. *Nature* **282**: 677-680

FALKOWSKI, P.G. 1994. The role of phytoplankton photosynthesis in global biogeochemical cycles. *Photosynthetic Research* **39**: 235-258

FALKOWSKI, P.G and RAVEN, J.A. 2007. Aquatic Photosynthesis (second edition). Princeton University Press, Princeton and Oxford

FALKOWSKI, P., SCHOLES, R.J., BOYLE, E., CANADELL, J., CANFIELD, D., *et al.,* 2000. The global carbon cycle: A test of our knowledge of earth as a system. *Science* **290** (5490): 291-296

FENG, Y., HARE, C. E., ROSE, J. M., HANDY, S. M., DITULLIO, G. R., *et al.*, 2010. Interactive effects of iron, irradiance and CO_2 on Ross Sea phytoplankton. *Deep-Sea Research Part I: Oceanography Research Paper* **57**: 368-83

FIELD, C. M., BEHRENFELD, RANDERSON, J. and FALKOWSKI. P. 1998. Primary production of the biosphere: integrating terrestrial and oceanic components. *Science* **281**: 237-240

FIELD, J.G., HEMPLE, G. and SUMMERHAYES, C.P. (editors) 2002. OCEANS 2020: Science, Trends, and the Challenge of Sustainability. Island Press, United States of America, ISBN 1 – 55963 -470-7

FIELDING, S., WARD, P., POLLARD, R.T., SEEYAVE, S., READ, J.F., *et al.,* 2007. Community structure and grazing impact of mesozooplankton during late spring/early summer 2004/2005 in the vicinity of the Crozet Islands (Southern Ocean). *Deep-Sea Research II: Topical Studies in Oceanography* **54** (18-20): 2106-2125

FONDA UMANI, S., ACCORNERO, A., BUDILLON, G., CAPELLO, M., TUCCI, S., *et al*., 2002. Particulate matter and plankton dynamics in the Ross Sea polynya of Terra Nova Bay during the austral summer 1997/98. *Journal of Marine Systems* **36**: 29-49

FONDA UMANI, S., MONTI, M., BERGAMASCO, A., CABRINI, M., DE VITTOR, C., *et al*., 2005. Plankton community structure and dynamics versus physical structure from Terra Nova Bay to Ross Ice Shelf (Antarctica). *Journal of Marine Systems* **55**: 31-46

FOUKALL, P., FROHLICH, C., SPRUIT, H. and WIGLEY, T. M. L.2006. Variations in solar luminosity and their effect on the Earth's climate. *Nature* **443**, [doi:10.1038/nature05072]

FREE, M. and ROBOCK, A. 1999. Global warming in the context of the Little Ice Age. *Journal of Geophysical Research.* **104:** 19057-19070

FRIEDLINGSTEIN, P., COX, P.M., BETTS, R., BOPP, L., VON BLOH, W., *et al.,* 2006. Climate-carbon cycle feedback analysis, results from the C^4MIP model intercomparison. *Journal of Climate* **19**: 3337-3353

FRIIS-CHRISTENSEN, E. and LASSEN, K. 1991. Length of the solar cycle: an indicator of solar activity closely associated with climate. *Science* **254**: 698-700

FUNG, Y., MEYN, S.K., TEGEN, I., DONEY, S.C., JOHN, J.G. and BISHOP, J.K.B. 2000. Iron supply and demand in the upper ocean. *Global Biogeochemical Cycles* **14** (1): 281-295

FUNG, I., DONEY, S.C., LINDSAY, K. and JOHN, J. 2005. Evolution of carbon sinks in a changing climate. *Proceedings of the National Academy of Sciences of the United States of America* **102 (**11): 201-11 206

GEIDER, R.J. and ROCHE, J. 1994. The role of iron in phytoplankton photosynthesis, and the potential for iron-limitation of primary productivity in the sea. *Photosynthesis Research* **39** (3): 275-301

GERVAIS, F., RIEBESELL, U., and GORBUNOV, M. Y. 2002. Changes in primary productivity and chlorophyll a in response to iron fertilization in the Southern Polar Frontal Zone. *Limnology and Oceanography* 47: 1324-1335

GIBBERD, M-J., KEAN, E., BARLOW, R., THOMALLA, S., LUCAS, M. 2013. Phytoplankton chemotaxonomy in the Atlantic sector of the Southern Ocean during the late summer 2009. *Deep-sea Reserch I* 78:70-78

GILMARTIN, M. 1967. Changes in inorganic phosphate concentration occurring during seawater sample storage. *Limnology and Oceanography* **12** (2): 325-328

GORDON, A. L. 1986. Interocean exchange of thermocline water. *Journal of geophysical Research* **91**: 5037-46

GORDON, A. L., LUTJEHARMS, J. R. E. and GRIIDLINGH, M. L. 1987. Stratification and circulation at the Agulhas Retroflection. *Deep-Sea Research Part I: Oceanography Research Paper* **34**: 565-599

GRASSHOFF, K.M., EHRHARDT, M. and KREMLING, K. 1983. Determination of urea (9.5). In: *Methods of seawater analysis* (second edition). Verlag Chemie, Wienheim, Germany. pp 158-162

GREENBLATT, J.B. and SARMIENTO, J.L. 2004. Variability and climate feedback mechanisms in ocean uptake of CO_2. In *The Global Carbon Cycle: Integrating Humans, Climate, and the Natural World, Scope 62*,. C.B. Field, M.R. Raupach (editors), ch. 2, Washington, DC: Island Press pp. 257-275

GREENE, R.M., GEIDER, R.J. and FALKOWSKI, P.G. 1991. Effect of iron limitation on photosynthesis in a marine diatom. *Limnology and Oceanography* **36**: 1772-1782

HAEBERLI, W., NOETZLI, J., ZEMP, M., BAUMANN, S., FRAUENFELDER, R. and HOELZLE, M. (editors) 2005a. Glacier mass balance bulletin, Bull. 8 (2002– 2003), 100 pp., World Glacier Monit. Serv., Zurich, Switzerland

HAEBERLI, W., ZEMP, M., FRAUENFELDER, R., HOELZLE, M. and. KAAB, A. (editors). 2005b. Fluctuations of glaciers 1995–2000, Volume VIII, report, 288 pp., World Glacier Monit. Serv., Zurich, Switzerland

HANSEN, J., SATO, M., LACIS, A., RUEDY, R., TEGEN, I and MATTHEWS, E. 1998. Perspective: Climate forcings in the industrial era. *Proceedings of the National Academy of Sciences of the United States of America* **22**: 12753-12758

HASSLER, C.S., SCHOEMANN, V., BOYE, M., TAGLIABUE, A., ROZMARYNOWYCZ, M. and MCKAY, R.M.L. 2012. Iron bioavailability in the Southern Ocean. *Oceanography and Marine Biology: An Annual Review* **50**: 1-64

HENDRIKS, C.A., WORRELL, E., DE JAGER, D., BLOK, K. and RIEMER, P. 2003. Greenhouse gas control technologies conference paper – cement. Emission Reduction of Greenhouse Gases from the Cement Industry
http://www.ieagreen.org.uk/prghgt42.htm (1 of 11) 13 July 2003

HIGGINS, S.I., SHACKLETON, C.M., and ROBINSON, R. 1999. Changes in woody community structure and composition under contrasting landuse systems in a semi-arid savanna, South Africa. *Journal of Biogeography* **26**: 619-627

HILLEL, D. and ROSENZWEIG, C. 2002. Desertification in relation to climate variability and change. Advances in Agronomy 77. Elsevier Science, USA, ISBN 0065 – 2113/02

HIRATA, T., AIKEN, J., HARDMAN-MOUNTFORD, N., SMYTH, T.J. and BARLOW, R.G. 2008. An absorption model to determine phytoplankton size classes from satiellite ocean colour. *Remote Sensing of Environment* **112**: 3153-3159

HISCOCK, M.R. 2004. (thesis) The regulation of primary productivity in the Southern Ocean. Nicholas School of the Environment and Earth Science, Duke University

HOEGH-GULDBERG, O. 1999. Climate change, coral bleaching and the future of the world's coral reefs. *Marine and Freshwater Research* **50** (8): 839-866

HOFFMANN, L.J., PEEKEN, I., LOCHTE, K., ASSMY, P. and VELDHUIS, M. 2006. Different reactions of Southern Ocean phytoplankton size classes to iron fertilization. *Limnology and Oceanography* **51** (3)

HOLETON, C.L., NEDELEC, F., SANDERS, R., BROWN, L., MOORE, C. M., *et al.,* 2005. Physiological state of phytoplankton communities in the Southwest Atlantic sector of the Southern Ocean, as measured by fast repetition rate fluorometry. *Polar Biology* **29**: 44-52

HOYT, D.V. 1979. Variations in sunspot structure and climate. *Climatic Change* **2** (1): 79-92

HUGHES, T. P., BAIRD, A. H., BELLWOOD, D. R., CARD M., CONNOLLY S. R., *et al.,* 2003. Climate change, human impacts and the resilience of coral reefs. *Science* **301**: 929

IPCC (2000). Land Use, Land Use Change and Forestry. R.T. Watson, I.R. Noble, B. Bolin, *et al.,* (editors). Cambridge University Press pp 375

IPCC (2001). R. T. Watson and Core Writing Team, Editors, *3rd Assessment Report of the Inter-Governmental Panel on Climate Change. Climate Change 2001: Synthesis Report,* www.ipcc.ch/pub/syreng.htm

IPCC (2007a). Summary for policymakers. In: *Climate Change 2007: The Physical Science Basis. Contribution of Working Group I to the Fourth Assessment Report of the Intergovernmental Panel on Climate Change*. S. Solomon, D. Qin, M. Manning, *et al.,* (editors), Cambridge University Press, Cambridge, United Kingdom and New York, NY, USA pp 1-18

IPCC (2007b). *Climate Change 2007: Synthesis Report. Contribution of Working Groups I, II and III to the Fourth Assessment Report of the Intergovernmental Panel on Climate Change* In: Core Writing Team, R.K. Pachauri, and A. Reisinger (Editors). IPCC, Geneva, Switzerland pp 104

IPCC (2007c). *Climate Change 2007: The Physical Science Basis. Contribution of Working Group I to the Fourth Assessment Report of the Intergovernmental Panel on Climate Change* (S. Solomon, D. Qin, M. Manning, *et al.,* [editors]). Cambridge University Press, Cambridge, United Kingdom and New York, NY, USA

IPCC (2007d). BINDOFF, N.L., WILLEBRAND, J., ARTALE, V., CAZENAVE, A., GREGORY, J., *et al.,* 2007: Observations: Oceanic Climate Change and Sea Level. *In: Climate Change 2007: The Physical Science Basis. Contribution of Working Group I to the Fourth*

Assessment Report of the Intergovernmental Panel on Climate Change (S. Solomon, D. Qin, M. Manning, *et al.,* [editors]). Cambridge University Press, Cambridge, United Kingdom and New York, NY, USA

IPCC (2011). MOOMAW, W., YAMBA, F., KAMIMOTO, M., MAURICE, L., NYBOER, J., *et al.,* 2011. Introduction. *In IPCC Special Report on Renewable Energy Sources and Climate Change Mitigation* (O. Edenhofer, R. Pichs P. Madruga, *et al.,* [editors]), Cambridge University Press, Cambridge, United Kingdom and New York, NY, USA

IPCC (2013). STOCKER, T.F., QIN, D., PLATTNER, G.-K., TIGNOR, M., ALLEM, S.K., *et al*., [editors] 2013. Summary for Policymakers. *In: Climate Change 2013: The Physical Science Basis. Contribution of Working Group 1 to the Fifth Assessment Report of the Intergovernmental Panal on Climate Change.* Cambridge University Press, Cambridge, United Kingdom and New York, NY, USA

ISMAIL, H., 1990. Surface nutrients in the vicinity of the Prince Edward Islands during April/May 1989. *South African Journal of Antarctic Research* **20** (1): 33-36

JEFFREY, S.W., MANTOURA, R.F.C. and WRIGHT, S.W. 1997. Phytoplankton pigments in oceanography; guidelines to modern methods. United Nations Educational, Scientific and Cultural Organization, Paris

JOHNSEN, G. and SAKSHAUG, E. 2007. Biooptical characteristics of PSII and PSI in 33 species (13 pigment groups) of marine phytoplankton, and the relevance for pulse amplitude modulated and fast repetition rate fluorometry. *Journal of Phycology* **43**: 1236-1251

JOUBERT, W.R., THOMALLA, S.J., WALDRON, H.N., LUCAS, M.I., BOYE, M., *et al*., 2011. Nitrogen uptake by phytoplankton in the Atlantic sector of the Southern Ocean during late austral summer. *Biogeosciences* **8**: 2947-2959

KASER, G., COGLEY, J. G., DYURGEROV, M. B., MEIER M. F. and OHMURA, A. 2006. Mass balance of glaciers and ice caps: Consensus estimates for 1961–2004. *Geophysical Research Letters* **33**, L19501, [doi:10.1029/2006GL027511]

KELLY, P.M. and WIGLEY, T.M.L. 1992. Solar cycle length, greenhouse forcing and global climate. *Nature* **360**: 382-330

KGOPE, B.S., BOND, W.J. and MIDGLEY, G.F. 2009. Growth responses of African savanna trees implicate atmospheric CO_2 as a driver of past and current changes in savanna tree cover. *Austral Ecology*

KOHFELD, K.E., LE QUERE, C., HARRISON, S.P. and ANDERSON, R.P. 2005. Role of Marine Biology in Glacial-Interglacial CO_2 Cycles. *Science* **308**(5718): 74-78, [doi: 10.1126/science.1105375]

KOLBER, Z. and FALKOWSKI, P. 1993. Use of active fluorescence to estimate phytoplankton photosynthesis in situ. *Limnology and Oceanography* **38**: 1646-1665

KOLBER, Z., ZEHR, J. and FALKOWSKI, P. 1988. Effects of growth irrandiance and nitrogen limitation on photosynthetic energy-conversion in photosystem-II. *Plant Physiology* **88**: 923-929

KOLBER, Z.S., PRASIL, O., FALKOWSKI, P.G. 1998. Measurements of variable chlorophyll fluorescence using fast repetition rate techniques: defining methodology and experimental protocols. *Biochimica et Biophysica Acta* **1367**: 88-106

KREMLING, K. and WENCK, A. 1986. On the storage of dissolved inorganic phosphate, nitrate and reactive silicate in the Atlantic Ocean water samples. *Meeresforschung* **31**: 69-74

KRUEGER, A., WALTER, J. S. L., BHARTIA, P.K., SCHNETZLER, C.C., KROTKOV, N. A., *et al.,* 1995. Volcanic sulphur dioxide measurements from the total ozone mapping spectrometer instruments. *Journal of geophysical research* **100**: 14057-76

KUDELA, R.M., COCHLAN, W.P. and DUGDALE, R.C. 1997. Carbon and nitrogen uptake response to light by phytoplankton during an upwelling event. *Journal of Plankton Research* **19** (5): 609-630

LANNUZEL, D., SCHOEMANN, V., DE JONG, J., TISON, J. and CHOU, L. 2006. Distribution and biogeochemical behaviour of iron in the East Antarctic sea ice. *Marine Chemistry* **106**: 18-32

LAUBSCHER, R. K., PERISSINOTTO, R. and MCQUAID, C. D. 1993. Phytoplankton production and biomass at frontal zones in the Atlantic sector of the Southern Ocean. *Polar Biology* **13**: 471-81

LAWRENCE, E (Ed.). 2005. Henderson's Dictionary of Biology (Thirteenth Edition). Pearson, Prentice Hall, Malaysia

LAWS, E.A. and BANNISTER, T.T. 1980. Nutrient- and light-limited growth of Thalassiosirafluviatilis in continuous culture, with implications for phytoplankton growth in the ocean. *Limnology and Oceanography* **25**: 457-473

LEAN, J and RIND, D. 1999. Evaluating sun-climate relationships since the Little Ice Age. *Journal of Atmospheric and Solar-Terrestrial Physics* **61**: 25-36

LEHNINGER, A.L. 1975. Biochemistry. The Molecular Basis of Cell Structure and Function (second Edition). New York, Worth Publishing

LE QUERE, C., RAUPACH, M.R., CANADELL, J.G., MARLAND, G., BOPP, L., *et al.,* 2009. Trends in the sources and sinks of carbon dioxide. *Nature Geoscience* **2**: 831-836, [doi:10.1038/ngeo689]

LEVITUS, S., CONKRIGHT, M.E., REID, J.L., NAJJAR, R.G. and MANTYLA, A.1993. Distribution of nitrate, phosphate and silicate in the world oceans. *Progress in Oceanography* **31** (3): 245-273

LEVITUS, S., ANTONOV, J.I. and BOYER, T.P. 2005: Warming of the World Ocean, 1955-2003. *Geophysical Research Letters* **32**, L02604, [doi:10.1029/ 2004GL021592]

LINDLEY, S., and BARBER, R.T. 1998. Phytoplankton response to natural and experimental iron addition. *Deep-Sea Research II: Topical Studies in Oceanography* **45**: 1135-1149

LONG, S.P., HUMPRIES, S. and FALKOWSKI P.G. 1994. Photoinhibition of photosynthesis in nature. *Annual Review of Plant Physiology and Plant Molecular Biology* **45**: 655-662

LONGHURST, A.R. 1991. Role of the Marine Biosphere in the Global Carbon Cycle. *Limnology and Oceanography* **36** (8): 1507-1526

LUCAS, M.I. 2009. Course material. Marine Ecology: BIO3002S. The University of Cape Town

LUCAS, M.I., SEEYAVE, S., SANDERS, R., MOORE, C.M., WILLIAMSON, R., and STINCHCOMBE, M., 2007. Nitrogen uptake responses to a naturally Fe-fertilised phytoplankton bloom during the 2004/5 CROZEX study. *Deep-Sea Research II: Topical Studies in Oceanography* **54** (18-20): 2138-2173

LUTJEHARMS, J. R. E. and COOPER, J. 1996. Interbasin leakage through Agulhas Current filaments. *Deep Sea Research Part I: Oceanographic Research Papers* **43**: 213-238

LUTZ, V.A., SATHYENDRANATH, S., HEAD, E.J.H., LI, W.K.W. 2001. Changes in the *in vivo* absorption and fluorescence excitation spectra with growth irradiance in three species of phytoplankton. *Journal of Plankton Research* **23**: 555-569

MACCARTHY, T. and RUBIDGE, B. 2005. The Story of Earth and Life: A southern African perspective on a 4.6-billion-year journey. Stuik nature, Cape Town, ISBN 978 1 77007 148 3

MACINTYRE, H.L., KANA, T.M., ANNING, T. and GEIDER, R.J. 2002. Photoacclimation of photosynthesis irradiance response curves and photosynthetic pigments in microalgae and cyanobacteria. *Journal of Phycology* **38**: 17-38

MACISAAC, J.J. and DUGDALE, R.C. 1972. Interactions of light and inorganic nitrogen in controlling nitrogen uptake in the sea. *Deep Sea Research and Oceanographic Abstracts* **19**: 209-232

MACKIE, D. S., BOYD, P. W., MCTAINSH, G. H., TINDALE, N. W., WESTBERRY, T. K. and HUNTER, K. A. 2008. Biogeochemistry of iron in Australian dust: From aeolian uplift to marine uptake. *Geochemical Geophysical Geosystems* **9**, Q03Q08, [doi:10.1029/2007GC001813]

MAHOWALD, N.M., BAKER, A.R., JICKELLS, T.D., KUBILAY, N., PROSPERO, J.M. and TEGEN, I. 2005. Atmospheric global dust cycle and iron inputs to the ocean. *Global Biogeochemical cycles* **19**, GB4025, [doi:10.1029/2004GB002402]

MANN, M. E., BRADLEY, R.S. and HUGHES, M.R. 1998. Global-scale temperature patterns and climate forcing over the past six centuries. *Nature* **392**: 779-787

MARTIN, J.H. 1990. Glacial-interglacial CO_2 change: the iron hypothesis. *Paleoceanograph*y **5**: 1-13

MARTIN, J.H. 1991. Iron. Leibig's Law and the Greenhouse. *Oceanography* **4**: 52-55

MARTIN, J.H. 1992. Iron as a limiting factor in oceanic productivity. *In* P. G. Falkowski, and A. D.Woodhead (editors). Primary Productivity and Biogeochemical. Plenum, New York pp 123-137

MARTIN, J. H. and FITZWATER, S. E. 1988. Iron deficiency limits phytoplankton growth in the north-east Pacific subarctic. *Nature* **331**: 341-343

MARTIN, J.H., COALE, K.H., JOHNSON, K.S., FITZWATER, S.E., GORDON, R.M., *et al.,* 1994. Testing the iron hypothesis in ecosystems of the equatorial Pacific Ocean. *Nature* **371**: 123-129

MATLAB The Language of Technical Computing. Version 7.8.0.347 (R2009a)

MENON, S., HANSEN, J., NAZARENKO, L. and LUO, Y. 2002. Climate Effects of Black Carbon Aerosols in China and India. *Science* **297** (5590): 2250-2253, [doi: 10.1126/science.1075159]

MICHEL, K-P. and PISTORIUS, E.K. 2004. Adaptation of the photosynthetic electron transport chain in cyanobacteria to iron deficiency: the function of idi a and isi a. *Physiologia Plantarum* **120**: 36-50

MILLER, G.W., PUSHNIK, J.C. and WELKIES, G.W. 1984. Iron chlorosis, a world wide problem, the relation of chlorophyll biosynthesis to iron. *Journal of Plant Nutrition* **7** (1-5): 1-22, [doi:10.1080/01904168409363172]

MOLEELE, N.M., RINGROSE, S., MATHESON, W. and VANDERPOST, C. 2002. More woody plants? The status of bush encroachment in Botswana's grazing areas. *Journal of Environmental Management* **64**: 3-11

MOORE, J.K. and ABBOTT, M.R. 2000. Phytoplankton chlorophyll distributions and primary production in the Southern Ocean. *Journal of Geophysical Research* **105** (C12): 28

MOORE, C.M., LUCAS, M.I., SANDERS, R. and DAVIDSON, R. 2005. Basin-scale variability of phytoplankton bio-optical characteristics in relation to bloom state and community structure in the Northeast Atlantic. *Deep-Sea Research Part I: Oceanography Research Paper* **52**: 401-419

MOORE, C.M., MILLS, M.M., MILNES, A., LANGLOISE, R., ACHTERBERG, E.P., *et al.,* 2006. Iron limits primary production during spring bloom development in the central North Atlantic. *Global Change Biology* **12**: 626-634

MOORE, C. M., HICKMAN, A.E., POULTON, A.J., SEEYAVE, S and LUCAS, M. 2007a. Iron-light interactions during the Crozet Natural Iron Bloom and Export Experiment (CROZEX) II: Taxonomic responses and elemental stoichiometry, *Deep-Sea Research II: Topical Studies in Oceanography* **54**: 2066-2084

MOORE, C. M., SEEYAVE, S., HICKMAN, A.E., ALLEN, J.T., LUCAS, M., *et al.,* 2007b. Iron-light interactions during the Crozet Natural Iron Bloom and Export Experiment (CROZEX) I: Phytoplankton growth and photophysiology, *Deep-Sea Research II: Topical Studies in Oceanography* **54**: 2045-2065

MORALES, F., ABADIA, A. and ABADIA, J. 1998. Photosynthesis, quenching of chlorophyll fluorescence and thermal energy dissipation in iron-deficient sugar beet leaves. *Australian Journal of Plant Physiology* **25** (4): 403-412

MOREL, F.M.M., RUETER, J.G. and PRICE, N.M. 1991. Iron nutrition of phytoplankton and its possible importance in the ecology of the ocean regions with high nutrient and low biomass. *Oceanography* **4**: 56-61

MORGAN, J.A., MILCHUNAS, D.G., LECAIN, D.R., WEST, M. and MOSIER, A.R. 2007. Carbon dioxide enrichment alters plant community structure and accelerates shrub growth in the shortgrass steppe. *Proceedings of the National Academy of Sciences of the United States of America* **104**: 14274-79

MOSTERT, S.A. 1983. Procedures used in South Africa for the automatic photometric determination of micronutrients in seawater. *South African Journal of Marine Science* **1**(1): 189-198

MURPHY, E.J., WATKINS, J.L., REID, K., TRATHA, P.N., EVERSON, I., *et al.,* 1998. Interannual variability of the South Georgia marine ecosystem: biological and physical sources of variation in the abundance of krill. *Fisheries Oceanography* **7**(3/4): 381-39

NSIDC 2012, National Snow and Ice Data Center. NASA Earth Observatory: http://www.earthobservatory.nasa.gov/Features/WorldOfChange/sea_ice_south.php http://nsidc.org/data/seaice_index/archives/image_select.html; 25 October 2012

NEALE, P. J. 1987. Algal photoinhibition and photosynthesis in the aquatic environment. In: Photoinhibition, D. J. Kyle, C. B. Osmond and C. J. Arntzen (editors). Elsevier, Amsterdam pp 39-65

NEY, R.A. and SCHNOOR, J.L. 2000. What Course for Carbon Trading? *Environmental Science and Technology* **34**: 176-182

Ocean Data View 2008. version 3.4.2. Reiner Schlitzer. http://odv.awi.de

ORR, J.C., MAIER-REIMER, E., MIKOLAJEWICZ, U., MONFRAY, P., SARMIENTO, J.L., *et al.,* 2001. Estimates of anthropogenic carbon uptake from four three-dimensional global ocean models. *Global Biogeochemical Cycles* **15**: 43-60

ORR, J.C., FABRY, V.J., AUMONT, O., BOPP, L., DONEY, S.C., *et al.,* 2005. Anthropogenic ocean acidification over the twenty-first century and its impact on calcifying organisms. *Nature* **437**: 681-686 [doi:10.1038/nature04095]

ORSI, A.H., WHITWORTH III, T. and NOWLIN, W.D. 1995. On the meridional extent and fronts of the Antarctic Circumpolar Current. *Deep Sea Research Part I: Oceanographic Research Papers* **42**: 641-673

PARK, Y.H., CHARRIAUD, E. and FIEUX, M 1998. Thermohaline structure of the Antarctic Surface Water/Winter Water in the Indian sector of the Southern Ocean. *Journal of Marine Systems* **17**: 5-23

PARSONS, T.R., MAITA, Y. and LALLI, C.M. 1984. *A manual of chemical and biological methods for seawater analysis*. Pergamon Press, Oxford pp 173

PETERSON, T.D., WHITNEY, F.A., HARRISON, P.J., 2005. Macronutrient dynamics in an anticyclonic mesoscale eddy in the Gulf of Alaska. *Deep-Sea Research II: Topical Studies in Oceanography* **52**: [**doi**:10.1016/j.dsr2.2005.02.004]

PETIT, J. R., JOUZEL, J., RAYNAUD, D., BARKOV, N. I., BARNOLA, J.M., *et al.,* 1999. Climate and atmospheric history of the past 420,000 years from the Vostok ice core, Antarctica. *Nature* **399**: 429-436

POLLARD, R. T., VENABLES, H.J., READ, J.F., and ALLEN, J.T. 2007. Large scale circulation around the Crozet Plateau controls an annual phytoplankton bloom in the Crozet Basin, *Deep-Sea Research Part II: Topical Studies in Oceanography* **54**: 1915-1929

POLLARD, R. T., SALTER, I., SANDERS, R.J., LUCAS, M.I., MOORE, C.M., *et al.,* 2009. Southern Ocean deep-water carbon export enhanced by natural iron fertilization. *Nature* **457**: 577-581

POULTON, A.J., ADEY, T.R., BALCH, W.A. and HOLLIGAN, P.M. 2007. Relating coccolithophore calcification rates to phytoplankton community dynamics: Regional differences and implications for carbon export. *Deep Sea Research II: Topical Studies in Oceanography* **54**: 538-557

POULTON, A.J., CHARALAMPOPOULOU, A., YOUNG, J.R., TARRAN, J.R., LUCAS, M.I., QUARTLY, G.D. 2010. Coccolithophore dynamics in non-bloom conditions during late summer in the central Iceland basin (july-august 2007)**.** *limnology and Oceanography* **44** (4): 1601-1613

PRICE, N.M., AHNER, B.A. and MOREL, F.M.M. 1994. The equatorial Pacific-Ocean-grazer-controlled phytoplankton populations in an iron-limited ecosystem. *Limnology and Oceanography* **39** (3): 520-534

R Development Core Team. 2011. R: A language and environment for statistical computing. R Foundation for Statistical Computing, Vienna, Austria. Version 2.14.0 (2011-10-31), ISBN 3-900051-07-0
http://www.R-project.org

RAMANATHAN, V., CRUTZEN, P.J., KIEHL, J.T. and ROSENFELD, D. 2001. Aerosols, Climate, and the Hydrological Cycle. *Science* **294**(5549): 2119-2124, [doi: 10.1126/science.1064034]

RAVEN, J.A. 1990. Predictions of Mn and Fe use efficiencies of phototrophic growth as a function of light availability for growth and C assimilation pathway. *New Phytology* **116**: 1-18

RAVEN, J.A., EVANS, M.C.W. and KORB, R.E. 1999. The role of trace metals in photosynthetic electron transport in O_2-evolving organisms. *Photosynthesis Research* **60**: 111-149

REDFIELD, A.C., KETCHUM, B.H., and F. A. RICHARDS, F.A. 1963. The influence of organisms on the composition of seawater. *In* M. N. Hill (editor). *The Sea* **2:** 26-77

RAGUENEAU, O., TREGUER, P., LEYNAERT, A., ANDERSON, R.F., BRZEZINSKI, M.A., *et al*., 2000. A review of the Si cycle in the modern ocean: recent progress and missing gaps in the application of biogenic opal as a paleoproductivity proxy. *Global and Planetary Change* **26**: 317-365

REID, K. and CROXALL, J.P. 2001. Environmental response of upper trophic-level predators reveals a system change in an Antarctic marine ecosystem. *Proceedings of the royal Society of Biological Sciences* **268**: 377-384

RIND, D. and OVERPECK, J. 1993. Hypothesized causes of decade-to-century-scale climate variability: Climate model results. *Quaternary Science Reviews* **12**: 357-374

RINTOUL *et al.,* (in press) http://www.sciencedaily.com/releases/2012/05/120521104635.htm

ROBOCK, A. 1979. The "Little Ice Age": Northern Hemisphere Average Observations and Model Calculations. *Science* **206**: 1402-1404

ROQUES, K.G., O'CONNOR, T.G. and WATKINSON, A.R. 2001. Dynamics of shrub encroachment in an African savanna: relative influences of fire, herbivory, rainfall and density dependence. *Journal of Applied Ecology* **38**: 268-280

ROSENZWEIG, C., KAROLY, D., VICARELLI, M., NEOFOTIS, P., WU, Q., CASASSA, G., *et al.,* 2008. Attributing physical and biological impacts to anthropogenic climate change. *Nature* **453**

SABINE, C.L., FEELY, R.A., GRUBER, N., KEY, R.M., LEE, K., *et al.,* 2004a. The Oceanic Sink for Anthropogenic CO_2. *Science* **305** (5682): 367-371, [doi: 10.1126/science.1097403]

SABINE, C.L., HEIMANN, M., ARTAXO, P., BAKKER, D., CHEN, C-T.A., *et al.,* 2004b. Current status and past trends of the global carbon cycle. In *The Global Carbon Cycle: Integrating Humans, Climate, and the Natural World, Scope 62*,. C.B. Field, M.R. Raupach (editors), ch. 2, Washington, DC: Island Press pp. 17-44b

SABINE, C.L. and TANHUA, T. 2010. Estimation of anthropogenic CO_2 inventories in the ocean. *Annual Review of Marine Science* **2**: 175-198

SAKSHAUG, E., SLAGSTAD, D. and HOLM-HANSEN, O. 1991. Factors controlling the development of phytoplankton blooms in the Antarctic Ocean - a mathematical model. *Marine Chemistry* **35**: 259-71

SARMIENTO, J. L., HUGHES, T. M. C., STOUFFER, R. J. and MANABE, S. 1998. Simulated response of the ocean carbon cycle to anthropogenic climate warming. *Nature* 393: 245-9

SATLANTIC, 2010. Operational manual for the FIRe fluorometer system, Document No. SAT-DN-00265. Satlantic Incorporated, Nova scotia

SCHLITZER, R. 2002. Carbon export fluxes in the Southern Ocean: results from inverse modeling and comparison with satellite-based estimates. *Deep Sea Research II: Topical Studies in Oceanography* **49**: 1623-1644

SCHMITZ, W. J. 1995. On the interbasin scale thermohaline circulation. *Reviews of geophysics* **33**: 151-173

SEEYAVE, S., LUCAS, M.I., MOORE, C.M., POULTON, A.J., 2007. Phytoplankton productivity and community structure in the vicinity of the Crozet Plateau during austral summer 2004/ 2005. *Deep Sea Research II: Topical Studies in Oceanography* **54** (18-20): 2020-2044

SEIBEL, B.A. and WALSH, P.J. 2001. Potential impacts of CO_2 injection on deep-sea biota. *Science* **294***:* 319-320

SIEGENTHALER, U. 1986. Carbon dioxide: its natural cycle and anthropogenic perturbation. In: The role of air-sea exchange in geochemical cycling. P. Buat-Menard (editor). Reidel pp 209-247

SIGMAN, D.M. and BOYLE, E.A. 2000. Glacial/interglacial variations in atmospheric carbon dioxide. *Nature* **407**: 859-869

SMETACEK, V. and NICOL, S. 2005. Polar ocean ecosystems in a changing world. *Nature* **437**: 362-368, [doi:10.1038/nature04161]

SMETACEK, V., DE BAAR, H. J., BATHMAN, U. V., LOCHTE, K. and RUTGERS VAN DER LOEFF, M. M. 1997. Ecology and biogeochemistry of the Antarctic Circumpolar Current

during austral spring: a summary of Southern Ocean JGOFS cruise *ANT X/6* of R.V. Polarstern. *Deep-Sea Research II: Topical Studies in Oceanography* **44**: 1-22

SMETACEK, V., ASSMY, P., HENJES, J., 2004. The role of grazing in structuring Southern Ocean pelagic ecosystems and biogeochemical cycles. *Antarctic Science* **16** (4): 541-558

SMETACEK, V., KLAAS, C., STRASS, V.H., ASSMY, P., MONTRESOR, M., *et al.,* 2012. Deep carbon export from a Southern Ocean iron-fertilized diatom bloom. *Nature* **489**: 313-319, [doi:10.1038/nature11229]

SMITH, W. O., and ASPER, V. L. 2001. The influence of phytoplankton assemblage composition on biogeochemical characteristics and cycles in the southern Ross Sea, Antarctica. *Deep-Sea Research Part I: Oceanography Research Paper* **48**:137-61

SMITH, W.O., DINNIMAN, M.S., TOZZI, S., DITULLIO, G.R., MANGONI, O., *et al*., 2010. Phytoplankton photosynthetic pigments in the Ross Sea: Patterns and relationships among functional groups. *Journal of Marine Systems* **82**: 177-185

SOKOLOV, S. and RINTOUL, R. 2007. On the relationship between fronts of the Antarctic Circumpolar Current and surface chlorophyll concentrations in the Southern Ocean. *Journal of Geophysical Research* **112**: C07030, [doi:10.1029/2006JC004072]

STRZEPEK, R.F., MALDONADO, M.T., HIGGINS, J.L., HALL, J., SAFI, K., *et al.,* 2005. Spinning the 'ferrous wheel': the importance of the microbial community in an iron budget during the Fe Cycle experiment. *Global Biogeochemical Cycles* **19**, GB4S26

STRZEPEK, R.F., MALDONADO, M.T., HUNTER, K.A., FREW, R.D. and BOYD. P.W. 2011. Adaptive strategies by Southern Ocean phytoplankton to lessen iron limitation: Uptake of organically complexed iron and reduced cellular iron requirements. *Limnology and Oceanography* **56** (6): 1983-2002

SUGGETT, D.J., MACINTYRE, H.L. and GEIDER, R.J. 2004. Evaluation of biophysical and optical determinations of light absorption by photosystem II in phytoplankton. *Limnology and Oceanography: Methods* **2**: 316-332

SUGGETT, D. J., MABERLY, S.C. and GEIDER, R.J. 2006. Gross photosynthesis and lake community metabolism during the spring phytoplankton bloom. *Limnology and Oceanography* **51**: 2064-2076

SUGGETT, D.J., MOORE, C.M., HICKMAN, A.E. and GEIDER, R.J. 2009. Interpretation of fast repetition rate (FRR) fluorescence: signatures of phytoplankton community structure versus physiological state. *Marine Ecology - Progress Series* **376**: 1-19

SULLIVAN, C.W., ARRIGO, K.R., MCCLAIN, C.R., COMISO, J.C. and FIRESTONE, J. 1993. Distributions of phytoplankton blooms in the Southern Ocean. *Science* **262**: 1832-1837

SUNDA, W.G. and HUNTSMAN, S.A. 1995. Iron uptake and growth limitation in oceanic and coastal phytoplankton. *Marine Chemistry* **50**: 189-206

SUNDA, W.G. and HUNTSMAN, S.A. 1997. Interrelated influence of iron, light and cell size on marine phytoplankton growth. *Nature* **390**: 389-392

SUNDQUIST, E.T. and VISSER ACKERMAN, K. 2014. The geologic history of the carbon cycle. Treatise on Geochemistry (Second Edition). *Biogeochemistry* 10: 361-398

TAKEDA, S. 1998. Influence of iron availability on nutrient consumption ratio of diatoms in oceanic waters. *Nature* **393**: 774-777

TAUCHER, J. and OSCHLIES, A. 2011. Can we predict the direction of marine primary production change under global warming. *Geophysical Research Letters* **38**, [doi:10.1029/2010GL045934]

TIMMERMANS, K.R., DAVEY, M.S., VAN DER WAGT, B., SNOEK, J., GEIDER, R.J., *et al.,* 2001. Co-limitation by iron and light of Chaetoceros brevis, C. dichaeta and C.calcitrans (Bacillariophyceae). *Marine Ecology - Progress Series* **217**: 287-297

TIMMERMANS, K.R., VER DER WAGT, B. and DE BAAR, H.J.W. 2004. Growth rates, half-saturation constants, and silicate, nitrate, and phosphate depletion in relation to iron availability of four large, open-ocean diatoms from the Southern Ocean. *Limnology and Oceanography* **49** (6): 2141-2151

TOGGWEILER, J.R. 2008.Origin of the 100,000-year timescale in Antarctic temperatures and atmospheric CO_2. *Paleoceanography* **23**: 2211, [doi:10.1029/2006PA001405]

TORTELL, P.D., PAYNE, C.D., LI, Y., TRIMBORN, S., ROST, B., *et al*., 2008. CO_2 sensitivity of Southern Ocean phytoplankton. *Geophysical Research Letters* **35**: L04605, [doi:10.1029/2007GL032583]

TRANVIK, L.J. and JANSSON, M. 2002. Climate change (communication arising): Terrestrial export of organic carbon. *Nature* **415**: 861-862

VASSILIEV, I. R., PRASIL, O., WYMAN, K. D., KOLBER, Z., HANSON JR, A. K., *et al.,* 1994. Inhibition of PSI1 photochemistry by PAR and UV radiation in natural phytoplankton communities. *Photosynthesis Research* **42**: 61-64

VENABLES, H. and MOORE, M. 2010. Phytoplankton and light limitation in the Southern Ocean: Learning from high-nutrient, high-chlorophyll areas. *Journal of Geophysical Research* **115**, C02015, [doi:10.1029/2009JC005361]

VENABLES, H.J., POLLARD, R.T. and POPOVA, E.E. 2007. Physical conditions controlling the development of a regular phytoplankton bloom north of the Crozet plateau, Southern Ocean. *Deep Sea research Part II: Tropical Studies in Oceanography* **54** (18-20): 1949-1965

VETH, C., PEEKEN, I. and SCHAREK, R 1997. Physical anatomy of fronts and surface waters in the ACC near the 6º W meridian during austral spring 1992. *Deep-Sea Research II: Topical Studies in Oceanography* **44**: 23-49

VOLK, T. and HOFFERT, M.I. 1985. Ocean carbon pumps: Analysis of relative strengths and efficiencies in ocean-driven atmospheric CO2 changes. In E.T. Sundquist and W.S. Broecker

(editor) The Carbon Cycle and atmospheric CO2: Natural Variations Archean to Present. 91-110 AGU Monograph 32, Am Geophys Union, Washington, DC

WAGENER, T., GUIEU, C., LOSNO, R., BONNET, S. and MAAHOWALD, N. 2008. Revisiting atmospheric dust export to the Southern Hemisphere ocean: Biogeochemical implications. *Global Biogeochemical Cycles* **22**, GB2006, [doi:10.1029/2007GB002984]

WARREN, B. A., and WUNSCH, C. 1981. Deep circulation of the world ocean. In B.A. Warren, (editor) Evolution of Physical Oceanography, 6-40. MIT Press, Cambridge

WATSON, A.J. and ORR, J.C. 2003. Carbon Dioxide fluxes in the global ocean. Ocean Biogeochemistry, Global Change – the IGBP series. Springer berlin Heidelberg, ISBN 978 – 3 – 642 – 55844 – 3

WESSEL, P. and SMITH, W.H.F. 1996. A global self-consistent, hierarchical, high-resolution shoreline database. *Journal of Geophysical Research* **101**: 8741-8743

WIGLEY, T.M.L. and RAPER, S.C.B. 1990. Natural variability of the climate system and the detection of the greenhouse effect. *Nature* **344**: 324-327

WIGLEY. B.J., BOND. W.J. and HOFFMAN. M.T. 2010. Thicket expansion in a South African savanna under divergent land use: local vs. global drivers? *Global Change Biology* **16**: 964-976

WHITNEY, F.A., CRAWFORD, D.W. and YOSHIMURA, T. 2005. The uptake and export of silicon and nitrogen in HNLC waters of the NE Pacific Ocean. *Deep-Sea Research II: Topical Studies in Oceanography* **52**: 1055-1067

WRIGHT, S. and JEFFREY, S. 2006. Marine Organic Matter: Biomarkers, Isotopes and DNA. Pigment Markers for Phytoplankton Production. J. Volkman (editor) The Handbook of Environmental Chemistry. Springer Berlin / Heidelberg, Isbn 978-3-540-28401-7. **2N**: 71-104, [Doi: 10.1007/698_2_003\]

YUNG, Y.L., LEE, T., WANG, C.H. and SHIH, W.T. 1996. Dust: a diagnostic of the hydrologic cycle during the Last Glacial Maximum. *Science* **271**: 962-963

ZAGHA, R. and NANKANI, G.T. 2005. Economic Growth in the 1990s: Learning from a Decade of Reform. The World Bank Washington, DC, ISBN 0-8213-6043-4

ZHANG, J. and ORTNER, P.B. 1998. Effects of thawing condition on the recovery of reactive silicic acid from frozen natural water samples. *Water Research* **32** (8): 2553-2555

ZHUANG, G. and DUCE, R.A. 1993. The adsorption of dissolved iron on marine aerosol particles in surface waters of the open ocean. *Deep Sea Research Part I: Oceanographic Research Papers* **40**: 1413-1429

http://www.acecrc.org.au/Research/Southern%20Ocean%20Carbon%20Sink on 13 August 2012

Acts

Air Pollution Prevention Act in 1965 (South Africa)

Clean Air Act of 1956, updated in 1993 (Britain)

Clean Air Act of 1999 (Philippine)

Clean Air Act of 1963, Public Law (United States) 88-206, 77 United States Statutes at Large 392, 1963-12-17

Clean Air Act Extension of 1970, 84 United States Statutes at Large 1676, Public Law (United States) 91-604, 1970-12-31

Clean Air Act Amendments of 1977, Public Law (United States) 95-95, 91 United States Statutes at Large 685, 1977-08-07

Clean Air Act Amendments of 1990, Public Law (United States) 101-549, 104 United States Statutes at Large 2399, 1990-11-15

National Environmental Management: Air Quality Act 2004 (South Africa)